Title
Biological and physical regulation of the oceanic fixed nitrogen reservoir

Author
Weber, Thomas Smith

Publication Date
2013

Peer reviewed|Thesis/dissertation

UNIVERSITY OF CALIFORNIA

Los Angeles

Biological and physical regulation of the oceanic fixed nitrogen reservoir

A dissertation submitted in partial satisfaction of the

requirements for the degree Doctor of Philosophy

in Atmospheric and Oceanic Sciences

by

Thomas Smith Weber

2013

ABSTRACT OF THE DISSERTATION

Biological and physical regulation of the oceanic fixed nitrogen reservoir

by

Thomas Smith Weber

Doctor of Philosophy in Atmospheric and Oceanic Sciences

University of California, Los Angeles, 2013

Professor Curtis Deutsch, Chair

Fixed nitrogen (N) limits phytoplankton growth throughout the low latitude ocean. The oceanic reservoir of this essential nutrient is therefore a critical determinant of the fertility of the ocean as a whole, and the strength of the biological pump that sequesters carbon in deep waters out of contact with the atmosphere. Two biological processes dominate the ocean's N budget: a source of N through N_2 fixation by diazotrophic plankton, and a sink through bacterial denitrification when oxygen is depleted. These processes are subject to external climate-related forces that push the N budget out of balance, but also coupled through internal feedbacks that strive to restore a balance and stabilize the N reservoir. The feedback mechanism can be thought to operate like a

"nutrient thermostat", in which the nitrogen-to-phosphorous (N:P) requirement of phytoplankton represents a setpoint towards which the ratio of N and P reservoirs is restored. This dissertation comprises four projects that address different aspects of the general question: *how flexible is the oceanic N reservoir?*

Chapters 2 and 3 examine the flexibility of the setpoint towards which the N reservoir is restored. In Chapter 2, a diagnostic model is used to show that the N:P of nutrient drawdown by marine phytoplankton, long considered to have a universal "Redfield ratio" of 16:1, varies significantly at the scale of marine biomes due to stoichiometric diversity between taxa. Thus the mean N:P of marine phytoplankton, previously thought of as a fundamental biological property, only reflects the balance of high and low N:P biomes under modern-ocean conditions. Chapter 3 explores the role of this variability in the nutrient thermostat feedbacks. An ecosystem model is used to show that the ratio of nutrient reservoirs it is biased upwards towards the high N:P requirements of subtropical phytoplankton that cohabit and compete directly with N_2-fixers. This resolves a discrepancy between the observed N reservoir and the predictions of "Redfieldian" models, which lose too much N before reaching equilibrium. We also demonstrate an important role in the nutrient thermostat for ocean circulation, which communicates stoichiometric signatures between biomes. Changes in the N reservoir may thus be driven, over millennial timescales, by a restructuring of plankton biomes and the circulation pathways that connect them.

Chapters 4 and 5 examine the potential for variations in the N reservoir via direct forcing of the oceanic N budget. Chapter 4 focuses on the process of N_2-fixation, which

may be limited either by an external supply of Fe through the atmosphere, or the internal generation of N deficits that allow diazotrophs to compete with faster-growing plankton, which are susceptible to N-limitation. Multiple geochemical constraints are used to show that N_2-fixation in the modern ocean is limited by Fe inputs at the community scale, but strongly coupled to N loss through denitrification at the basin scale. These results reconcile biochemical evidence for Fe-stress in diazotroph communities with the existence of regulatory feedbacks that maintain a balanced the N budget. Within the regime of intermediate Fe-control, the oceanic N reservoir would respond weakly to the enhanced dust fluxes hypothesized for a glacial climate, but strongly to the reduced fluxes expected under climate warming.

Chapter 5 uses a biogeochemical model to derive a simple framework for understanding the strength of N cycle feedbacks. A feedback response to any N-budget forcing comprises two components: a fast initial adjustment period involving only the upper ocean, in which changes in the N reservoir are minor, and a slow millennial response involving deep ocean circulation. The magnitude of changes in the N reservoir depend on the fraction of forced anomalies that "leak" into the deep ocean, and the timescale over which those deep-ocean anomalies are removed. Feedbacks through N_2-fixation, rather than denitrification, are most efficient at preventing leakage and removing deep-ocean anomalies, and are strong enough to prevent major perturbation to the N reservoir, unless Fe shortages confine diazotrophs to small regions of the ocean.

The dissertation of Thomas Smith Weber is approved.

James McWilliams

Aradhna Tripati

Peggy Fong

Curtis Deutsch, Committee Chair

University of California, Los Angeles

2013

TABLE OF CONTENTS

LIST OF FIGURES

LIST OF TABLES

ACKNOWLEDGEMENTS

I acknowledge with gratitude the many people that have contributed, both directly and indirectly, to my work and education over the last five years.

First and foremost I would like to thank my Ph.D. supervisor, mentor and friend Professor Curtis Deutsch. He has invested a great deal of his time grounding me in the disciplines of oceanography and mathematical modeling, and helping me to develop the mindset of a research scientist. He taught me how to ask the right questions, and equipped me with the tools to seek their solutions. He allowed me the freedom to pursue my own interests, but provided the guidance to prevent me straying too far. Most of all, he always approaches science problems with excitement and enthusiasm, and inspires me to do the same. For all of these things I am extremely grateful.

I acknowledge and thank Professors Jim McWilliams, Aradhna Tripati and Peggy Fong for joining my Ph.D. committee and providing valuable feedback and constructive criticism of my work. I am also grateful to all the members of the Biogeochemistry Working Group at UCLA, with whom I have discussed my research and sought assistance innumerable times. In particular, Tim DeVries has taught me methods that proved indispensible in my dissertation work and Hartmut Frenzel has patiently helped me improve my programming skills, provided expert IT support, and helped correct my many computing errors. Junhong Liang has always shown a deep interest in my work, and has provided many useful suggestions and insights, which I greatly appreciate. The

group as a whole has been a pleasure to both work with and take breaks with, including our lively lunchtime discussions, and Friday pizza nights.

I must express my deep gratitude to the organizers of the C-MORE Summer Course in Microbial Oceanography at the University of Hawaii: Matt Church, Mike Rappe, Grieg Steward and Dave Karl. This course exposed me to many new facets of my discipline, bringing me closer to the diverse and beautiful microbes whose activity I attempt to simulate, albeit incompletely, in my models. It served to deepen my interests in marine ecology and microbiology and provided me the opportunity to participate in a research cruise – a rare treat for a computer modeler! Furthermore, the course introduced me to Andi, Bryn, Kerry, Sara and Thiska – excellent young scientists who have taught me so much by explaining their exciting research, and helped me present my own work to those less familiar with models. I look forward to future reunions and discussions.

My time in Los Angeles would have been all the duller without my officemates and good friends both inside and outside the department. Anton, Anu, Ian and Tom made sure that I took the time to step back from work once in a while, and helped me discover that there is more to this city than the part between Gayley and Hilgard. For all the Thanksgivings, Superbowls and Quiz Nights I thank you, and will miss you much.

A special thank you to my wonderful family, who have supported me not only during the last five years, but for my whole life. Mum and Dad taught me to work hard and enjoy learning, and have always encouraged me to follow my interests and passions, even when they took me so far away from home. I know it must have been hard. They have always been there when I needed them, to console, comfort or congratulate me, and

for that I cannot thank them enough. I am fortunate to have grown up with Sam and Charley, dedicated and loving siblings who share so many of my interests and beliefs, and are both doing work that I admire so much. They inspire me to do better.

I dedicate this work to the two strongest and kindest people I have known – Granny and Freddy. Fred was a fountain of knowledge, and had an answer to all of my questions, about life, the universe and everything; he inspired me to understand the world around me, and sparked my interest in science. Granny has the warmest heart, and the delight she takes in my accomplishments has always spurred me on. She was never far from my thoughts during the preparation of this dissertation.

Somehow the most important people end up at the bottom of acknowledgements, perhaps because they are the foundation upon which all else is built. For the last four years Elizabeth Evans Weber has been the cornerstone of my life, and both my work and wellbeing have benefited immeasurably. She motivates me, brings me peace, and most of all believes in me even when I do not. Our chance meeting in the Westwood Trader Joes still amazes me, and I am thankful for it above all else.

Introductory material in Chapter 1 and data compilation in Chapter 2 are adapted from an article published in the Annual Review of Marine Science. The full citation is: Deutsch, C. & Weber, T. Nutrient Ratios as a Tracer and Driver of Ocean Biogeochemistry. *Annual Review of Marine Science* **4**, 113-141 (2012). I thank the primary author Curtis Deutsch, and NASA for support through an Earth System Science fellowship.

The majority of Chapter 2 is adapted from a Research Article published in Nature. The full citation is: Weber, T.S. Deutsch, C. Ocean nutrient ratios governed by plankton biogeography. *Nature* **467**, 550-554 (2010). I thank my co-author Curtis Deutsch, and the UCLA Pauley Foundation for support.

Chapter 3 is adapted from a Letter published in Nature. The full citation is: Weber, T. and C. Deutsch, Oceanic nitrogen reservoir regulated by plankton diversity and ocean circulation. *Nature* **489**, 419 (2012). I thank my co-author Curtis Deutsch and NASA for support through an Earth System Science Fellowship.

Chapter 4 is adapted from a Report under review for publication in Science. The full citation is: Weber, T. and C. Deutsch, Local versus basin-scale limitation of marine N_2-fixation. *Submitted to Science* (2013). I thank my co-author Curtis Deutsch and NASA for support through an Earth System Science Fellowship.

VITA

Education

University of California, Los Angeles:

Atmospheric and Oceanic Sciences	M.Sc.,	2010

University of Leeds:

Earth Sciences	B.Sc., M.Sc.,	2008

Publications

Weber, T. S., C. Deutsch, Local vs. basin-scale limitation of marine nitrogen fixation, in review for *Science*

Durham, B.P., M. Rappe & the CMORE 2011 collective (includes T.S.W.) Genome sequence of marine alphaproteobacterial strain HIMB11, the first cultivated representative of a unique lineage within the Roseobacter clade possessing a remarkably small genome, in review for *Standards in Genomic Sciences*

Weber, T. S. and C. Deutsch (2012), Oceanic nitrogen reservoir regulated by plankton diversity and ocean circulation, *Nature,* in the press.

Deutsch, C. and T. Weber (2012), Nutrient ratios as a tracer and driver of ocean biogeochemistry, **4**, 113-141.

Weber, T. S. and C. Deutsch (2010). Ocean nutrient ratios governed by plankton biogeography, *Nature*, **467**, p550-554.

Service Activities

Reviewer of journal articles for: Nature, Environmental Monitoring and Assessment.

Fellowships and Awards

- Outstanding Student Presentation Award, V.M. Goldschmidt Conference 2012.
- Outstanding Student Presentation Award, Annual Meeting of the American Geophysical Union 2012.
- Mautner Award for graduate research, UCLA 2011.
- NASA Earth Systems Science Fellowship, 2011-2013.
- Pauley Graduate Fellowship for highly recruited incoming graduate students, UCLA 2008.
- Vardy Award for best undergraduate dissertation, University of Leeds 2008.

Positions of Responsibility

- Secretary, UCLA XEP Atmospheric and Oceanic Sciences Graduate Student Society, 2010-2011.
- Recruitment representative, UCLA XEP Atmospheric and Oceanic Sciences Graduate Student Society, 2010-2011.
- President, University of Leeds Earth Sciences Society, 2005-2006.

CHAPTER 1

Introduction: Dynamics of the oceanic N reservoir

Nitrogen (N) is one of the fundamental building blocks of life. It is an essential component of all protein-forming amino acids and the bases that comprise nucleic acids. Although N is an abundant element in the ocean, the vast majority (>90%) occurs as dissolved dinitrogen (N_2) gas that is not readily available to autotrophic organisms (Galloway et al 2004, Zehr & Kudela 2011). Instead, phytoplankton at the base of the marine food web rely on "fixed" forms of nitrogen such as ammonia (NH_3), nitrite (NO_2^-) and nitrate (NO_3^-), which are scarce relative to the requirements of those organisms (Zehr & Ward 2002). When nutrient-laden deep waters upwell to the sunlit surface, where conditions are conducive to photosynthesis, NO_3^- (the dominant form of fixed N) is rapidly consumed by the microscopic plants and usually becomes depleted before any other nutrient.

Throughout vast expanses of the low latitude ocean, NO_3^- scarcity limits primary production and the rain of organic matter from the surface to the deep ocean – a process responsible for sequestering carbon in deep waters, where it cannot exchange with the atmosphere (Codispoti 1989). The strength of this "biological carbon pump" is thus closely tied to the quantity of fixed N available in deep ocean waters, i.e. the magnitude of the oceanic N reservoir. Through its influence on ocean productivity and the air-sea

partition of CO_2, changes in the N reservoir have been hypothesized to a drive long-term global climate change, including a potential role in the Pleistocene Glacial-Interglacial cycles (Broecker & Henderson 1998, Falkowski 1997).

This chapter reviews the dynamics of the oceanic N reservoir, beginning with the dominant sources and sinks of the N budget and their environmental sensitivities. A picture emerges of an N reservoir that is buffered by internal regulatory feedbacks, but also subject to external climate forcing, and ultimately regulated by the very phytoplankton whose growth it sustains.

1.1 The ocean's N budget

In contrast to the other bio-limiting elements like phosphorous (P), biological rather than geological processes dominate the oceanic N budget (Fig. 1.1). To first order, the P budget reflects a balance between river inputs and organic matter burial in sediments – slow, geological processes that are small relative to the size of the P reservoir (predominantly PO_4^{3-}). Consequently, P has an oceanic residence time (equilibration timescale) on the order of 50,000 years, and is likely subject to change only on geological timescales of hundreds of thousands or millions of years (Benitez-Nelson 2000). In contrast, N exchanges with the atmospheric reservoir, through fast biological processes that are much larger relative to its reservoir.

Early in the evolutionary history of marine plankton, specialized diazotrophic clades developed the ability to tap into the inexhaustible pool of gaseous N_2, by

converting it into bioavailable ammonia (Karl et al 2002). The process, known as biological N_2 fixation, employs the enzyme nitrogenase and chemical energy to overcome the large energetic barrier required to break the strong dinitrogen triple bond (Zehr & Kudela 2011). Although relatively few taxa invest in the strategy of N_2-fixation, all marine phytoplankton benefit from the activity of diazotrophs, which provide newly fixed N to the broader community when their organic matter is remineralized upon mortality (Redfield 1958). This constitutes the largest single source of fixed N (Gruber 2004), and maintains the productivity of ocean by counteracting the continual removal of N in deeper waters.

Removal of fixed N is closely related to the activity of heterotrophic microbes in subsurface environments (Fig. 1.1), which respire the sinking organic matter that rains through the water column and onto the seafloor sediments. Molecular oxygen (O_2) is preferentially used as the electron acceptor (oxidizing agent) during respiration, as aerobic respiration provides the highest energetic yield per mole of organic matter consumed (Lam & Kuypers 2011). While the majority of oceanic waters are well oxygenated, a combination of global circulation and local dynamics conspire to create regions of O_2 depletion. After subducting from the surface ocean, where O_2 re-equilibrates with the atmosphere, watermasses are subject to a steady removal of O_2 by bacterial respiration. The ocean's oldest waters (measured as time since exposure), which are found at the far end of the deep "conveyor-belt" circulation in the North Pacific and Indian Oceans, therefore have the lowest oxygen content. In the wind-driven upwelling systems along the west coast of America and the Arabian Peninsula, high rates of primary

production result in an elevated oxygen demand in underlying thermocline waters, where O_2 is already in short supply. Consequently, three zones of permanent suboxia ($[O_2]<5\mu M$) are located in the Eastern Tropical North and South Pacific (ETNP, ETSP) and the Arabian Sea (AS) (Keeling et al 2010).

Under these suboxic conditions, bacteria use NO_3^- to replace O_2 as the terminal electron acceptor in respiration – a process termed denitrification that yields only slightly less energy than aerobic respiration. The net result is to reduce NO_3^- (through NO_2^- and NO interims) to gaseous N_2 that enters the dissolved pool (Gruber & Sarmiento 1997). Note, the term "denitrification" will be used here to blanket both canonical denitrification and the newly recognized process of anaerobic ammonium oxidation, which have a similar net effect on fixed N and similar environmental sensitivities (Kuypers et al 2003). Through direct rate measurements and geochemical surveys, ETNP, ETSP and AS have all been identified as sites of active water-column denitrification.

Although suboxia is a rare condition in the water column, it occurs much more readily in marine sediments, where oxygen is rapidly consumed by respiration and its influx constrained by diffusion across the sediment-water interface. Again denitrification takes over in the absence of O_2, reducing NO_3^- that also diffuses into the sediments from overlying waters (Middelburg 1989). This process of benthic denitrification is though to remove 1.5 to 4-fold more N than the water-column process, and is more evenly distributed across latitude and between ocean basins. It concentrates along shallow continental margins where fluxes of organic matter to the seafloor are largest.

Over the last few decades, much effort has been made to quantify these sources and sinks and assess the status of the ocean's N budget. Some have argued for a balanced budget in which N_2-fixation inputs closely match denitrification losses (Gruber 2004), while others propose a budget is in severe deficit, with denitrification rates up to double those of N_2-fixation (Codispoti 1995, Codispoti et al 2001). The most recent constraints (DeVries et al 2012a, Großkopf et al 2012) suggest that both processes have annual rates on the order of 200TgN/yr, which given the oceanic reservoir of $6x10^5$TgN indicates an oceanic residence time on the order of just a few millennia.

This dissertation will not focus not on constraining the magnitudes of N fluxes, but rather on understanding the mechanisms that couple or decouple the sources and sinks, controlling of the dynamics of the oceanic N reservoir.

1.2 Internal regulatory feedbacks

The short residence time of oceanic N and possible imbalance of its sources and sinks creates the potential for large swings in the N reservoir and productivity of the ocean over millennial timescales. However, evidence for relatively constant marine productivity over the entire Holocene period (Gruber 2004) indicates that mechanisms exists to prevent sustained imbalances, effectively coupling N_2-fixation and denitrification over some timescale. Because the two processes occur in different regions of the ocean under different environmental conditions, this cannot be achieved by a direct biological

coupling within individual organisms or microbial communities. Instead, the coupling arises from the sensitivity of each process to the magnitude of the N reservoir itself.

Rates of denitrification are linked to N availability through two related mechanisms. First, global export production determines the degree of O_2 consumption in subsurface waters, and controls the size of suboxic zones and diffusion of O_2 into sediments. Second, local export fluxes above the suboxic zones and above shallow sediments determine the oxidant demand that must be met by NO_3^- in these denitrification zones (Codispoti et al 2001). In turn, export fluxes are limited by the supply of NO_3^- to the surface to fuel primary production, thus an ocean with a larger N reservoir must support higher rates of denitrification (Fig. 1.2).

The dependence of N_2-fixation on the ocean N reservoir rests on competitive dynamics between diazotrophs and other, non-fixing phytoplankton. Because fixing N_2 is an energetically costly process, it is a poor strategy to pursue when fixed forms of N are available in the ambient seawater (Redfield et al 1963). Diazotrophs are thus selected for when NO_3^- is scarce, as in the stratified subtropical gyres, but outcompeted by faster growing non-fixers when NO_3^- is replete. A larger oceanic N reservoir selects against diazotrophy, and must be associated with smaller N inputs through N_2-fixation (Fig. 1.2).

Their sensitivity to fixed-N availability reveals the propensity for these source and sink processes to regulate the oceanic N reservoir within tight bounds. A surplus of N_2-fixation over denitrification will cause NO_3^- to accumulate in the ocean, both selecting against further N_2-fixation and stimulating extra productivity that expands suboxic zones and promotes denitrification in the water column and sediments. A combination of

reduced N_2-fixation and heightened denitrification then acts to restore a close balance between these processes, providing a stabilizing feedback on the oceanic N reservoir (Deutsch & Weber 2012). On the other hand, a surplus of denitrification above N_2-fixation will gradually deplete the NO_3^- pool, providing a competitive boost to diazotrophic plankton while stifling primary production and organic matter export. In this case, enhanced N_2-fixation and the slowdown of denitrification again force the N budget towards a balance and stabilize the reservoir.

The existence of negative feedbacks between N sources and sinks not only predicts a tendency towards a balanced N budget, but also predicts the magnitude of the oceanic N reservoir at which this balance can be attained. Even when NO_3^- is exhausted, and the growth of their competitors is strongly N-limited, diazotroph growth cannot proceed indefinitely as it soon become limited by PO_4^{3-} (Tyrrell 1999). Marine N_2-fixation rates are thus limited by the quantity of "excess" PO_4^{3-} available in upwelling deep water – the portion remaining once non-fixing phytoplankton have reached N-limitation (Deutsch et al 2007). By adding fixed N to the ocean, diazotrophs postpone the onset of N-limitation, allowing their competitors to consume a larger portion of the available PO_4^{3-} and eroding their own ecological niche. Once the deep-ocean ratio of $[NO_3^-]$:$[PO_4^{3-}]$ approaches the metabolic N:P requirements of non-fixing plankton, PO_4 becomes the limiting nutrient for the broader community and no excess will remain to fuel N_2-fixation. A balanced N budget can be maintained only when the excess of PO_4^{3-} is sufficient to excite just enough N_2-fixation to balance losses through denitrification (Redfield 1958, Tyrrell 1999).

Taken together, the ocean's N-cycle feedbacks operate like a *nutrient thermostat* that stabilizes the N reservoir by coupling it to the inertia of the P reservoi, leading to the geochemical paradigm that "N is a slave to P". The biomass N:P ratio of marine phytoplankton takes special significance in this feedback mechanism, providing the "setpoint" towards which the ratio of nutrient inventories is continually restored (Tyrrell 1999). Since Alfred Redfield documented the mean ratio of 16N:1P (the canonical "Redfield ratio"), much work has focused on understanding its variations at different levels of biological organization, and its biomolecular underpinning.

1.3 External forcing

Although N_2-fixation and denitrification must be coupled to some extent through their mutual dependence on the oceanic N reservoir, each process is influenced by other environmental factors that may force the N budget towards imbalance. Because water-column denitrification occurs under the condition of thermocline suboxia, its global rate hinges on the myriad climatic factors that control ocean oxygenation: the temperature of surface waters that equilibrate with the atmosphere; the speed of thermohaline circulation; and the strength of local wind-driven upwelling. Conventional wisdom predicts enhanced water-column denitrification during warmer climate regimes, when O_2 is less soluble and more intense stratification favors sluggish deep circulation and greater oxygen utilization in the ocean interior (Keeling et al 2010). Over shorter timescales,

however, the response to climate warming may be more complex than implied by this conceptual model (Deutsch, in prep).

Sediment denitrification is also sensitive to the oxygen content of bottom waters, but depends more strongly on the area of shallow continental margins that receive large sediment loads. Its global rate is likely subject to forcing by oceanic sea level, whereby lower sea levels associated with cooler climate regimes would expose large shelf regions and reduce the sediment denitrification sink (Christensen et al 1987).

The supply of Fe to the ocean through windblown dust has been hypothesized as an overriding control on marine N_2-fixation, owing to the high Fe requirement of diazotrophic plankton for building the nitrogenase enzyme (Falkowski 1997). It follows that the enhanced dust fluxes expected under cooler, drier climatic conditions should stimulate diazotroph growth and cause NO_3 to accumulate in the ocean. Warmer, damper climate regimes on the other hand, might be expected to suppress N_2-fixation through a weakening of Fe inputs (Lambert et al 2008, Mahowald et al 1999).

1.4 Ocean N reservoir and climate

The emerging view of the oceanic N reservoir is one of "dynamic homeostasis", in which N sources and sink may be driven apart by external forcings, but are restored towards one another by internal feedbacks. The potential for the oceanic N reservoir to drive global climate change, through its influence on deep-ocean carbon storage, depends on the relative strength of forced variations and stabilizing feedbacks, raising two questions.

First, how strongly do N_2-fixation and denitrification respond to their external stimuli? Isotopic records indicate the enhanced ventilation of thermocline waters during the Last Glacial Maximum resulted in significantly lower rates of water column denitrification (Altabet et al 1995, Ganeshram et al 2000). On shorter timescales, inter-decadal oscillations in suboxia have been hypothesized to drive twofold variations in the denitrification rates of the Eastern Tropical Pacific (Deutsch et al 2011). Second, over what timescales do negative feedbacks compensate these forcings? A large forced imbalance in the oceanic N budget may still be of little consequence to the N reservoir if damped out over just a few years. The timescale of ocean overturning has been posited as limitation on feedback speeds (Codispoti 2007) but a more complete understanding is still lacking.

The ocean N cycle gains greatest leverage over global climate in a scenario where N sources and sinks are so strongly influenced by external forcings that the regulatory feedbacks can be broken or bypassed altogether (Fig. 1.2). In this case, ocean oxygenation and enhanced and Fe inputs associated with climate cooling would favor a large surplus of N_2-fixation over denitrification, resulting in the accumulation of N that stimulates further productivity, carbon storage and cooling. Should these positive feedbacks dominate, small orbitally-forced variations in global temperature may be amplified by the N cycle into larger climatic cycles, providing a possible driving mechanism for the Pleistocene glaciations (Ganeshram et al 1995).

Irrespective of the relative strength of forcings and feedbacks, the N:P ratio of marine phytoplankton imposes a fundamental constraint on the N reservoir and ocean

fertility that is independent of N budget processes (Deutsch & Weber 2012). Although the understanding of phytoplankon stoichiometry at organism scale has improved dramatically since Redfield's observations, its flexibility at the community scale and ability to shift the setpoint of the nutrient thermostat is not known.

1.5 Scope of the dissertation

This dissertation will address a number of unanswered questions regarding the long-term regulation of the N reservoir. The first half of the dissertation will focus on the most poorly understood aspect of the ocean's nutrient thermostat – the biomass N:P ratio of marine phytoplankton. Specific questions to be addressed include:

- How constant are plankton N:P ratios over large scales in the ocean?
- Do variations in plankton N:P play a role in determining the "setpoint" of the nutrient thermostat, or is the global-mean N:P ratio the only important factor?

The remainder of the dissertation will address uncertainties regarding the response of N budget process to external forcing, and the strength of their coupling through internal feedbacks. The motivating questions include:

- Is N_2-fixation controlled more strongly by external Fe inputs, or internally generated N deficits? To what extent does the Fe supply limit stabilizing N-cycle feedbacks?

- Over what timescales do the stabilizing feedbacks operate? How do biological and physical factors determine these timescales, and what limitations do they place on N reservoir perturbations?

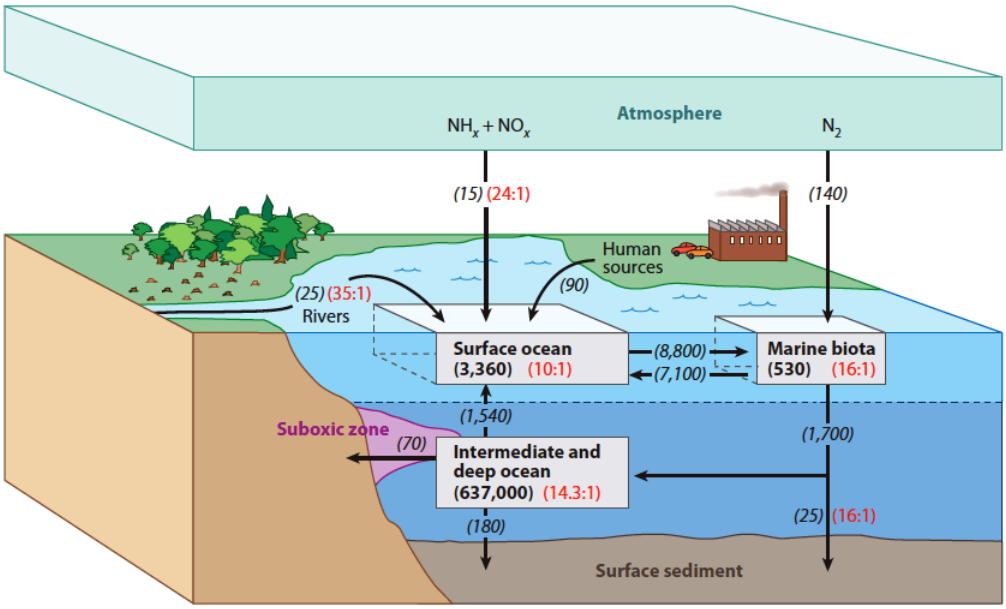

Figure 1.1 Schematic of the ocean nitrogen budget. The pre-anthropogenic budget is dominated by biological fluxes, comprising a source through N2-fixation, and sinks through sediment and benthic denitrification. These sources are relatively large compared to the deep-ocean N reservoir, yielding a residence time of just a few thousand years. N:P ratios of fluxes are shown in red, demonstrating that deep-ocean nutrient reservoirs are not held in the ratio supplied externally from rivers, and their ratio must be set by internal processes. From Deutsch & Weber, 2012.

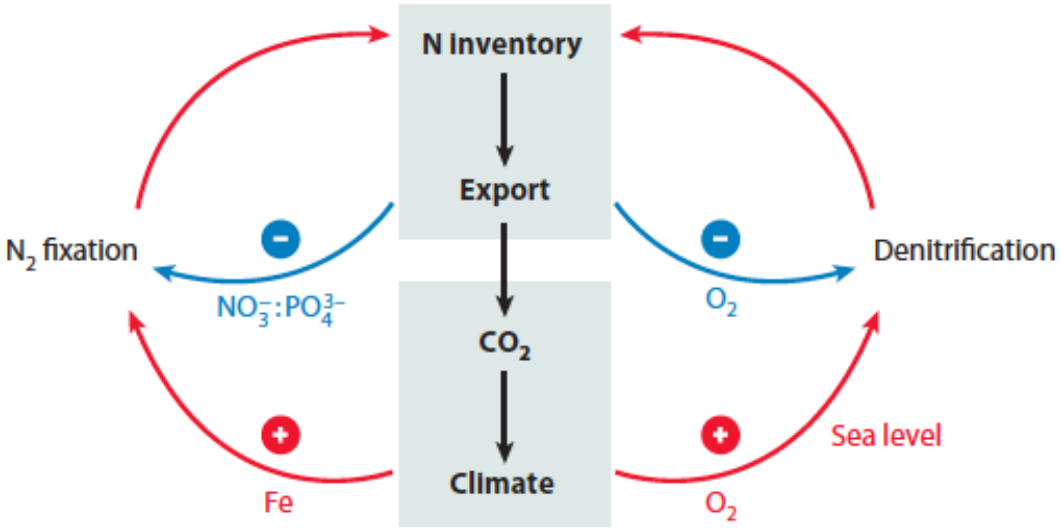

Figure 1.2 Feedbacks and forcings in the ocean N cycle. Each step in a feedback involves a direct proportionality (plus sign) or inverse proportionality (minus sign). Warmer climates leading to deoxygenation of the ocean and reduced Fe inputs, leading to greater denitrification and reduced N_2-fixation. Both factors force a reduction in the N oceanic N reservoir, weakening the biological pump and amplifying the initial forcing. However, these positive feedbacks may be bypassed by negative feedbacks in which sources and sinks respond to the N reservoir itself. Reduced productivity stifles denitrification, whereas N shortages select for N_2-fixing plankton, both counteracting the climate-forced changes. From Deutsch & Weber, 2012.

CHAPTER 2

Large-scale variations in nitrogen to phosphorous ratios of marine phytoplankton

Abstract

The major nutrients nitrate and phosphate exhibit one of the strongest correlations in the sea, with a slope similar to the average composition of plankton biomass (16N:1P). The processes through which this global relationship emerges despite the wide range of N:P ratios at the organism level are not known. Here we use an ocean circulation model and observed nutrient distributions to show that the N:P of biological nutrient removal varies across latitude in Southern Ocean surface waters from 12:1 in the polar ocean to 20:1 in the Subantarctic Zone. These variations are governed by regional differences in the species composition of the plankton community. The covariation of dissolved nitrate and phosphate is maintained by ocean circulation, which mixes the shallow subsurface nutrients between distinct biogeographic provinces. Climate-driven shifts in these marine biomes may alter the mean N:P ratio of marine phytoplankton, and in so doing shift the "setpoint" of the ocean's nutrient thermostat.

2.1 Introduction

The oceanic cycles of life's essential elements - nitrogen, phosphorus and carbon - are closely coupled through the metabolic requirements of phytoplankton, whose average proportions of 106C:16N:1P are known as the Redfield ratios (Falkowski 2000, Redfield 1958, Sterner & Elser 2002). The global distributions of dissolved nitrate (NO_3^-) and phosphate (PO_4^{3-}) are among the most highly correlated properties in the ocean, with a slope remarkably similar to the average N:P of plankton biomass (Fig. 2.1a). This has long been taken to imply that a relatively constant number of N atoms per atom of P are assimilated by phytoplankton throughout the surface ocean, and released by the respiration of organic matter at depth (the "geochemist's view)(Anderson & Sarmiento 1994, Takahashi et al 1985). The Redfield N:P ratio is therefore viewed as a critical global threshold between N-limitation and P-limitation of marine photosynthesis and the carbon it sequesters (Broecker 1982, Codispoti 1989). Over millennial timescales, the oceanic reservoirs of N and P are thought to be maintained near the Redfield ratio by diazotrophic species that add N to the ocean via biological N2 fixation when N is limiting, but are out-competed by other plankton when it is not (Tyrrell 1999). The Redfield ratio thus underpins the geochemical understanding of species competition and coexistence and the long-term regulation of ocean fertility and carbon storage.

At the cellular scale, different physiological processes drive an organism's requirement for N and P. The organic molecules used for resource acquisition, such as proteins and chlorophyll, require substantial N but little P, while the molecular machinery

of growth and reproduction, DNA and RNA, are rich in P but contain little N (Elser et al 2000). The partition of biomass among these different classes of organic molecules largely determines overall cellular stoichiometry (Geider & La Roche 2002), and reflects both the evolutionary history of plankton lineages (Falkowski 2000, Quigg et al 2003), and physiological adaptation of organisms to environmental conditions (Finkel et al 2006, Price 2005). As a result, the biomass N:P ratio of measured phytoplankton species varies by at least an order of magnitude around its mean value (Fig 2.1b, the "biologist's view"). The Redfield ratio of 16N:1P thus has no biological basis apart from being an approximate average across a wide range of species and environmental conditions (Falkowski 2000, Klausmeier et al 2004).

To reconcile the biological and geochemical perspectives on Redfield N:P ratios, some process is required to effectively average out the wide variations in N:P at the organism level ($N:P_{org}$) and maintain the covariation of NO_3^- and PO_4^{3-} observed in seawater. Two such mechanisms can be hypothesized. On one hand, the local balance of species and phenotypes and their seasonal succession may average deviations from Redfield stoichiometry over small spatial scales within the plankton ecosystem. This process, referred to here as "ecosystem averaging", would lead to the export of organic matter from the surface with a relatively uniform N:P ratio ($N:P_{exp}$) of ~16:1, consistent with the current paradigm. Alternatively, $N:P_{exp}$ may vary between marine biomes due to sustained regional differences in the physiological state or species composition of the plankton community. The tight correlation between NO_3^- and PO_4^{3-} could still be achieved however, if circulation and mixing in the ocean interior were to effectively

integrate the nutrients exported and remineralized from regions both above and below the Redfield ratio, a mechanism we refer to as circulation averaging.

2.2 Data compilation

These two hypotheses may be tested against the relative N and P content of organic particles filtered from suspension in surface waters, which reflect the composition of the marine ecosystem as a whole. Such measurements include both intracellular pools alongside non-living phytoplankton and zooplankton detritus, as well as a P adsorption onto particles (Fu et al 2005). Particle N:P observations from numerous sources in the published literature . A wide range of N:P ratios (5-33.5) are represented, around a mean value (16.11) very close to Redfield stoichiometry, but the sparse nature of this data precludes the identification of systematic spatial trends (Fig. 2.2 circles). A more fundamental limitation of this data set is that most points represent only a single observation or brief observational period. At the few stations where longer time series have been recorded (Fig. 2.2 squares), particle composition is found to vary widely over seasonal, interrannual and decadal time scales, so a single 'snapshot' is unlikely to be representative of mean conditions.

A more integrated view of N and P export fluxes and their ratio $N:P_{exp}$ can be obtained from the ratio between NO_3 and PO_4 removed from surface waters by the net effect of all ecosystem processes. Most studies have examined local nutrient removal based on time series data in high latitude regions with a strong seasonal cycle (Arrigo et

al 1999, De Baar et al 1997, Green & Sambrotto 2006a, Rubin et al 1998). Throughout the Antarctic Zone of the Southern Ocean (55-70°S), seasonal NO_3 and PO_4 drawdown yield a relatively consistent view of N:P stoichiometry significantly lower than 16:1 (Fig. 2.2, diamonds). Again however, the utility of these observations is limited by their spatial extent and the possibility that stoichiometric averaging within plankton communities occurs on timescales longer than the duration of these studies.

In the remainder of this chapter, we develop a method to assess to the time-mean N:P ratio of nutrient utilization by plankton communities, at the scale of an entire ocean basin.

2.3 Southern Ocean export ratios

The two averaging mechanisms outlined in section 2.1 can be distinguished based on their effects on the distributions of dissolved NO_3^- and PO_4^{3-} in the upper ocean. In the case of ecosystem averaging, the biological removal and subsequent remineralization of nutrients at the Redfield ratio would conserve the tracer N* ($[NO_3^-]$-16$[PO_4^{3-}]$) along the transport path of a water parcel(Gruber & Sarmiento 1997). The only sources of variation in N* would be addition of nitrate via N_2-fixation or atmospheric N deposition, and nitrate removal through anaerobic denitrification (Gruber & Sarmiento 1997). In the case of circulation averaging, regions of high N:P uptake at the surface would cause N* to decrease along flow lines, whereas regions with low uptake ratios would increase N*. To detect changes in N* that are caused by stoichiometric variability of plankton, rather

than sources or sinks of fixed N, we focus on the Southern Ocean poleward of 35°S. Here, N_2-fixation is virtually excluded by the abundance of dissolved NO3- and low iron concentrations(Karl & Michaels 2001), terrestrial N sources to the atmosphere are remote(Dentener et al 2006), and high O_2 concentrations inhibit denitrification (Codispoti & Christensen 1985). We also restrict our analysis to the open ocean north of 70°S, where over 100,000 measurements of NO_3^- and PO_4^{3-} concentrations are widely distributed throughout the water column (Garcia et al 2010).

In the Southern Ocean, physical and chemical properties are efficiently communicated between ocean basins by rapid circumpolar currents, and the largest hydrographic gradients are across latitude (Orsi et al 1995). There is no systematic zonal variation of N* in this region, but its zonal mean values show pronounced gradients along pathways of the large-scale meridional overturning circulation (Fig. 2.3a). In the Antarctic Zone, N* is higher at the surface than in the Circumpolar Deep Water upwelling from depth. As these high N* surface waters are driven northwards across the Antarctic Polar Front and Subantarctic Front by westerly winds, they become depleted in NO_3^- relative to PO_4^{3-}, reducing N* by ~2 $\mu molL^{-1}$ between 65°S and 40°S. The opposite gradient is observed below the surface: N* increases towards the north in the thermocline from which nutrients are entrained into the surface during winter mixing. Consequently, the vertical difference in N* between the surface and thermocline ($\Delta N^* = N^*_{0\text{-}75m} - N^*_{200\text{-}800m}$) reverses sign from positive in the Antarctic Zone to negative in the Subantarctic (Fig. 2.3b). This trend is independently observed in the Pacific, Atlantic and Indian sectors of the Southern Ocean, indicating that the zonal mean N* gradients are robust

The compatibility of these observations with the ecosystem and circulation averaging hypotheses can be tested using an ocean circulation and biogeochemical model to predict nutrient distributions and diagnose nutrient uptake under different conditions.

2.3.1 Southern Ocean model

The physical transport and biological cycling of nutrients was simulated in an ocean general circulation model (OGCM) using the transport matrix method (Khatiwala et al 2005), in which the physical transport through both advection and eddy diffusion are captured in the matrix **A**. This matrix can be extracted from the parent circulation model by probing it with a passive tracer, computing its transport between each grid cell over a short time interval. Our default simulations were conducted using a transport matrix that represents annual-mean flow from the ECCO ('Estimating the Currents and Climate of the Ocean') circulation model, with a horizontal resolution of 1° and 23 vertical layers (Khatiwala 2007). The model domain was divided into an interior solution region (I) in which tracer distributions were simulated, and a boundary region (B) in which nutrients are held at their observed concentrations (Garcia et al 2010). To facilitate this, the transport matrix is separated into a component ($\mathbf{A}_I$) that transports simulated nutrients within the interior, and a component ($\mathbf{A}_B$) that carries observed nutrients from the boundary into the interior. The conservation equations for nutrients ($C = NO_3^-$ or PO_4^{3-}) and their dissolved organic counterparts (C_{org} = dissolved organic N or P) are:

$$\partial C_I / \partial t = \mathbf{A}_I C_I + \mathbf{A}_B C_B - J_{ex} + J_{rem} - J_{org} + k_{org} C_{org,I} \quad (1)$$

$$\partial C_{org,I} / \partial t = \mathbf{A}_I C_I + \mathbf{A}_B C_{org,B} + J_{org} - k_{org} C_{org,I} \quad (2)$$

Here, the *I* and *B* subscripts denote concentrations in interior and boundary regions. The *J* terms represent net biological nutrient removal (J_{ex}) from the surface euphotic zone (top 75m, 5 layers), remineralization in the subsurface (J_{rem}), and production of dissolved organic nutrients (J_{org}). C_{org} degrades by first order decay at rate k_{org}, and the remineralization of particulate organic matter is parameterized by assuming the sinking flux (J_{POM}) of nutrient *C* decreases with depth below z_{comp} following:

$$J_{POM,C}(z) = J_{ex} . (z / z_{comp})^b \quad (3)$$

where J_{ex} is the sinking flux of *C* at z_{comp}, and the parameter *b* controls the shape of the remineralization profile (Martin et al 1987). The production of dissolved organic matter (J_{org}) is simulated by assuming that equal fractions of total production are partitioned into DOM and sinking particles ($J_{org} = J_{ex}$), although our results are insensitive to this formulation. Parameters used in the initial set of simulations are given in Table 2.1 below, and are subject to sensitivity testing (Appendix 2A, below). In each simulatiuon, equations 1 and 2 were integrated to a steady state, in which biological uptake balances the transport convergence of nutrients into the surface ocean.

2.3.2 Redfield prediction

To test the ecosystem averaging hypothesis, we used this model to predict nutrient distributions throughout the Southern Ocean water column under the assumption that uptake and remineralization occur universally at the Redfield N:P ratio. In this simulation the boundary was set at 35°S, and NO_3^- and PO_4^{3-} were held at climatological concentrations to the North. Biological export of PO_4^{3-} was diagnosed by damping surface concentrations towards their observed values over timescale τ_{damp}:

$$J_{ex}(C_I) = \max\left(\frac{C_I - C_{I,obs}}{\tau_{damp}},\ 0\right) \quad (4)$$

and NO_3^- export and remineralization were computed assuming a constant ratio of 16N:1P.

Predicted export production rates were 10-100 mmolP/m^2/yr, with a peak at ~50°S latitude, in good agreement with other model and data-derived estimates (Schlitzer 2002). However, the predicted surface N* gradient increases northwards from -4 μmolL^{-1} in the Antarctic Zone to -2.5 μmolL^{-1} in the Subantarctic, and there is little variation in N* with depth (Fig. 2.4). This gradient reflects the isopycnal transport of N* values from the subtropical boundary into the Southern Ocean, but is inconsistent with the observations (Fig. 2.3a). The observed N* distribution contradicts the ecosystem

averaging hypothesis, and implies nutrient removal below the Redfield ratio polewards of ~55°S, and above the Redfield ratio to the north.

2.3.3 Diagnosed export ratios

To derive a quantitative picture of $N:P_{exp}$ consistent with all nutrient observations, we conducted a second simulation in which the export of NO_3^- and PO_4^{3-} were independently diagnosed throughout the Southern Ocean, using eq. 4 for both niutrients. In this simulation, the nutrient supply from below the surface layer was computed using observed nutrient concentrations in the subsurface, eliminating errors that might arise from uncertainty in the model's treatment of particle remineralization. This was achieved by incorporating the subsurface south of 35°S into the boundary region.

The basin-integrated export fluxes are 0.125 MmolP/yr and 2.05 MmolN/yr, yielding a basinwide export ratio of ~16.5N:1P, nearly identical to the Redfield ratio. However, large deviations from the Redfield ratio are revealed at the regional scale, with $N:P_{exp}<16$ throughout most of the polar ocean and $N:P_{exp}>16$ in the Subantarctic (Fig. 2.5a), as anticipated from N*. The zonal mean export ratio varies almost two-fold with latitude, increasing from 12.5±2 at 60°S to 20±1 at 40°S (Fig. 2.5b), consistent with the limited observations of nutrient drawdown ratios (Green & Sambrotto 2006b). Rigorous sensitivity testing (Appendix 2A, below) demonstrated that this meridional trend is not dependent on the choice of circulation model, biological parameterizations, depth of net nutrient uptake, and dissolved organic matter dynamics. It derives from the northward

increase in surface N* and its vertical gradient along shallow pathways of the meridional overturning circulation.

2.4 Sources of N:P variability

The latitudinal variation in $N:P_{exp}$ reflects the elemental composition of the plankton that assimilate nutrients and export them from the surface. Nutrient uptake ratios measured in algal monocultures are highly species-dependent (Quigg et al 2003), suggesting that species distributions could influence $N:P_{exp}$ over large scales in the ocean. The region from 35-70°S encompasses two distinct ecological biomes, the Antarctic Polar biome polewards of 55°S and the Westerly Winds biome to the north, each with characteristic plankton communities and trophic interactions (Longhurst 1995). Direct observations are too sparse to determine the community structure at the scales required here, but diatoms are consistently reported as a major component of Southern Ocean assemblages (Kopczynska et al 1986). Because diatoms are the only algal family to build silica-based frustules, so their fractional contribution to exported organic matter (ϕ_{diat}) can be diagnosed from the observed silicic acid distribution (Jin et al 2006). First, the sinking flux of biogenic Si was diagnosed by restoring surface silicic acid concentrations towards observed values from the World Ocean Atlas climatology (Garcia et al 2010) using eq. 2. The export of N by diatoms was then estimated assuming Fe-dependent Si:N of diatoms (Brzezinski et al 2002):

$$Si:N = \begin{Bmatrix} 5, & if\ [\mathrm{Fe}] < 0.2\mathrm{nM} \\ 1, & if\ [\mathrm{Fe}] > 0.2\mathrm{nM} \end{Bmatrix} \quad (5)$$

This was then used to determine the fraction of total N export that can be attributed to diatoms.

Consistent with direct observations (Kopczynska et al 1986), silica export fluxes show that diatoms account for over 80% of N-export throughout the Si-replete Antarctic Polar biome, and less than 20% in the Si-poor Westerly Winds biome (Fig. 2.5b). A strong negative correlation exists between the N:P of nutrient export and the fraction of that export attributed to diatoms ($N:P = 20.39 - 9.6\phi_{diat}$, $P<0.0001$), indicating that Southern Ocean communities comprise diatoms with a low N:P of ~10, and a remaining population with a high average N:P of ~20. This simple characterization of the plankton community structure accounts for 50% of the spatial variance in the N:P of nutrient drawdown, and 98% of the variance in its zonal-mean value.

We also considered a range of environmental properties that can influence phytoplankton N:P at the phenotypic level (Table 2.2). Observations and theoretical considerations suggest that cellular resources are selectively allocated to P-rich reproductive biomolecules during exponential growth (Klausmeier et al 2004, Sterner & Elser 2002), and to N-rich protein-pigment complexes during slow growth under light limitation (Finkel et al 2006). In diatom cultures biomass N:P varies as a function of Fe availability (Price 2005), whereas in picoplankton cultures it is moderately sensitive to temperature (Fu et al 2007). To assess the contribution of phenotypic factors to variations in the N:P of Southern Ocean plankton communities, we correlated spatial patterns of the

relevant environmental parameters against the diagnosed latitudinal trend in $N:P_{exp}$. Solar Radiation Dose data was used to characterize the annual average light intensity experienced by the community, and was taken from the ISCCP climatology (Zhang et al 2004). We used temperature data from World Ocean Atlas and a simulated Fe distribution from the NCAR Community Climate System Model (Moore et al 2004). Summertime growth rates were estimated from December-February temperature, nutrients and SRD using standard multiplicative functions (Sarmiento & Gruber 2006):

$$\mu = \mu_{\max} \exp(k(T - T_{\max})) \cdot \frac{I}{\sqrt{I^2 + K_I^2}} \cdot \min\left\{\frac{N}{N + K_N}, \frac{P}{P + K_P}, \frac{Fe}{Fe + K_{Fe}}\right\} \quad (6)$$

In each case, $N:P_{exp}$ was either weakly correlated with these drivers of phenotypic variability, or inconsistent with the direction or magnitude of its predicted effect (Table 2.2).

These findings indicate that large-scale variability in nutrient uptake ratios stem primarily from the relative abundance of species with distinct metabolic requirements. Similar species-driven deviations from the Redfield ratio have been observed at smaller scales in the Southern Ocean (Arrigo et al 1999, Green & Sambrotto 2006b). In the coastal waters of the Ross Sea, the local balance of low N:P diatoms and high N:P prymnesiophytes was found to maintain an export ratio of ~16N:1P over relatively small spatial scales (Arrigo et al 1999). In contrast, we find that the long-term biogeography of plankton communities produces regional deviations from Redfield uptake ratios across vast expanses of the open Southern Ocean.

2.5 Averaging mechanisms

The nutrient export ratios diagnosed for the Southern Ocean, in conjunction with a compilation of stoichiomnetric observations (Fig. 2.1, 2.2), illustrate the contribution of both ecosystem averaging and circulation averaging in reconciling the relative constancy of deep ocean nutrient ratios with the wide ranging N:P values among plankton species. As summarized in Fig. 2.6, N:P ratios vary widely between phytoplankton, with taxonomic variations appearing dominant. Because plankton assemblages contain numerous species, part of the organism-scale variability is averaged out locally within the ecosystem, and is not reflected in aggregate particle ratios or net nutrient fluxes from the surface (Fig. 2.6). However, each assemblage does not contain the same balance of species: plankton biogeography is organized by physical properties of the ocean into biomes (Longhurst 1995) with distinct species composition and elemental stoichiometry. A large degree of N:P variability therefore persists at the biome scale.

In the presence of large spatial variations in $N:P_{exp}$, physical mixing is needed to enforce the observed covariation between NO_3^- and PO_4^{3-}. To test this circulation averaging mechanism, we conduct a third simulation in which $N:P_{exp}$ is diagnosed from surface nutrients (as in the second simulation), and organic particles transmit the signature of variable plankton stoichiometry into the subsurface, where they remineralize. This was facilitated by re-extending the model's interior region to include the subsurface of the Southern Ocean, in which the remineralization of N and P were simulated independently based on their export fluxes following eq. 3.

Subsurface nutrient concentrations (C) can be considered the sum of the accumulated product of remineralization within the Southern Ocean (C_{rem}), and a "preformed" component that is transported either from outside the Southern Ocean, or from surface waters as unutilized nutrient:

$$C = C_{pref} + C_{rem} \quad (7)$$

At steady state, the preformed component can be isolated using the transport matrix by incorporating the Southern Ocean surface into the boundary region, and solving the conservation equation for C_I in the absence of biological fluxes. Using the transport matrix method, this be achieved through direct matrix inversion:

$$C_I = \mathbf{A_I^{-1}}(-\mathbf{A_B}C_B) \quad (8)$$

Eq. 7 can then be solved for the remineralized components of subsurface NO_3^- and PO_4^{3-} ($[NO_3^-]_{rem}$ and $[PO_4^{3-}]_{rem}$).

Directly beneath the zone of net community production, $[NO_3^-]_{rem}$:$[PO_4^{3-}]_{rem}$ increases northwards from ~12.5 in the Antarctic Zone to ~21 in the Subantarctic, reflecting the full range of latitudinal variability in $N:P_{exp}$ (Fig. 2.7). However, within 100m of the compensation depth mixing has reduced this variability by >50%, and below 500m horizontal differences in $[NO_3^-]_{rem}$:$[PO_4^{3-}]_{rem}$ are negligible. The mixing of remineralized nutrients is sufficient to maintain the strong correlation (R^2=0.99) of NO_3^- and PO_4^{3-} in the subsurface, with a slope of 15.6N:1P that is indistinguishable from the observed slope. Mixing is not strong enough, however, to entirely homogenize the remineralized nutrient ratios, and the small variations that remain bring the thermocline N* distribution into better agreement with the observations than in the Redfield

prediction. While the ecosystem averaging hypothesis alone cannot account for N* gradients in the surface of the Southern Ocean, circulation averaging is consistent with both surface and subsurface observations. The canonical covariation of NO_3^- and PO_4^{3-} in the deep ocean is thus maintained not by a uniform N:P of nutrient assimilation and remineralization, but by physical mixing across biogeographic provinces that are stoichiometrically distinct.

2.6 Implications

Deviations from the Redfield N:P ratio at the scale of ocean biomes has broad implications for the understanding of nutrient limitation and the marine carbon cycle. The relationship between diatom production and community N:P in the Southern Ocean is likely to exist throughout the surface ocean, although its detection from observations is confounded by exogenous inputs of fixed N and possibly a wider range of physiological acclimations at the global scale. A recent exhaustive compilation of published and unpublished particulate organic matter observations has revealed global stoichiometric variations driven by plankton community structure that are in line with those reported here for the Southern Ocean (Martiny et al 2013). In oligotrophic regions of the low latitude ocean where Si is scarce, this relationship implies a nutrient drawdown of ~20:1, consistent with the observed stoichiometry of sinking organic matter in the North Pacific. This suggests that plankton communities of the subtropical ocean gyres may be more strongly N-limited than previously recognized. The high metabolic N:P requirements in

these biomes would expand the environmental selection for N_2 fixation by diazotrophs, which is in turn essential to sustaining the high N demand of the non-diazotrophic community. In this sense, the relationship between diazotrophs and other plankton may be more mutualistic than competitive. This helps resolve a previously noted paradox in the North Atlantic, where diazotrophs create a basin-scale excess of NO_3^- relative to a Redfield PO_4^{3-} quota, but do not erase their ecological niche (Wu et al 2000).

The stoichiometry of macronutrients also influences the amount of carbon sequestered in the deep ocean (Broecker 1982). Because the cellular C:P ratios of plankton vary most strongly with N:P (Geider & La Roche 2002), the carbon export and air-sea CO_2 fluxes associated with a given degree of PO_4^{3-} drawdown depend on the balance of biomes with distinct N:P requirements. Recent evidence for reduced upwelling and opal production during the Last Glacial Maximum (Anderson et al 2009) suggests that diatoms were less prevalent in the glacial Southern Ocean. This would have increased the N:P of nutrient removal, reconciling the apparent increase in NO_3^- utilization while PO_4^{3-} concentrations remained constant (Elderfield & Rickaby 2000). According to a simple 3-box model of the oceanic carbon cycle (Sarmiento & Toggweiler 1984), a 25% increase in high latitude C:P ratios reflecting an increase in N:P from 16 to 20, would reduce atmospheric pCO_2 by ~15ppm from interglacial levels.

2.7 Summary and outlook

This study has demonstrated that variations in plankton N:P ratios, which have which have been widely reported at the organism scale, manifest all the way up to the scale of ocean biomes. In the Southern Ocean, the dominant driver of large-scale stoichiometric variations is the partition of the plankton community between low N:P diatoms, and a residual community with high N:P ratios. The canonical correlation between deep-ocean NO_3^- and PO_4^{3-}, which has long been used to argue for a universal stoichiometry in plankton communities, can be maintained by ocean circulation even when organic matter with highly variable N:P content remineralizes in deep water.

Returning to the broader theme of this dissertation, the prospect of an ocean with large-scale structure in N:P requirements poses important questions concerning the regulation of the oceanic N reservoir. How does the N homeostasis imagined by Redfield operate in an ocean in which diazotrophs compete not with the "average" plankton, but only with subtropical species that likely have elevated N:P requirements relative to the global mean? This may also give rise to a role for ocean circulation in the thermostat mechanism, by communicating the N:P requirements of remote plankton communities to diazotrophs through the supply of residual high latitude nutrients into the subtropics. These hypotheses are laid out more explicitly in Deutsch & Weber (2012) their analysis becomes the focus of the following chapter in this dissertation.

If the Redfield ratio of 16N:1P merely reflects the current balance of stoichiometrically distinct biomes, might climate-driven changes in the marine environment upset that balance and shift the "set-point" of the ocean's nutrient thermostat? Currently, no theoretical framework exists to answer this question. A

necessary first step would be to develop a deeper understanding of the biological basis for N:P variability over large scales in the modern ocean, which gives rise to three further questions:

- What is the quantitative relationship between N:P stoichiometry and cellular allocation among different classes of biomolecule?
- How does that allocation strategy control the ecological traits of a species, such as its maximum growth rate and susceptibility to nutrient limitation?
- How do features of the physical ocean, such as circulation patterns and seasonality select among plankton that differ in those traits?

The first of these questions has been answered over the last two decades by careful biochemical and physiological measurements. Recently, new insights into the third question emerged from models of self-assembling plankton communities in which physical and chemical properties of the ocean select among a wide array of viable "species". Our ability to incorporate elemental stoichiometry into such models is currently limited by unanswered aspects of the second question - quantitative relationships linking cellular allocation strategies to biological rates and sensitivities have yet to be established. Nevertheless, cursory attempts to model the emergence of stoichiometric diversity from environmental selection have produced large-scale patterns in the N:P that are broadly consistent with the results presented in this chapter (Daines, pers. Comm.).

Appendix 2A: Sensitivity testing

We tested our central result, the spatial distribution of export ratios in the Southern Ocean, against a number of methodological uncertainties. We repeated the diagnosis of nutrient export numerous times, varying the factors that could influence the diagnosed pattern of $N:P_{exp}$. The range of zonal mean values of $N:P_{exp}$ was taken as a measure of uncertainty. Factors tested were:

- **Compensation depth**. Nutrient export is diagnosed by damping nutrient concentrations towards their observed values above the compensation depth (z_{comp}). In the original diagnosis, z_{comp} was set at 75m, in agreement with the estimated global-mean value. In the sensitivity testing we used the largest range of reasonable depths afforded by the model resolution: 30, 50, 75 and 100m. Nutrient export fluxes differed in each simulation, but the best agreement with other published modeled and data-derived estimates was obtained in the original simulation using z_{comp} of 75m. The spatial pattern of $N:P_{exp}$ also varied in each simulation (Fig. 2.8) particularly in the Antarctic Zone, where the high N* signal is confined to the shallow surface. However, the meridional transition from low $N:P_{exp}$ in the Antarctic Zone to high $N:P_{exp}$ in the Subantarctic is not sensitive to the choice of compensation depth.

- **DOM cycling parameters**. Dissolved organic N and P are advected with the flow until they are bacterially degraded into inorganic forms. This represents another nutrient supply process that could influence the export of NO_3^- and PO_4^{3-} diagnosed by the model. To determine whether this contributed to the diagnosed pattern of $N:P_{exp}$, we repeated our diagnosis without DOM cycling (all DOM fluxes set to zero in Eq. 1). We also tested the sensitivity of our results to the degradation timescales prescribed for DON and DOP by repeating the experiment with $\tau_{DON} = 2$ years and $\tau_{DOP} = 0.5$ years. The simulation with no DOM cycling yielded almost identical results to the original experiment (Fig. 2.9). Changing the degradation timescales resulted in slightly lower $N:P_{exp}$ throughout the Southern Ocean, particularly in the Antarctic region, as more N was advected out of the domain as DON (Fig. 2.9). However, the difference in the meridional trend was not large.

- **Damping timescale**. The timescale over which surface nutrient concentrations are damped towards their observed values controls the relative strength of biological fluxes, which produce the N* signal in the surface, and physical fluxes that mix across nutrient gradients and destroy the N* signal. A shorter timescale increases the relative strength of biological fluxes, whereas longer timescales allow a higher degree of mixing. We tested the robustness of our results against a wide range of damping timescales, between 2 weeks and 1 year. Although the magnitude of export fluxes was highly sensitive to these changes, the meridional gradient in

$N:P_{exp}$ was not. The original experiment, with a damping timescale of 2 months produced export fluxes most consistent with previous estimates.

- **Circulation model**. The largest source of possible error in our experiments is in the ability of the ocean circulation model to simulate real transport processes. These errors are also the most difficult to quantify, but a good test of our results robustness is to see whether a similar pattern of $N:P_{exp}$ emerges using a different circulation model. For this purpose we use a coarse resolution configuration of the MITgcm, with horizontal resolution of 2.8° and 15 vertical layers and no data assimilation. When we compare simulations with similar compensation depths (those closest to 50m and 100m) we find good agreement between the two models (Fig. 2.10). From the observed distribution of N* (Fig. 2.3) it is apparent that any circulation scheme that captures the broad pattern of Southern Ocean overturning will diagnose low $N:P_{exp}$ in the Antarctic ocean and high $N:P_{exp}$ in the Subantarctic.

Parameter	Units	Value
k_{org}	yr^{-1}	1
τ_{damp}	months	2
z_{comp}	meters	75
b	-	1.04

Table 2.1 Parameters used in default simulations.

			Expected relationship	
	Zonal (n=35)	1° x 1° (n=11408)	Direction	N:P range
Community composition[a]	-98	-50	Negative	10-31
Light (SRD)	62	19	Negative	7-41
Summertime growth rate[b]	86	39	Negative	8-45[c]
[Fe]	72	22	Positive	9-14
Temperature	89	38	Positive	20-25

[a] Characterized by % export by diatoms.
[b] Estimated from nutrients, light, iron, and temperature (see Supplementary Information).
[c] Range obtained by varying allocation to reproductive machinery in cellular model.

Table 2.2 Correlation of $N:P_{exp}$ with potential sources of variability. Zonal and 1°x1° values are correlation coefficients (R^2x100), with negative values indicating negative correlations. The expected direction and N:P range are obtained from culture/modeling studies that varied the property independently. The direction of the relationship is opposite to that expected for growth rate and light, while the magnitude is too large to be explained by Fe or temperature.

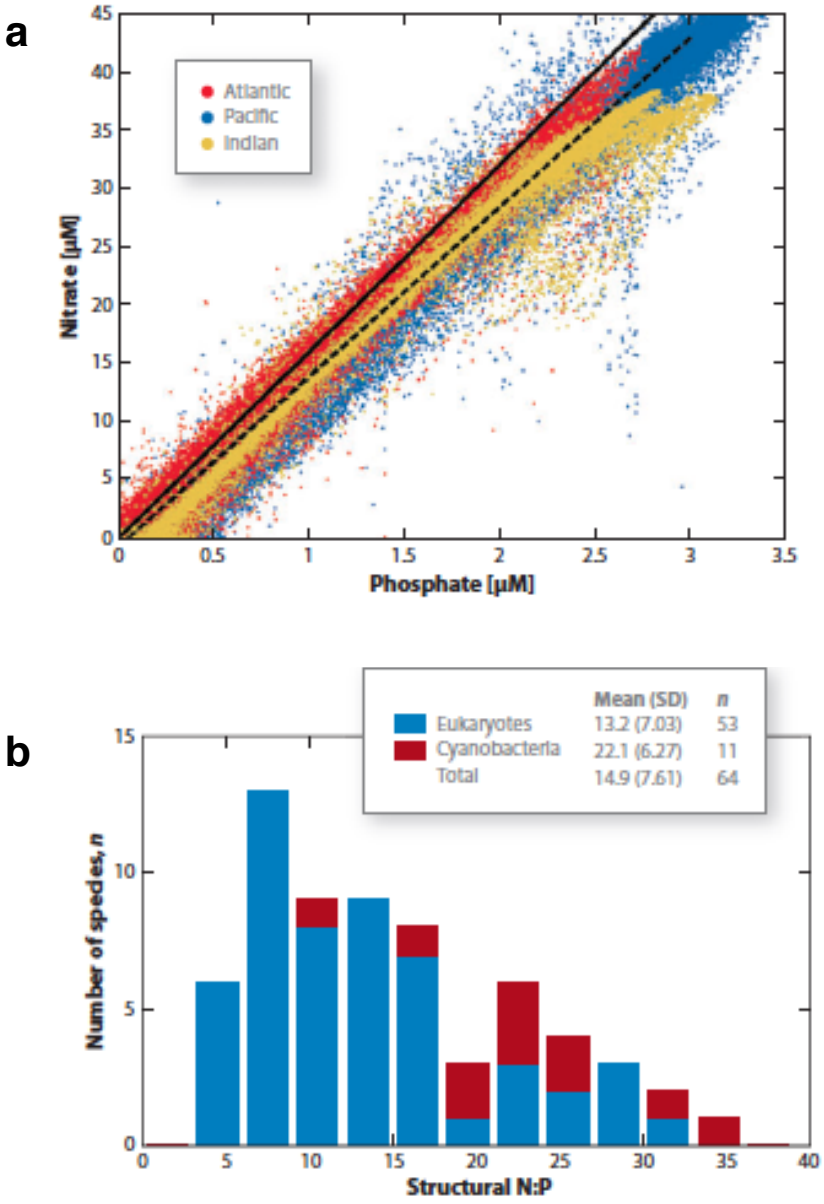

Figure 2.1 Geochemical and biological views of plankton N:P ratios. **a** the strong correlation between ocean NO_3 and PO_4 concentrations, with a slope of 16:1, suggests cycling at constant N:P ratios. **b** Phytoplankton species cultured in the laboratory exhibit a broad range of N:P ratios, from which 16:1 emerges as the average. From Deutsch & Weber, 2012

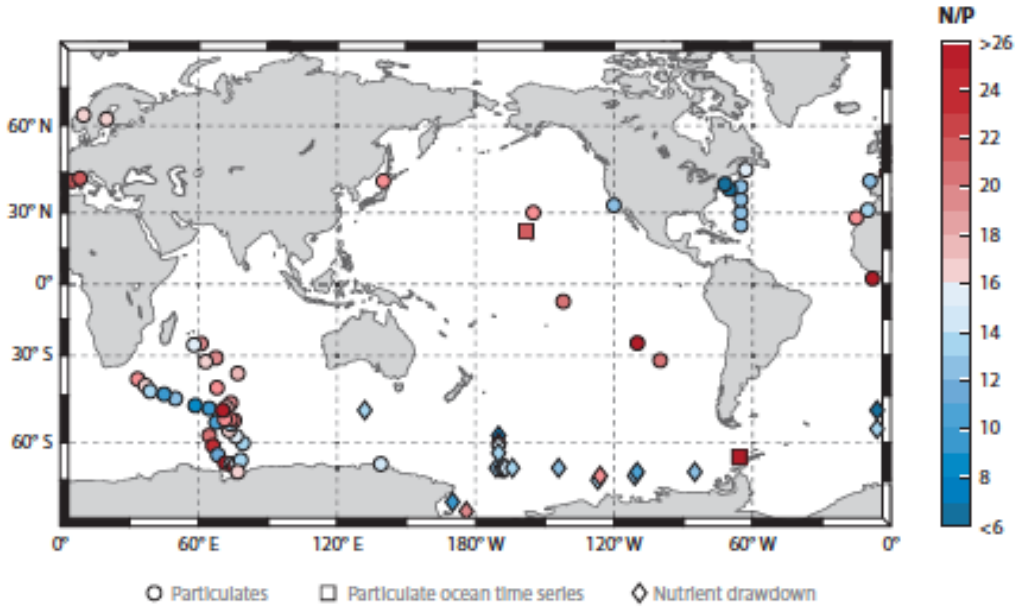

Figure 2.2 Global distribution of observed N:P stoichiometry in suspended organic particles from single observations (circles) and timeseries (squares – time mean), and in the drawdown ratios of inorganic nutrients NO_3 and PO_4. From Deutsch & Weber, 2012.

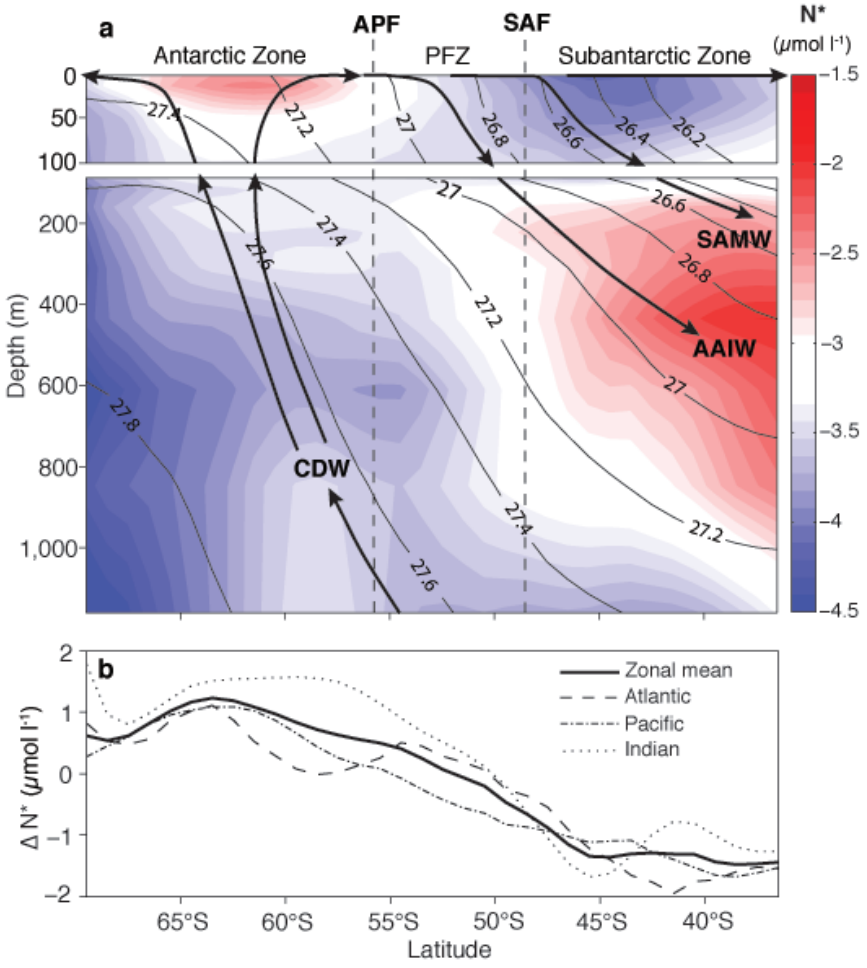

Figure 2.3 Observed N* distribution in the Southern Ocean. **a,** Zonal-mean section of N* (N*=[NO_3^-]-16*[PO_4^{3-}]), with potential density contours (thin lines) and schematic large-scale meridional overturning circulation patterns (arrows). Upwelling Circumpolar Deep Water (CDW) is driven across the Antarctic Polar Front (APF) and Subantarctic Front (SAF) by Ekman transport, and subsides in the Polar Frontal Zone (PFZ) to form Antarctic Intermediate Water (AAIW) and Subantarctic Mode Water (SAMW). **b,** Zonal-mean vertical difference in N* between the surface and thermocline ($\Delta N^* = [N^*_{0\text{-}75m}] - [N^*_{200\text{-}800m}]$), globally and in individual sectors of the Southern Ocean. From Weber & Deutsch, 2010.

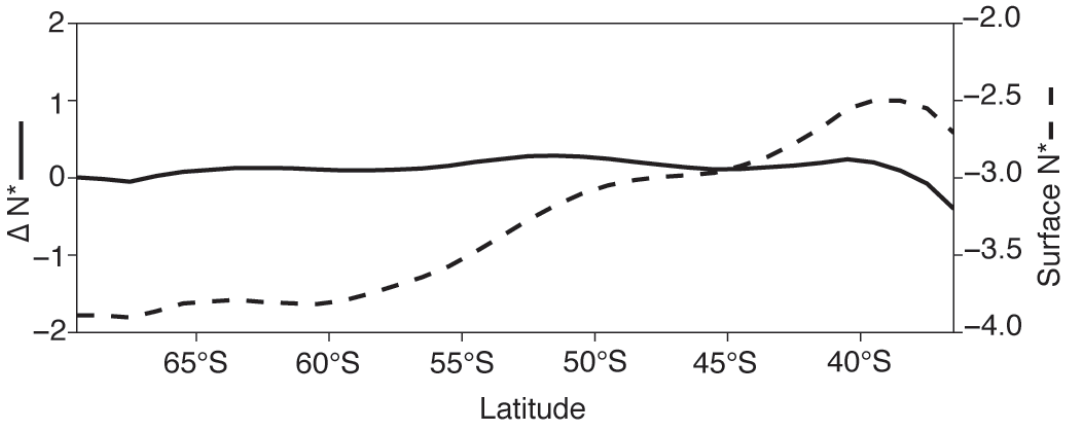

Figure 2.4 Redfield N* prediction. Southern Ocean surface N* gradient (broken line) and ΔN* (solid line) predicted in Model 1, assuming nutrient uptake and remineralization at the Redfield ratio. The northwards increase in surface N* and low ΔN* values are inconsistent with observations. From Weber & Deutsch, 2010.

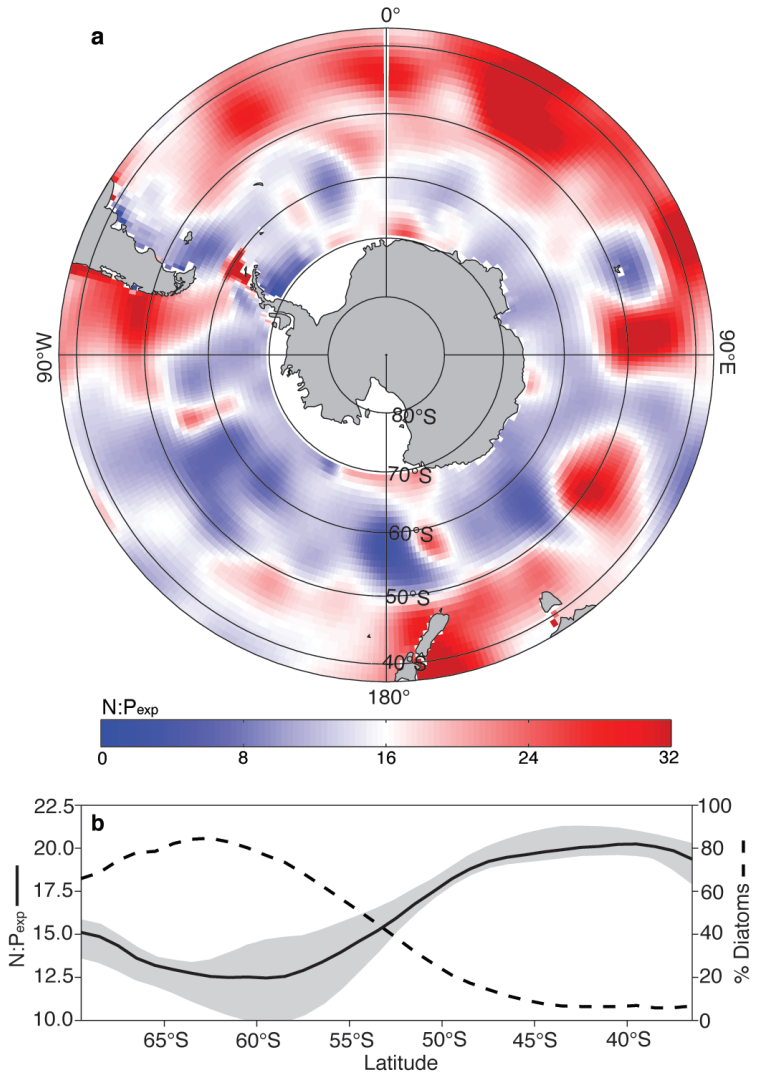

Figure 2.5 Diagnosed nutrient export ratios. **a,** Spatial pattern of $N:P_{exp}$, derived by diagnosing the export of NO_3^- and PO_4^{3-} independently. **b,** Zonal mean export ratio (solid line), and diagnosed contribution of diatoms to N export (broken line). The grey envelope is an estimate of errors associated with the choice of model compensation depth (50-100m), biological damping timescale (2 weeks-1 year) and DOM parameterization. From Weber & Deutsch, 2010.

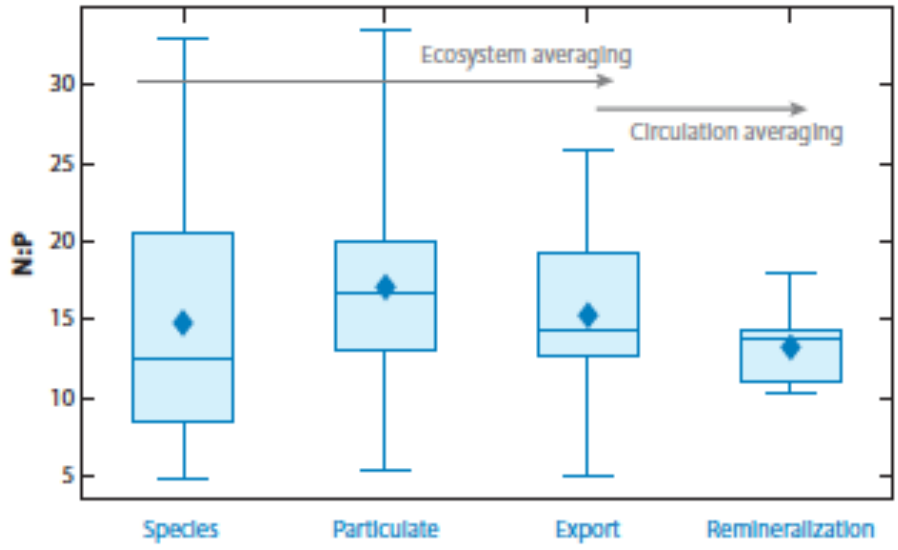

Figure 2.6 Summary of N:P averaging mechanisms. The reductiuon in variability between species, organic particles, and drawdown ratios represents the effects of ecosystem averaging. The further reduction in variability at the remineralization level represents the effects of circulation averaging, mixing remineralized nutrients to maintain a relatively constant stoichiometry at depth. From Deutsch & Weber, 2012.

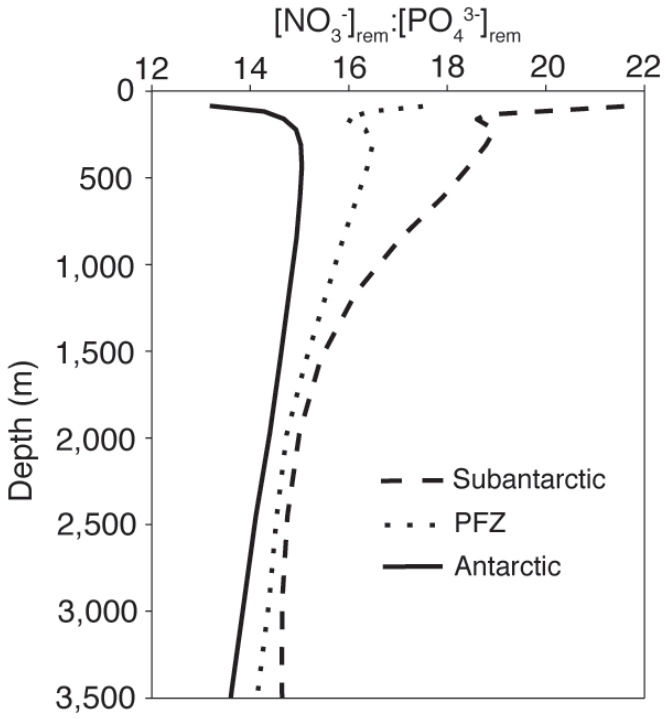

Figure 2.7 Circulation averaging of remineralized nutrients. Depth profiles of $[NO_3]_{rem}$:$[PO_4^{3-}]_{rem}$ predicted in the Antarctic, Polar Frontal and Subantarctic zone. The reduction in variability with depth results from the mixing of remineralized nutrients. From Weber & Deutsch, 2010.

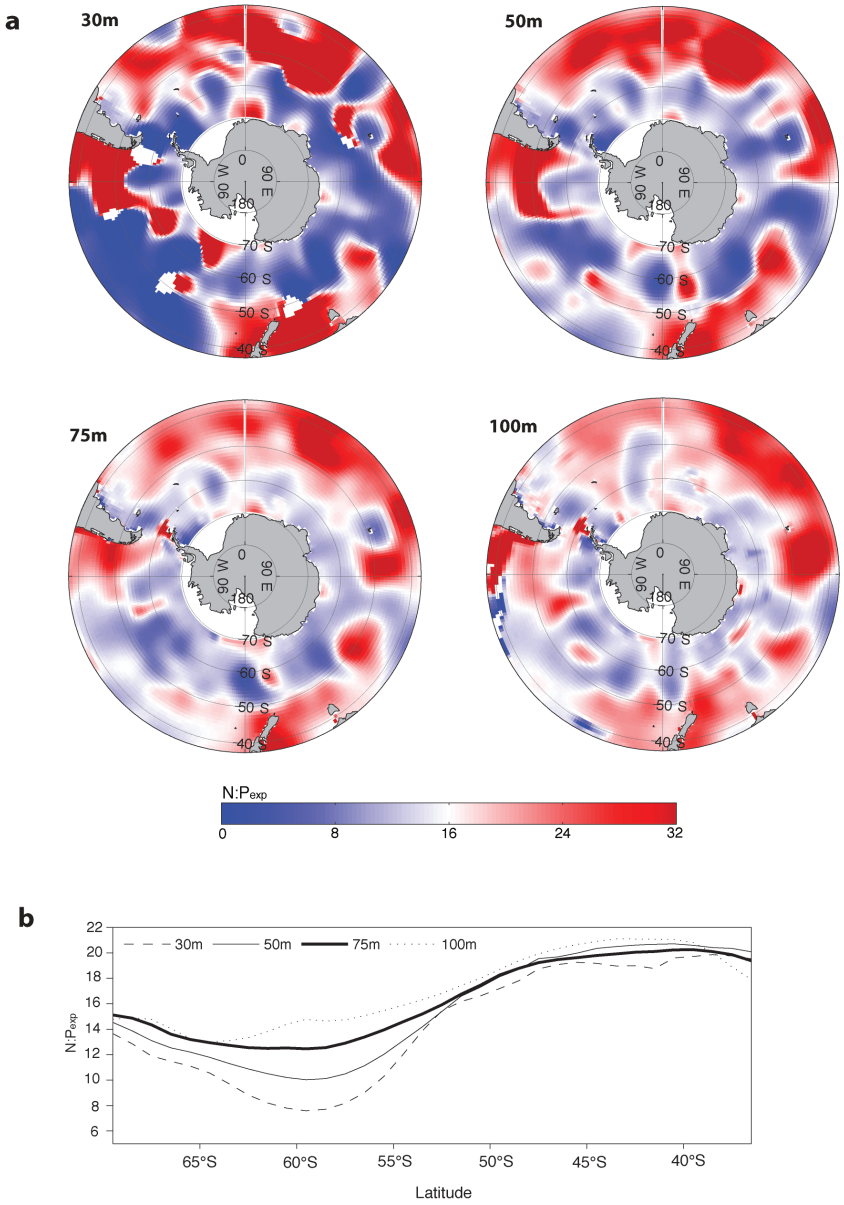

Figure 2.8 Sensitivity to compensation depth. Spatial pattern (**a**) and zonal mean trend (**b**) of $N{:}P_{exp}$ diagnosed by repeating our experiments with compensation depths of 30, 50 and 100m.

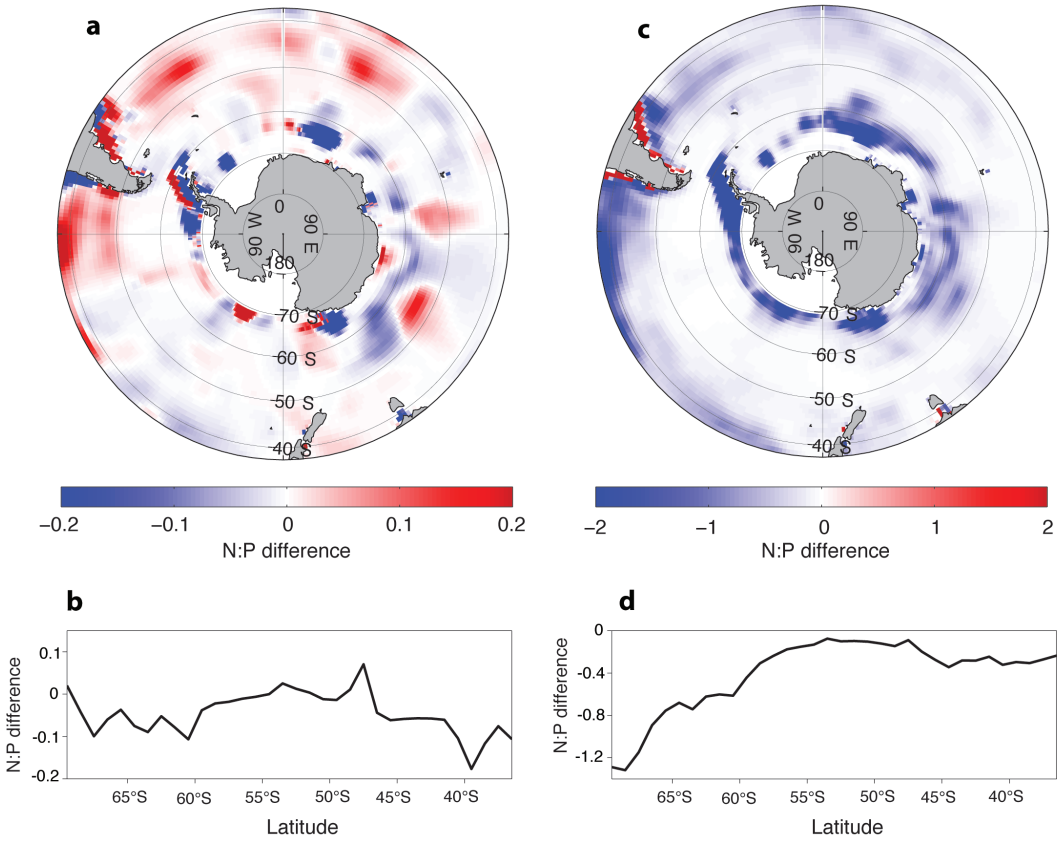

Figure 2.9 Sensitivity to DOM cycling**.** Differences between $N:P_{exp}$ between default configuration and repeats that included (**a,b**) no DOM cycling and (**c,d**) different degradation timescales for DON and DOP (τ_{DON} = 2 years, τ_{DOP} = 0.5 years).

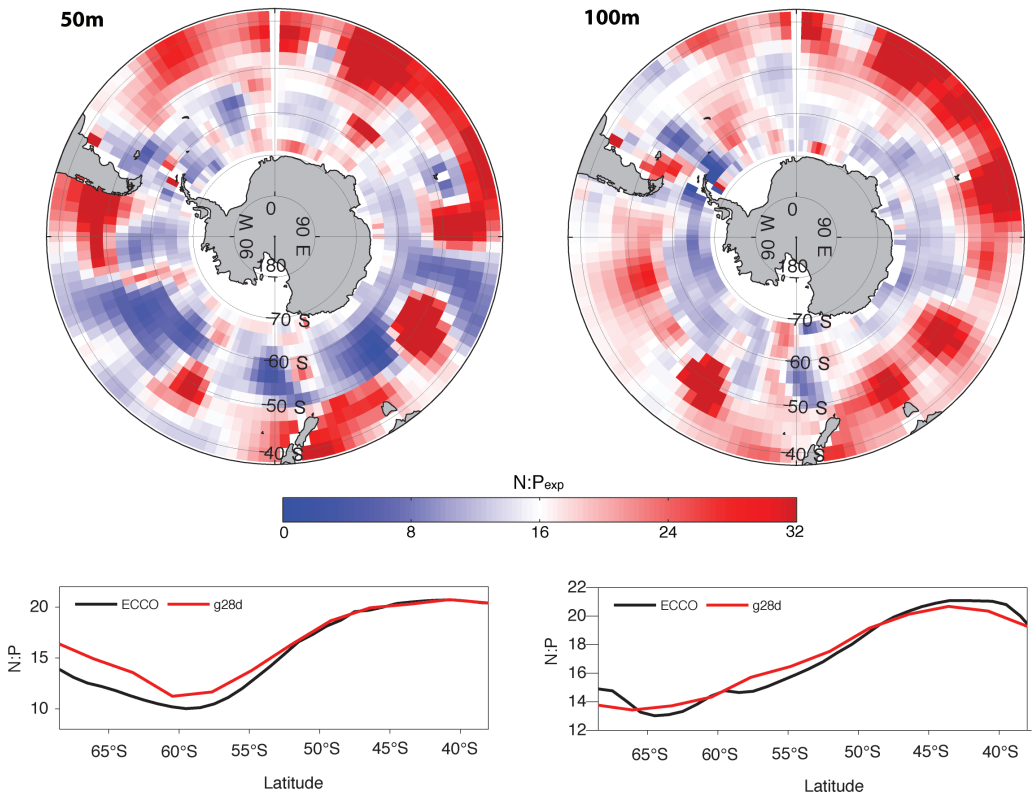

Figure 2.10 Sensitivity to OGCM. Spatial pattern of $N:P_{exp}$ diagnosed by repeating simulations with a coarse resolution OGCM (top two panels), and their zonal mean comparison (bottom two panels) to similar compensation depth simulations using the standard model (ECCO)

CHAPTER 3

Plankton diversity and ocean circulation regulate the ocean nitrogen reservoir

Abstract

The average nitrogen-to-phosphorous ratio of marine phytoplankton (16N:1P) is closely matched to the nutrient content of mean ocean waters (14.3N:1P). This condition is thought to arise from biological control over the ocean's N budget, in which removal of bioavailable N by denitrifying bacteria ensures widespread selection for diazotrophic phytoplankton that replenish this essential nutrient when it limits the growth of other species. Here we show that in the context of a realistic ocean circulation and a uniform N:P ratio of plankton biomass, this feedback mechanism yields an oceanic nitrate deficit more than double its observed value. The critical missing phenomenon is diversity in the metabolic N:P requirement of plankton, which has recently been shown to exhibit large-scale patterns associated with species composition. When these variations are accounted for, and diazotrophs compete with high N:P communities in subtropical regions, the ocean N inventory rises and may even exceed the average N:P ratio of plankton. The latter condition, previously considered impossible, is prevented in the modern ocean by shallow circulations that communicate stoichiometric signals from remote biomes

dominated by diatoms with low N:P ratios. Large-scale patterns of plankton diversity and the circulation pathways connecting them are thus key factors determining the availability of fixed nitrogen in the ocean.

3.1 Introduction

The biologically mediated feedback between marine denitrification and N_2-fixation operates like a "nutrient thermostat" (refs (Redfield 1958, Redfield et al 1963, Tyrrell 1999)) that couples the ocean's fixed N reservoir (primarily nitrate, NO_3^-) to its less dynamic reservoir of P (primarily phosphate, PO_4^{3-}). A central element of this self-regulating mechanism is the partition of ecological niches between diazotrophic (N_2-fixing) phytoplankton, which grow slowly but do not require external fixed N (Capone et al 1997, Karl et al 2002), and other plankton that grow quickly but are often N-limited due to persistent N removal in anoxic environments (Codispoti 1989, Lam & Kuypers 2011, Ward et al 2009). To date, this mechanism has been assessed quantitatively only in box models, in which diazotrophs maintain the ocean's ratio of major nutrient reservoirs ($\Sigma N/\Sigma P$) close to, but slightly below, the N:P requirements of plankton with whom they compete for PO_4^{3-} (Lenton & Klausmeier 2007, Lenton & Watson 2000, Tyrrell 1999).

Box model depictions make two major simplifications however. First, diazotrophs are assumed to compete with plankton having a universal Redfield ratio of 16N:1P,

which sets a threshold for N_2 fixation and constitutes the "setpoint" of the nutrient thermostat. In reality, the Redfield ratio is only an average value and plankton N:P varies systematically between marine species and their preferred biomes (Arrigo et al 1999, Green & Sambrotto 2006b, Quigg et al 2003, Weber & Deutsch 2010). It has thus been hypothesized that the regulation of $\Sigma N/\Sigma P$ is biased towards the nutrient requirements of those species cohabiting with diazotrophs in subtropical biomes. Second, the circulation pathways that transport nutrients between surface regions with different species composition and N:P ratios are not represented in box models, but may play a central role in shaping the ecological niche of diazotrophs (Deutsch & Weber 2012). A realistic physical model is required to identify the processes maintaining the N reservoir of an ocean with diverse plankton stoichiometry.

Such a model is described in the following section (2.2), and then used to compare the steady-state N reservoir of a Redfieldian ocean and one which plankton diversity drives large-scale variations in community N:P ratios.

3.2 Model and methods

A suitable model for this study must contain a realistic representation of those factors hypothesized to influence the ratio of the nutrient reservoirs in the ocean – resource competition between diazotrophic and non-fixing phytoplankton that may vary in their N:P requirements, appropriate spatial separation of denitrification and N_2-fixation regions, and large scale circulation patterns that those regions. The model must be simple

enough however to facilitate simulations over the millennial timescales required for N budget equilibration. To meet these requirements, we developed a simple biogeochemical model that can be combined with a coarse-resolution circulation model, using a transport matrix approach.

3.2.1 Circulation model

We used an observationally constrained ocean general circulation model (OGCM) which optimizes circulation to fit the linearized momentum equations and observed distributions of temperature and salinity, and ^{14}C (DeVries & Primeau 2011). It has horizontal resolution of 4°x4°, and 24 vertical layers including 2 in the top 75m. Annual-mean flow fields were extracted (as a matrix **A**) for offline tracer transport simulations.

3.2.2 Biogeochemical model

A simple ecosystem model was adopted, similar to those previously used in box model studies of N cycle dynamics (Tyrrell 1999). It includes four prognostic variables: NO_3^- (*N*), PO_4^{3-} (*P*), diazotrophic phytoplankton (*F*) that fix dissolved N_2, and "general" phytoplankton (*O*) that assimilate N and P in the ratio R_o. These variables are governed by:

$$\frac{dO}{dt} = \mu_o \min\left(\frac{P}{P+K_P}, \frac{N}{N+K_N}\right) O - MO \quad (1)$$

$$\frac{dF}{dt} = \mu_F \frac{P}{P+K_P} F - MF \quad (2)$$

$$\frac{dP}{dt} = \mathbf{A}P - (J_{up,O} + J_{up,F}) + \mathbf{Q}_{rem}\left(M(O+F)\right) \quad (3)$$

$$\frac{dN}{dt} = \mathbf{A}N - R_o J_{up,O} + \mathbf{Q}_{rem}\left(M(R_o O + R_F F)\right) - D \quad (4)$$

Parameters of the ecosystem model are discussed below and their numeric values listed in Table 3.1.

The first terms on the right hand side of Eq. 1 and 2 represent plankton growth, as a function of environmental factors. The maximum growth rate of O (μ_o) is given by:

$$\mu_o(T,I) = \mu_{opt} \exp(k(T-T'))(1-\exp(-I/K_I)) \quad (5)$$

Here, μ_{opt} is the growth rate under optimal conditions, and k, T', K_I, K_P and K_N control the sensitivity of growth to temperature (T), light (I) and nutrient concentrations. Sensitivity parameters are tuned to reproduce observed surface nutrient distributions (Garcia et al 2010) in the model, ensuring a realistic pattern of biological nutrient drawdown (Fig. 3.1). We account for the competitive handicap of diazotrophs by reducing their maximum growth rate (μ_F) relative to general plankton. It is scaled by a constant factor (δ_F), representing an intrinsic energetic expenditure on nitrogenase activity, and by a Fe-limitation parameter to represent the heightened requirement by diazotrophs for Fe:

$$\mu_F(T,I,Fe) = \mu_o \delta_F \frac{J_{Fe}}{J_{Fe} + K_{Fe}} \quad (6)$$

J_{Fe} is the simulated distribution of atmospheric Fe deposition onto the surface ocean (Mahowald et al 2006), and the strength of the Fe-limitation is varied through K_{Fe} (Fig. 3.2). In Eq. 1 and 2, M represents phytoplankton mortality, and includes a quadratic term that scales with total biomass ($M = m_1+m_2B,$ where $B=O+F$) and can be thought to represent grazing by zooplankton, which are not simulated explicitly.

Nutrients are transported by the circulation operator (**A**), and are assimilated into biological pools in the top 75m through plankton growth. In Eq. 3 and 4, $J_{up,O}$ and $J_{up,F}$ are the same as the first terms on the right hand side of Eq. 1 and 2 respectively. R_o is the biomass N:P ratio of general phytoplankton, and R_F is the amount of N fixed per unit P uptake by diazotrophs. Following phytoplankton mortality, the recycling and remineralization of organic matter is simulated using the operator $\mathbf{Q}_{rem}$. The majority is recycled in the surface ocean, and restored to local inorganic pools. A small fraction (ϕ_e) is exported from the surface layers as organic particles, and remineralized over depth following a power-law relation (Martin et al 1989).

Newly fixed N is assumed to derive from an abundant dissolved N_2 pool that is not simulated explicitly. In Eq. 4, D represents the sum of water-column and sediment denitrification, which are simulated as sinks of NO_3^-. Water-column denitrification is proportional to the remineralization rate of organic matter in grid cells with climatological oxygen concentrations below a critical threshold $[O_2]_{crit}$. Sediment denitrification is determined by the flux of organic matter to seafloor grid cells (Middelburg et al 1996). Because global denitrification rates are one of the primary determinants of the steady-state N inventory (Deutsch & Weber 2012), but are not well

constrained observationally, *D* is scaled to maintain a specified global rate, and a constant partition among water column and sediments (F_{wc}). The global rate is then varied between simulations over the interval 50-300TgN/yr, which is more extensive than the range of recent observational estimates. Simulated distributions of N sources and sinks are shown in Fig. 3.3.

3.3 N reservoir of a Redfieldian ocean

The model described in the preceding section was first used to predict the N reservoir of a "Redfieldian" ocean, in which non-fixing plankton have uniform N:P requirments (R_o) of 16:1. Consistent with box models (Tyrrell 1999), we find that under this assumption the steady-state value of $\Sigma N/\Sigma P$ hinges on two parameters: (1) The globally-integrated rate of denitrification, and (2) The competitive handicap faced by diazotrophs (μ_F/μ_O). The decrease in $\Sigma N/\Sigma P$ at higher denitrification rates and/or stronger Fe limitation (Fig. 3.4) reflects the proportions of PO_4^{3-} and NO_3^- required to support global N_2 fixation rates that balance N removal through denitrification. Because diazotrophs have slow growth rates, they compete successfully for PO_4^{3-} only when NO_3^- is low enough to hinder their competitors to a similar degree. The diazotrophic niche is thus determined, through competitive dynamics, by the NO_3^-: PO_4^{3-} ratio of ambient seawater, even though their growth is explicitly independent of NO_3^-. When strong Fe-limitation exacerbates their competitive handicap, the deep ocean must accumulate a larger deficit of NO_3^- (lower

ΣN/ΣP) to support the needed N_2 fixation rate. Similarly, higher global rates of denitrification must be balanced by enhanced N_2-fixation that, for a given diazotrophic growth rate, can only be achieved with a greater excess of PO_4^{3-} (lower ΣN/ΣP).

Throughout the observationally supported range of global denitrification rates – 150-250TgN/yr (Gruber 2003) – simulated ΣN/ΣP is considerably lower than its observed value of ~14.3. For the average plankton, this amounts to a global deficit of NO_3^- relative to PO_4^- of 6-13 μM, which is 2-4 times larger than observed. Even when Fe limitation is eliminated, unrealistically low denitrification rates (<100 TgN/yr) are required to reconcile the model with observations (Fig. 3.4). Rigorous sensitivity testing (Appendix 3A, below) demonstrated that this discrepancy cannot be eliminated by greater model complexity, including the addition of dissolved organic matter, a complete iron cycle, and minor N budget terms. Similar discrepancies have been noted in other studies using global biogeochemical models (Landolfi et al 2013, Moore & Doney 2007, Somes et al 2010), but their causes have not been explored in detail.

3.3.1 Accumulation of N deficits

The underlying causes of our model's low simulated N reservoir can be elucidated using a simpler model configuration that neglects ecosystem dynamics, and simply tracks the distribution of N deficits that are produced denitrification and annihilated by N_2-fixation. N deficits can be quantified as an excess of PO_4^{3-} relative to Redfield proportions: P* =

$[PO_4^{3-}] - [NO_3^-]/16$. Assuming that diazotrophic plankton fix 16 moles of N per mole of PO_4^{3-} assimilated (although the result is not sensitive to this assumption), the conservation equation for P* can be written:

$$\frac{dP*}{dt} = \mathbf{A}P* + \frac{D}{16} - \frac{P*}{\tau} \quad (7)$$

The last term represents the damping of excess PO_4^{3-} by N_2-fixation in the subtropical surface ocean only. The steady-state P* distribution can be solved for by matrix inversion:

$$P* = (\mathbf{A} - \mathbf{Q}_{bio})^{-1}(-D/16) \quad (8)$$

Here $\mathbf{Q}_{bio}$ is a matrix with $1/\tau$ on the diagonal. Eq. 8 can be solved separately for scenarios with water column or benthic denitrification only, revealing the magnitude of N deficits that must accumulate before the damping of that P* by N_2-fixation can balance its production through denitrification. In order for N_2-fixation to balance 50TgN/yr water column denitrification and 100TgN/yr benthic denitrification – at the lower bound of rates estimated for those processes – N deficits of 1.76×10^4 and 9.29×10^4TgN accumulated respectively. Fig. 3.5 tracks these deficits through time, showing that although they are produced largely in the upper ocean, they must eventually penetrate the deep ocean before the N budget reaches a balance.

The accumulation of N deficits reflects the connectivity via ocean circulation between denitrification zones to the subtropical surface ocean where N deficits are replenished. When transport is less direct, N deficits carve out a larger swath of the ocean before reaching the subtropical surface ocean. In each case, but particularly for sediment

denitrification, large deficits of N are able penetrate into the deep ocean before reaching diazotrophic habitats, reflecting indirect or 'leaky' transport of P* between its source and sink regions. A scenario combining both water column and sediment denitrification must therefore accumulate an N deficit greater than 10^5TgN/yr, much larger than observed deficit of $6x10^4$Tg. More realistic (higher) denitrification rates would give rise to even larger discrepancies. Box models are able to reproduce a more realistic N reservoir, because the connectivity between regions of N_2-fixation and denitrification is often exaggerated. For example, the box model of Tyrrell (1999) partitions 75% of denitrification into the surface region, spatially coincident with diazotrophs. The majority of denitrification can therefore be compensated by N_2-fixation without any significant accumulation of P* in the ocean as a whole. The more realistic circulation of the OGCM precludes such a tight coupling between N sources and sinks.

The inability of Redfieldian model to reproduce the observed N reservoir therefore stems simply from the geographic location of regions conducive to N source and sink processes, and the rates of watermass transport between them. The discrepancy can only be overcome by stimulating additional N_2-fixation for a given supply of PO_4^{3-}, over that allowed in the Redfield model, effectively expanding the ecological niche of diazotrophs. This cannot be accomplished by increasing their growth rate, which already reaches near parity with other plankton in our simulations (Fig. 3.4). It requires a process through which the availability of PO_4^{3-} is enhanced relative to NO_3^- in the subtropics. A likely candidate is large-scale deviations from Redfield stoichiometry in nutrient uptake by non-fixing phytoplankton (Deutsch & Weber 2012).

3.4 Role of variable stoichiometry

In Chapter 2, large-scale variations in R_o were diagnosed throughout the Southern Ocean, where polar latitudes dominated by diatoms export low N:P organic matter, while Subantarctic latitudes are characterized by high N:P ratios (Weber & Deutsch 2010). More recently, an exhaustive compilation of particulate organic matter measurements demonstrated that similar trends hold throughout the global ocean (Martiny et al 2013). We developed a simple parameterization of N:P variability among non-fixing plankton to use in the ecosystem of this study.

3.4.1 Parameterizing N:P variability

We assume that stoichiometric variability occurs primarily at the taxonomic level, and largely reflects the partition among diatoms and other taxa in the non-fixing phytoplankton assemblage (Weber & Deutsch 2010). Community-level N:P (R_o) can therefore be thought of as the sum of diatom and non-diatom components:

$$R_o = R_{o,diat}\phi_{diat} + R_{o,other}(1-\phi_{diat}) \quad (9)$$

Here, ϕ_{diat} is the fractional contribution of diatoms to nutrient export, and $R_{o,diat}$ and $R_{o,other}$ are the biomass N:P ratios of diatoms and other non-diazotropic phytoplankton respectively. Rather than explicitly simulate different taxonomic groups explicitly, we used a prior estimate of ϕ_{diat} combined with Eq. 7 to apply a spatially varying pattern of

R_o to the single class of non-diazotrophic plankton. Three different approaches were considered for estimating ϕ_{diat} (Fig. 3.6). Method 1 assumes that the relative abundance of diatoms scales with the observed surface concentration of $Si(OH)_4$ (Egge & Aksnes 1992):

$$\phi_{diat} = \frac{Si}{Si + K_{Si}} \tag{10}$$

K_{Si} is tuned to accommodate the observational constraint that diatoms contribute 40-50% of global export production (Jin et al 2006). Methods 2 and 3 compute ϕ_{diat} from the relative export fluxes of N and Si, similar to the method used in chapter 2:

$$\phi_{diat} = \frac{\Phi_{Si} / R_{Si:N}}{\Phi_N} \tag{11}$$

The Φ terms represent nutrient export (of Si and N) from the surface, and $R_{Si:N}$ is the biomass Si:N ratio of diatoms, which can be estimated as a function of Fe availability (Eq. 5, Chapter 2). In Method 2, the export flux ratio (Φ_{Si}/Φ_N) is estimated from observations only (Sarmiento & Gruber 2006), based on the vertical gradients of Si and N between the thermocline and surface, whereas Method 3 diagnoses the fluxes in an OGCM (Eq. 4, Chapter 1). We note that the two diagnostic methods are less appropriate in regions where N_2-fixation confounds the diagnosis of N export. In the majority of simulations, the simplest approach (Method 1) was used, which agrees most closely with satellite-derived estimates of diatom biogeography (Alvain et al 2008). Methods 2 and 3 were used to derive an estimate of uncertainty associated with the community-composition parameterization.

Initially, $R_{o,di}$ and $R_{o,other}$ were held close to the values diagnosed in Weber & Deustch (2010) for the Southern Ocean (10 and 20 respectively), with additional constraint that the global mean N:P export ratio by non-fixing plankton is equal to the Redfield ratio of 16:1. This allows us identify changes in ΣN/ΣP (relative to the Redfield case) that are caused by the spatial pattern of R_o and not by its mean value.

The resulting pattern of community-level R_o (Fig. 3.7) is low (~10:1) in high latitude regions where diatoms dominate, but high in the subtropical gyres where nutrient starvation selects against bloom-forming diatoms. The mean N:P of plankton that compete directly with diazotrophs in these subtropical regions, denoted $R_{o,ST}$, is therefore close to 20. This is consistent with the elemental composition of cyanobacteria that dominate oligotrophic waters (Bertilsson et al 2003, Heldal et al 2003), the observed N:P of organic matter in the North Pacific Subtropical Gyre (Karl et al 2001b), and theoretical predictions of high N:P allocation strategies during resource competition (Klausmeier et al 2004).

3.4.2 Influence on N reservoir

The introduction of stoichiometric diversity raises the model's steady-state ΣN/ΣP, bringing it into close agreement with the observed value across a wide range of plausible denitrification and Fe-limitation scenarios (Fig. 3.8). This increase is driven by the high N:P requirements of oligotrophic phytoplankton, which exacerbates N-limitation in the subtropical gyres. A larger excess of PO_4^{3-} then remains to fuel N_2-fixation, expanding

the niche of diazotrophs beyond that created by subsurface denitrification. This allows a balanced N budget to be achieved at higher ΣN/ΣP values of the modern ocean. Under weak Fe-limitation and low denitrification rates, ΣN/ΣP actually exceeds the average N:P of marine plankton (Fig. 3.8) – a condition that cannot be attained in previous box-model depictions. The ocean's ratio of nutrient reservoirs thus depends not only on the mean N:P of it's plankton, but also on their stoichiometric diversity.

To investigate the sensitivity of ΣN/ΣP to different degrees of stoichiometric diversity, we varied the N:P quota of diatom and non-diatom end-member communities, while maintaining a constant average export ratio of 16N:1P. As plankton stoichiometry becomes more diverse, global ΣN/ΣP steadily rises (Fig. 3.9), reflecting the expansion of the diazotrophic niche caused by the increasing N:P requirements of non-fixing plankton cohabiting subtropical regions with diazotrophs (i.e. increasing $R_{o,ST}$). However, for every increase in $R_{o,ST}$, the increase in ΣN/ΣP is only 40% as large, much less than would be expected based on Redfield's hypotheses that diazotrophs keep ΣN/ΣP in line with the stoichiometric needs of their local competitors (that hypothesis would predict a 1:1 relation between $R_{o,ST}$ and ΣN/ΣP. This implies that the ecological niche of diazotrophs is determined not only by local competition with high N:P plankton, but also by remote diatom-dominated communities with a lower N:P quota. Since these communities largely occupy different ocean biomes, their stoichiometric signatures must be communicated over long distances by ocean circulation.

3.5 Role of ocean circulation

To further explore the role of circulation in controlling ΣN/ΣP, we turned to a much simplified model framework, in which the circulation patterns that transport nutrients between the surface and deep-ocean, and between plankton biomes with different stoichiometry, can be abstracted and manipulated.

3.5.1 Ocean box model

We used a 3-box model of the ocean that can capture the important features of the GCM and aid in its interpretation. The geometry and nutrient fluxes of the model are shown in FIGURE 9. It comprises a deep-ocean box (below 500m), and two surface/upper thermocline boxes (top 500m). The surface is divided laterally into an upwelling region (*UW*) that not inhabited by diazotrophs, and is dominated by diatoms with N:P requirements below 16:1, and a subtropical region (*ST*) that is cohabited by diazotrophs and high N:P non-fixing plankton ($R_{o,ST}$>16). Each surface box mixes independently with the deep ocean, (Fig. 3.10a), but an overturning circulation can also be added, through which nutrients upwell in *UW* and are transported laterally into *ST*. The model's ecosystem and biogeochemistry components are held as close to the OGCM as possible for ease of comparison, with the following simplifications:

(a) Phytoplankton growth rates are set to the optimal value in *ST*, and reduced by a factor of 0.5 in the *UW*, so that residual nutrients remain in the surface as observed.

(b) The competitive handicap of diazotrophs is determined only by δ_F in *ST* (no Fe-limitation), and μ_F is set to zero in *UW,* so that diazotrophs do not grow.

(c) Denitrification is distributed with 50% in the surface/upper thermocline box, and 50% in the deep ocean.

When surface nutrients are supplied only from vertical exchange with the deep ocean (**M**), the niche of diazotrophs is governed by their local competitors only, so every change in $R_{o,ST}$ produces an equal change in $\Sigma N/\Sigma P$, even though the global mean R_o is anchored at 16 (Fig. 3.10b, f_Ψ=0). However, when the nutrients are predominantly supplied through shallow overturning and near-surface lateral circulations (**Ψ**), the signature of low N:P uptake – a higher residual NO_3^-: PO_4^{3-} ratio in surface waters – is transported directly from diatom-dominated upwelling regions into the subtropics. This reduces the excess PO_4^{3-} available to diazotrophs, and must be compensated by lower NO_3^-: PO_4^{3-} in upwelling deep water to maintain a given N_2-fixation rate. The response of the ocean's $\Sigma N/\Sigma P$ to increases in $R_{o,ST}$ is thus damped as lateral circulations strengthen relative to vertical exchange. In the extreme case where all subtropical nutrients pass first through surface communities with low N:P ratios (Fig. 3.10b, f_Ψ=1), the ocean N reservoir is entirely independent of spatial variations in R_o, and $\Sigma N/\Sigma P$ is regulated through the global-mean N:P of plankton, as originally hypothesized by Redfield (Redfield 1958).

3.5.2 Comparison to OGCM

In light of these box model results, the tendency of ΣN/ΣP in the GCM to track only ~40% of a change in $R_{o,ST}$ (Fig. 3.9) suggests that about half the waters reaching subtropical sites of N_2-fixation are first influenced by low N:P plankton communities outside the subtropics. The dependence of global ΣN/ΣP on the spatial pattern of plankton N:P ratios can be quantified further by introducing taxon-dependent deviations from a constant Redfield N:P one grid cell at a time and computing the new steady-state N reservoir in each case.

For each surface grid cell (with *x,y* coordinates *i,j*), a simulation was conducted in which the local R_o was set to its stoichiometrically diverse value, as computed from ϕ_{diat} (Fig. 3.7a). In all other surface regions, R_o was held equal to the Redfield ratio. The difference between the steady-state ΣN/ΣP in this simulation, and that in a uniform Redfieldian case, was then computed:

$$\Delta_{\Sigma N/\Sigma P}\Big|_{\substack{x=i\\y=j}} = \frac{\Sigma N}{\Sigma P}\left(\begin{cases} R_o = f(\phi_{diat}), & x=i, y=j \\ R_o = 16, & x\neq i, y\neq j \end{cases}\right) - \frac{\Sigma N}{\Sigma P}\left(R_o = 16\right) \tag{11}$$

This value is taken as measure the sensitivity of ΣN/ΣP to the uptake stoichiometry of plankton communities in the perturbed surface region. The efficiency of these computations was enhanced using a Quasi Steady-State Assumption (QSSA) for the 'fast' biological variables *O* and *F*:

$$O = \frac{\mu_o}{M}\min\left(\frac{P}{P+K_P}, \frac{N}{N+K_N}\right) \tag{12}$$

$$F = \frac{\mu_F}{M} \frac{P}{P + K_P} \quad (13)$$

This reduces the model to a 2-equation system that can be solved directly for steady state using Newton's Method (Kwon & Primeau 2006). Sensitivity testing demonstrated that the solutions derived from the QSSA approach and full 4-equation model were almost indistinguishable.

This calculation can be used to divide regions between those whose stoichiometric deviation from 16:1 tends to raise ΣN/ΣP compared to the Redfieldian case (positive values, Fig. 3.11a), and those that tend to reduce it (negative values, Fig.3.11a). Large negative values are found in the North and Equatorial Pacific and, to a lesser extent, the polar regions of the Southern Ocean. The transport of nutrients from these source regions into the subtropics, through surface Ekman currents and shallow overturning, creates a "biogeochemical teleconnection" by which remote low N:P communities reduce the availability of PO_4^{3-} to fuel N_2-fixation. This counteracts the expanded niche of diazotrophs produced by local competition with high N:P subtropical communities, offsetting roughly half of the upwards pressure on ΣN/ΣP (Fig. 3.11b). Ocean circulation thus plays a critical role in the nutrient thermostat, reducing the bias of ΣN/ΣP towards the stoichiometry of subtropical communities, and holding the nutrient content of seawater closer to the global average requirements of phytoplankton.

3.6 Implications

The ratio of oceanic N and P reservoirs is a simple but powerful observational constraint on the dynamics of the marine N cycle. It appears fundamentally incompatible with a universal Redfield ratio of plankton biomass, lending global support to the large-scale association between biogeography and plankton nutrient metabolism inferred from Southern Ocean nutrient data (Weber & Deutsch 2010).

The modern ocean $\Sigma N/\Sigma P$ also places new bounds on global denitrification rates and the limitations to diazotroph growth. Denitrification rates at the upper end of the estimated range (>250TgN/yr) are unable to yield the observed $\Sigma N/\Sigma P$ ratio, even with a high degree of stoichiometric diversity. At the same time, the net effect of stoichiometric diversity among plankton taxa is to expand the ecological niche of marine diazotrophs. In geochemical estimates of N_2-fixation based on surface nutrients (Deutsch et al 2007), this would translate into higher diagnosed N_2-fixation rates in the subtropics, rather than the lower rates suggested by Mills & Arrigo (2010). Thus, stoichiometric diversity helps close the long-standing gap between estimates of N sources and sinks (Codispoti 1995).

From a mechanistic perspective, the expanded niche for diazotrophs yields a higher $\Sigma N/\Sigma P$ for a given denitrification rate, but this is still insufficient to achieve observed $\Sigma N/\Sigma P$ when diazotrophs are strongly limited by airborne Fe. At most, the overall growth rate handicap of diazotrophs can approach 50%, and then only if denitrification rates are at the lower end of the estimated range. If the intrinsic cost of diazotrophy were greater than the conservative value we use ($\mu_F/\mu_O = 0.95$), or if diazotroph growth is also slowed by other factors such as temperature and light not included here (Karl et al 2002), then the observed $\Sigma N/\Sigma P$ would require even weaker Fe

limitation. These findings imply a secondary role for atmospheric Fe deposition in controlling rates of N_2 fixation in the modern ocean.

Temporal changes in the mean N:P of plankton have been hypothesized to drive long-term trends in ocean fertility and carbon storage, by shifting the setpoint of its nutrient thermostat (Broecker & Henderson 1998, Falkowski 2000). Our model shows that this setpoint is also controlled by the biogeography of distinct plankton taxa, and ocean circulation patterns that transport nutrients between biomes – two factors known to vary with climatic conditions. Future stratification of the upper ocean and the expansion of oligotrophic biomes expected under a warming climate (Polovina et al 2008) could reshape the ecological niche of diazotrophs, and initiate a long-term perturbation in the ocean's nutrient thermostat.

3.7 Summary and outlook

This study demonstrated that stoichiometric variability among marine phytoplankton, and just their global-mean N:P ratio, is critical in regulating the ocean's steady-state N reservoir. It is the N:P requirement of plankton that compete directly with diazotrophs that governs the availability of excess PO_4^{3-} to fuel diazotroph grows, and determines the ability of N_2-fixation to compensate N deficits produced by denitrification. Diazotrophs thus tend to restore $\Sigma N/\Sigma P$ towards the high N:P of subtropical phytoplankton, rather the global mean, resulting in a larger N reservoir than under Redfield conditions. This

reconciles a discrepancy between the predictions of Redfieldian models and the observed ΣN/ΣP. In those models, the spatial separation of N source and sink regions, and the "leaky" circulation pathways connecting them, cause a larger accumulation of N deficits in the deep ocean than is observed.

The study revealed an important and previously unknown role for ocean circulation in the "nutrient thermostat" feedbacks: it transports residual nutrients from non-diazotrophic habitats, such as the high latitudes, into the subtropics. In so doing, it communicates the elemental requirements of remote plankton communities through the nutrient supply, giving them leverage over the ecological niche of diazotrophs. The net effect is to reduce the upwards bias of ΣN/ΣP towards the N:P demands of plankton competing directly with diazotrophs. Results of this study also allowed new bounds to be placed on other N-cycle processes. Even when stoichiometric variability was accounted for, the observed ΣN/ΣP could not be reconciled with dentrificiation rates greater than 250TgN/yr, or a stong limitation of N_2-fixation by Fe inputs.

As well as advancing our understanding of the modern-ocean N reservoir, this study raises two new potential mechanisms for driving its variations through time, independent of forcings on. Large-scale patterns of plankton N:P are a critical factor controlling N_2-fixation. Because those patterns are largely controlled by differences in the species composition of plankton communities, the changing biogeography of different plankton taxa could reshape the ecological niche of diazotrophs and reset the "setpoint" of the ocean's nutrient thermostat. Large-scale biogeographical changes have been hypothesized both under past and future climate change. It has been suggested that

enhanced Fe inputs and the "leakage" of silicic acid out of the high latitudes allowed an expansion of diatoms into the subtropics during the Last Glacial Maximum (Brzezinski et al 2002). Their direct competition with diazotrophs may then have biased ΣN/ΣP towards the low N:P requirement of diatoms, resulting in significant N loss from the oceans and weakening the biological pump. However, this would work against enhanced carbon drawdown during glacial periods, and must be counteracted by further, unknown mechanisms. In contrast, anthropogenic climate warming is projected to expand the stratified subtropics, potentially expanding the habitat of high N:P plankton and raising the oceanic N reservoir.

Ocean circulation provides a second mechanism for driving variations in ΣN, without direct forcing of the N budget. A change in circulation patterns that tends to enhance the nutrient supply from the high latitude surface, relative to the supply from the deep ocean, will tend to reduce the bias of ΣN/ΣP towards the needs of subtropical plankton. Under such conditions, the "setpoint" of the nutrient thermostat would more closely reflect the mean N:P of phytoplankton, as hypothesized by Redfield. On the other hand, changes in circulation that lead to greater isolation of the high latitudes from the subtropics would tend to increase the bias of ΣN/ΣP towards the needs of low latitude communities.

The efficiency of these two mechanisms could be explored and predicted for different climate regimes using the same model framework outlined in the outlook of Chapter 2. Modeling efforts have already precited circulation changes under a range of climate scenarios, including those of the Last Glacial Maximum and the warmer near-

future. The changing oceanic conditions would select for different plankton traits in an emergent ecosystem model, and thus select for communities with changed N:P requirements. Again, such a modeling effort is limited by our understanding of the relationship between resource allocation among pools of cellular machinery, and the trait parameters that are needed for ecosystem modeling, such as growth rates and nutrient affinities. It is hoped that the studies presented in this dissertation will motivate new work in this area, so that the modeling framework outlined above can soon be realized.

Appendix 3A: Sensitivity Testing

We tested the sensitivity of our results to changes in model parameters that could affect ΣN/ΣP. We discuss the significance of each parameter and test results below.

- **Distribution of denitrification.** The distribution of denitrification controls how rapidly denitrified waters are transported to sites of N_2-fixation, so influences the strength of feedbacks between N sources and sinks. Anoxic regions of the water column occur in upwelling margins, which are an important source of nutrients to the surface of the subtropical Pacific and Indian Oceans. The NO_3:PO_4 signature of water-column denitrification is thus efficiently transported to diazotrophic habitats, prompting a strong response from N_2-fixation. We would therefore expect a higher steady state N reservoir in an ocean where a greater fraction of total denitrification occurs in the water column (i.e. high F_{WC}), rather than sediments. We tested the sensitivity to this parameter by varying F_{WC} between 0 and 1 (Fig. 3.12a). Although our model exhibits the expected increase in ΣN/ΣP at high F_{WC}, the response was relatively weak: ΣN/ΣP changes by ~0.5 over the whole range of simulations. Isotopic constraints suggest that F_{WC} is confined to the range 0.2-0.5, within which ΣN/ΣP varies by just 0.1. The inability of our Redfieldian simulations to reproduce observed ΣN/ΣP values cannot therefore be attributed to the distribution of denitrification.

- **Additional N budget terms.** Our default simulations assume that N_2-fixation and denitrification are the only sources and sinks of fixed N to and from the ocean. For a given rate of denitrification, additional sources of N would allow a balanced N budget to be achieved at lower N_2-fixation rates, reducing the requirement for excess PO_4 in the deep ocean. Additional sources of N should therefore raise steady-state ΣN/ΣP in our model. In the pre-industrial era, the most important such sources were atmospheric deposition from lightning, which is thought to have supplied no more than 20TgN/yr to the ocean (Brandes et al 2007). Adding additional N sources of this magnitude to our model, evenly distributed over the surface ocean, had a negligible effect on its N reservoir (Fig. 3.12b). The simplifications made to the N budget in our default simulations are therefore not responsible for the low predicted ΣN/ΣP under Redfieldian conditions.

- **Diatom scheme.** The response of ΣN/ΣP to stoichiometric diversity in our model may be sensitive to the inferred distribution of diatoms upon which R_o is patterned. Using Method 1 (Si-based), we found that stoichiometric diversity increased the ocean N reservoir to observed values, but that ocean circulation damped the upwards bias of ΣN/ΣP towards high N:P communities (see main text). We tested the robustness of these findings using Method 2 (nutrient gradient) and Method 3 (nutrient-OGCM) outlined above. In each case, ΣN/ΣP raised as stoichiometric diversity became more pronounced, and reached observed

values within the estimated range of global denitrification rates. Relative to our default simulations, the response of ΣN/ΣP to $R_{o,ST}$ (~40%) was only slightly stronger using Method 2 (~50%) and slightly weaker using Method 3 (~35%). Our conclusions are robust against the precise distribution of diatoms used in simulations, as long as the broad, well-known, pattern of their biogeography is captured.

- **Dissolved organic matter dynamics.** Other non-Redfieldian processes may contribute to enhancing PO_4 availability and raising ΣN/ΣP towards its observed value. For example, a faster re-supply of P than N from dissolved organic matter in the subtropics would expand the niche of diazotrophs relative the Redfield case. We tested whether such dynamics might contribute to resolving the discrepancy of low ΣN/ΣP in the Redfield model by including explicit DON and DOP pools using two different formulations. The first assumes that the two pools behave similarly, with production rates proportional to their biological quotas and equal decay rates ("DOM Equal" scenario). The second accounts for potential differences in the dynamics of the pools. High quality measurements of dissolved organic matter are scarce, but the available data suggests a faster turnover (higher production and a faster decay rate) for DOP than for DON. Deutsch et al (2007) derived the best-fit production and decay parameters to reproduce the observed distributions of DON and DOP in the Pacific. We use this parameter set in our second formulation ("DOM Unequal" scenario). A comparison between steady-

state ΣN/ΣP in our original simulations and those with explicit DOM cycles (Table 2) reveal no large changes, suggesting that these processes cannot reproduce the observed ΣN/ΣP.

Parameter	Symbol	Fixed Value	Range	Units
Plankton growth rate under optimal conditions	μ^{∞}	1		day^{-1}
Temperature sensitivity parameter	k	0.02		$°C^{-1}$
Optimal growth temperature	T'	30		°C
Light sensitivity parameter	K_I	10		Wm^{-2}
Intrinsic growth-rate handicap of diazotrophs	δ_F	0.95		dimensionless
Fe-sensitivity of diazotroph growth rate	K_{Fe}		0-0.5	$g/m^2/yr$
Phosphate half-saturation constant	K_P	0.1		µM
Nitrate half-saturation constant	K_N		$K_P \times R_o$	µM
Linear mortality constant	m_1	0.1		day^{-1}
Quadratic mortality constant	m_2	10		$\mu M^{-1}day^{-1}$
Si concentration at which diatoms become dominant	K_{Si}	8		µM
N:P ratio of diatoms	$R_{o,di}$		5-16	mol/mol
N:P ratio of other non-fixers	$R_{o,other}$		16-25	mol/mol
Si:N ratio of diatoms	$R_{Si:N}$		1-5	mol/mol
N:P ratio of diazotrophs	R_f	50		mol/mol
Depth of euphotic zone	z_0	75		m
Export ratio	ϕ_e	0.1		dimensionless
Shape of Martin curve	b	0.858		dimensionless
critical oxygen concentration for water column denitrification	$[O_2]_{crit}$	10		µM
Fraction of total denitrification that occurs in water column	F_{WC}	0.33 (main text)	0-1 (sensitivity testing)	dimesionless
Scaling constant for water-column deitrification	c_{WC}		0.25-1.5 (determined by model	dimensionless

			constraints)	
Scaling constant for sedimentary denitrification	c_S		0.2-1.25 (determined by model constraints)	dimensionless

Table 3.1. Parameters of ecosystem and biogeochemistry model.

Scenario	No DOM	DOM Equal	DOM Unequal
ΣN/ΣP	13.17	13.23	13.31

Table 3.2. Influence of DOM dynamics on ΣN/ΣP. Simulations have denitrification rates of 150TgN/yr and moderate Fe-limitation.

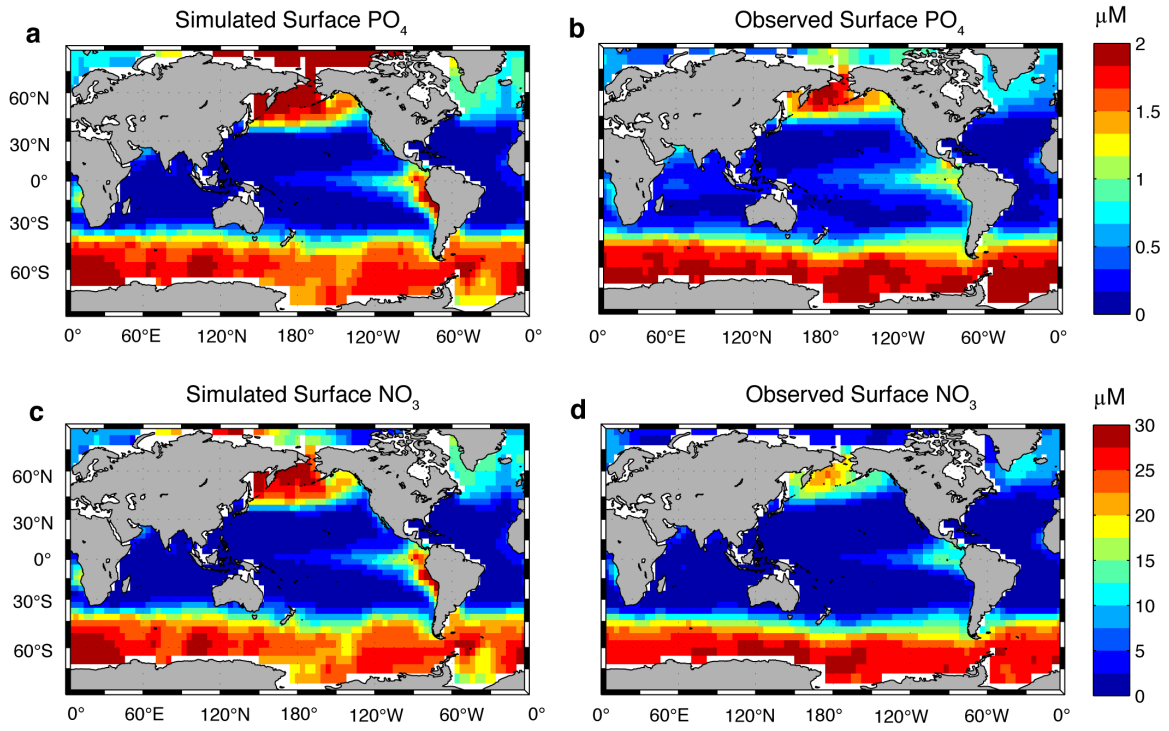

Figure 3.1. Comparison between simulated and observed (World Ocean Atlas 2009) distributions of PO_4 (**a,b**) and NO_3 (**c,d**). Unlike PO_4, the total inventory of NO_3 deviates from observations in many of simulations, leading to discrepancies between observed and simulated NO_3 distributions. However, in simulations that reproduce a realistic N inventory, surface NO_3 is close to observations (**c,d**), indicating that our ecosystem model produces realistic patterns of nutrient drawdown.

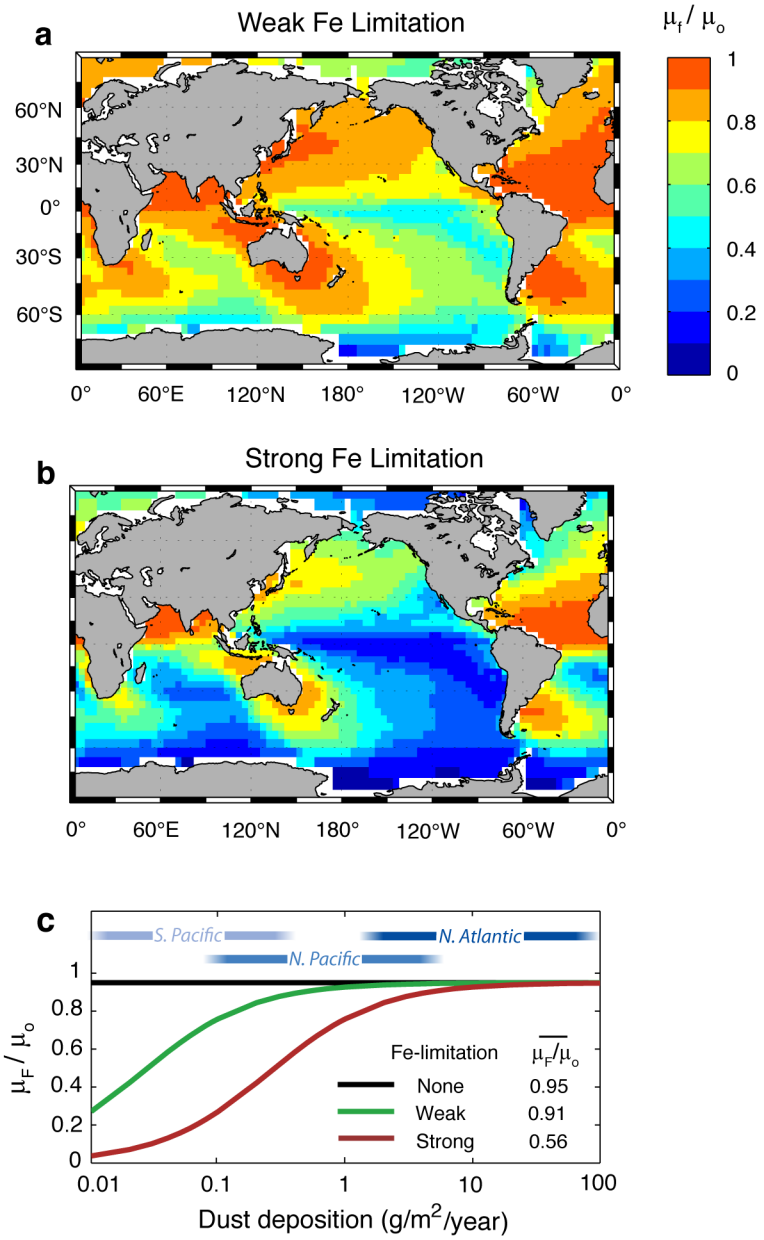

Figure 3.2. Competitve handicap faced by diazotrophs under different Fe limitation scenarios. Values in **a&b** represent the maximum growth rate of diazotrophs relative to non-fixing plankton. **a,** Weak Fe-limitation: K_{Fe} = 0.05g/m^2/yr. **b,** Strong Fe-limitation: K_{Fe} = 0.25g/m^2/y. As Fe limitation strengthens, μ'_F/μ'_O becomes more variable between regions of high and low Fe inputs, and its mean value is reduced (**c**). In the following figures, different Fe limitation scenarios are denoted by their mean μ'_F/μ'_O value. From Weber & Deutsch, 2012.

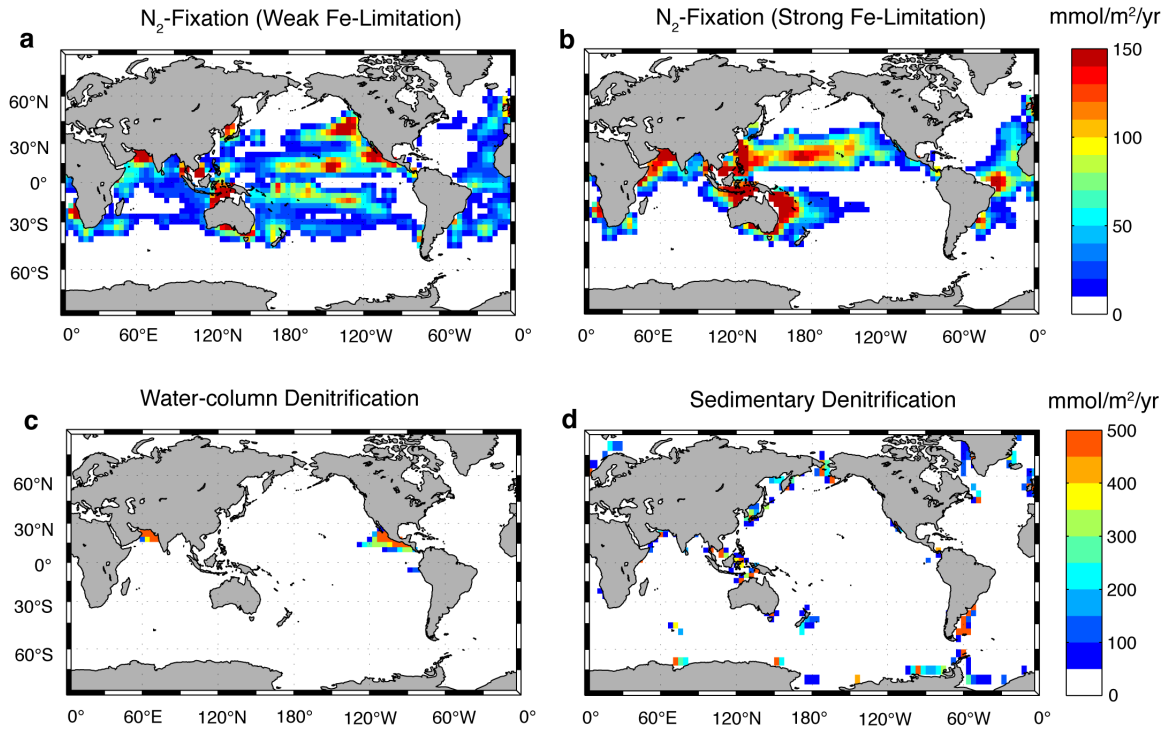

Figure 3.3. Model distributions of N_2-fixation (**a,b**) and denitrification (**c,d**). Fixation is shown for weak (**a**) and strong (**b**) Fe-limitation scenarios. Denitrification is shown separately for water-column (**c**) and sedimentary (**d**) fractions. Total fixation/denitrification is 150TgN/yr in all cases.

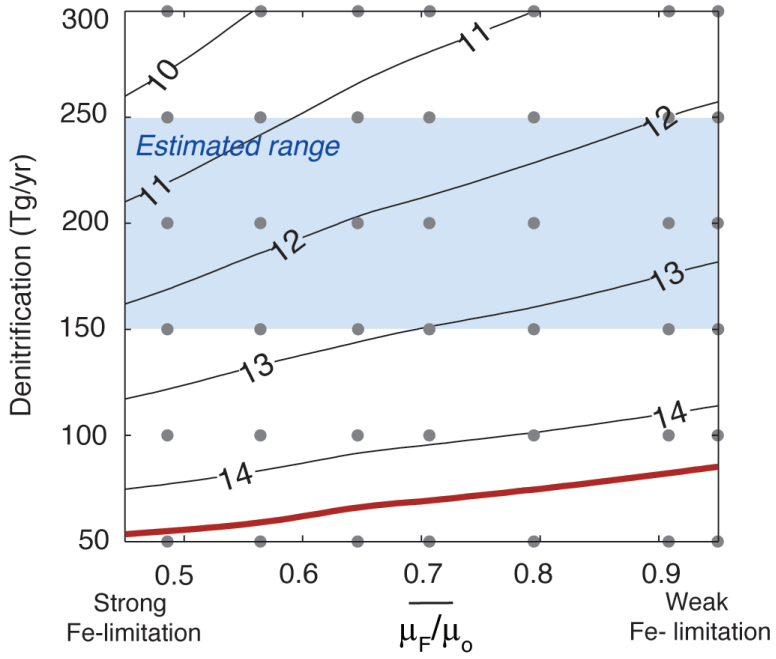

Figure 3.4 Predicted steady-state ΣN/ΣP for a Redfieldian ocean, across a range of denitrification and Fe-limitation scenarios. Blue shading represents observational constraints on denitrification range; red line indicates observed ΣN/ΣP; grey dots are solutions of individual simulations. From Weber & Deutsch, 2012.

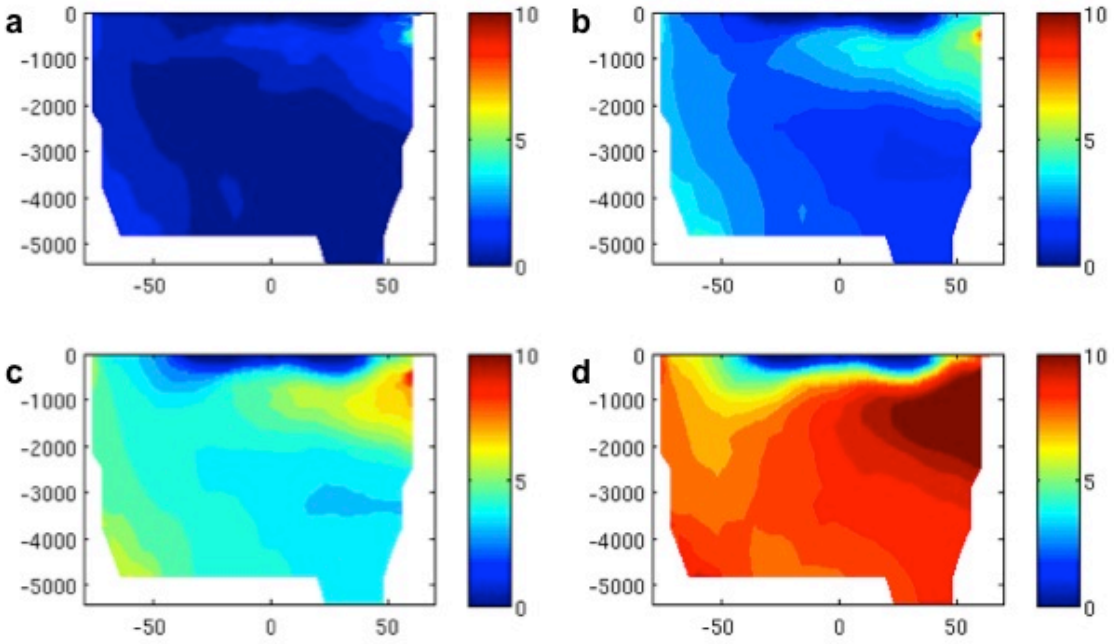

Figure 3.5 Distribution of N deficits (16[PO_4]-[NO_3]) at times **a** 100yrs, **b** 500yrs, **c** 1000yrs, **d** 5000yrs. Deficits are produced by 50TgN/yr water column denitrification and 100TgN/yr benthic denitrification, and are circulated until they reach the subtropical surface ocean, where they removed to represent N_2-fixation. Despite their formation predominantly in upper ocean waters (<1000m), N deficits penetrate and accumulate in the deep ocean before the removal rate (in the subtropics) balances their production. The indirectness of circulation between sites where N deficits are produced and destroyed explains why the Redfieldian model has a low N reservoir compared to box models, in which denitrification and N_2-fixation are more tightly coupled.

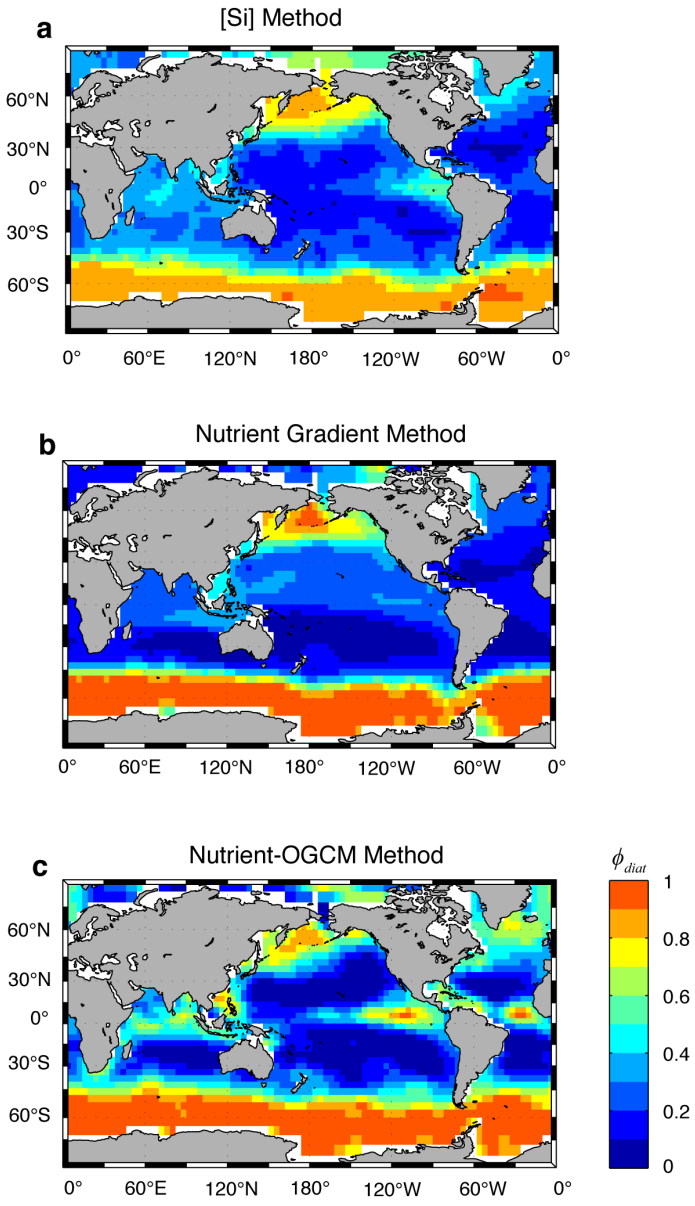

Figure 3.6 Fraction of nutrient export attributed to diatoms (ϕ_{diat}), estimated using three different methods: **a,** Method 1 scales the surface distribution of $Si(OH)_4$; **b,** Method 2 uses the vertical gradients of N and Si between the surface and thermocline; **c,** Method 3 diagnoses ϕ_{diat} from nutrient fluxes in an OGCM. Each can be combined with biomass N:P ratios of diatom and non-diatom end-members to derive a spatial pattern of R_o.

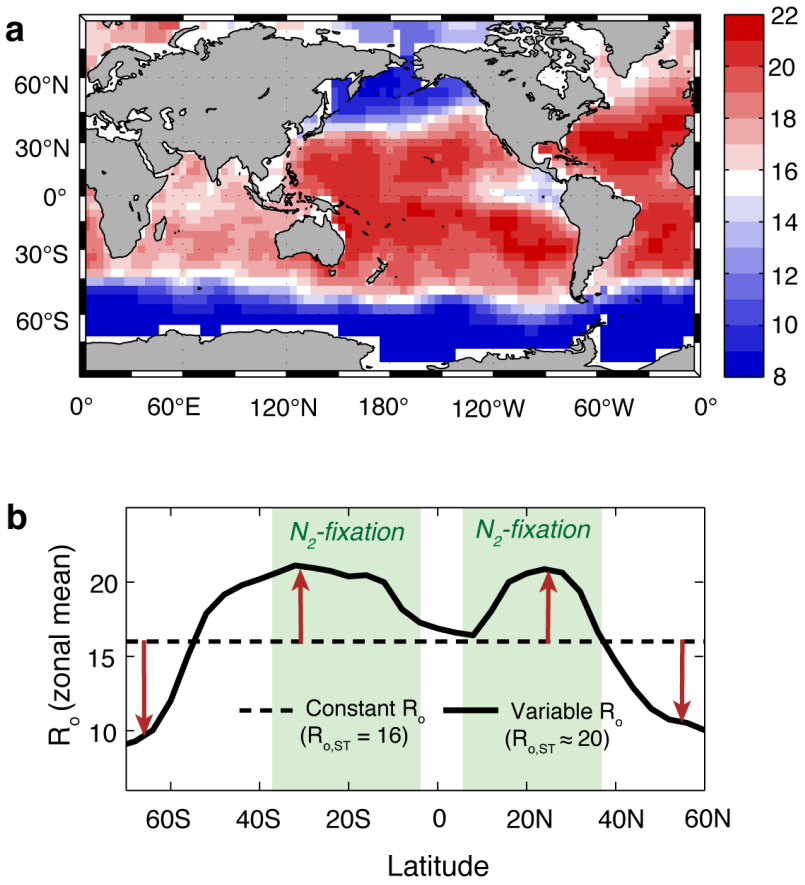

Figure 3.7 Pattern of community R_o derived using Method 1 ([Si] method) for diatom distributions, and applying taxon-dependent N:P ratios. **a** R_o is low throughout high latitude and Equatorial Pacific upwelling regions, and high throughout the subtropics. **b** Diazotrophs, which are confined to subtropical gyres, therefore cohabit and compete almost exclusively with plankton that have N:P requirements above the global mean. From Weber & Deutsch, 2012.

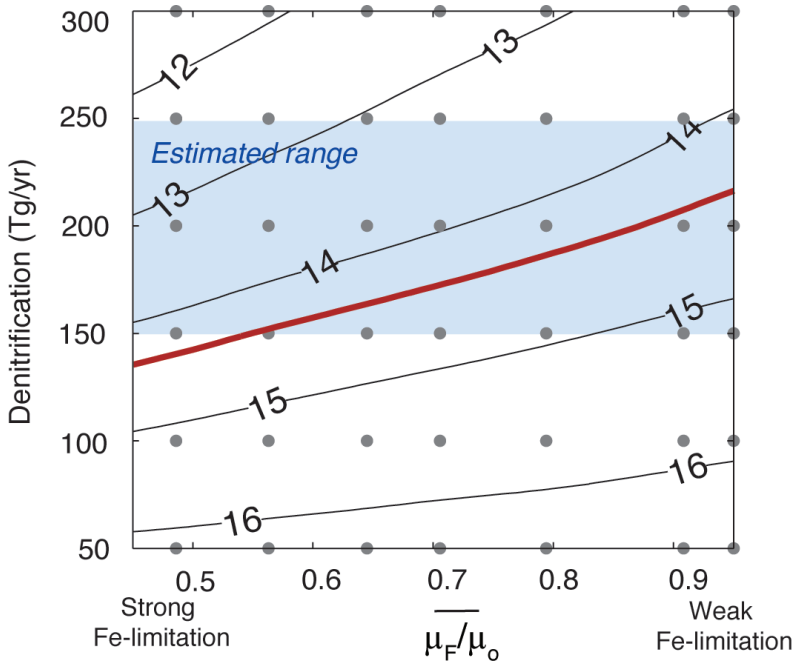

Figure 3.8 As **3.4**, except for stoichiometrically diverse scenarios ($R_{o,ST}$≈20). From Weber & Deutsch, 2012.

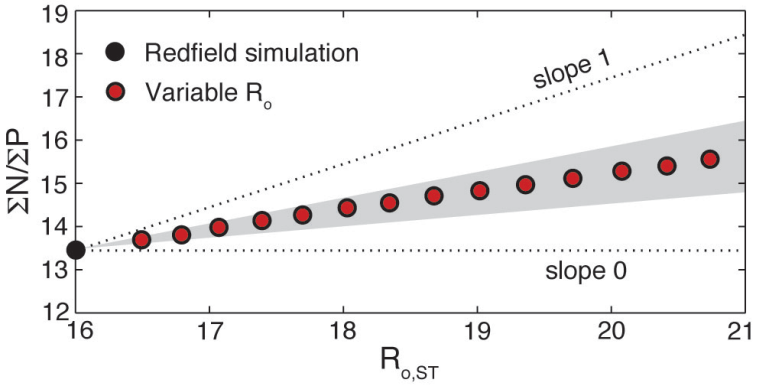

Figure 3.9. Response of ΣN/ΣP to the degree of stoichiometric diversity ($R_{o,ST}$). Each simulation has 150TgN/yr denitrification and no Fe-limitation. If the "setpoint" of the nutrient thermostat were determined through local competition only, ΣN/ΣP would raise with $R_{o,ST}$ along a line of slope 1, yet a much weaker response is observed in our model. Grey shading represents an estimate of error for the slope of this line, derived using the three different estimates of diatom abundance as the basis for R_o. From Weber & Deutsch, 2012.

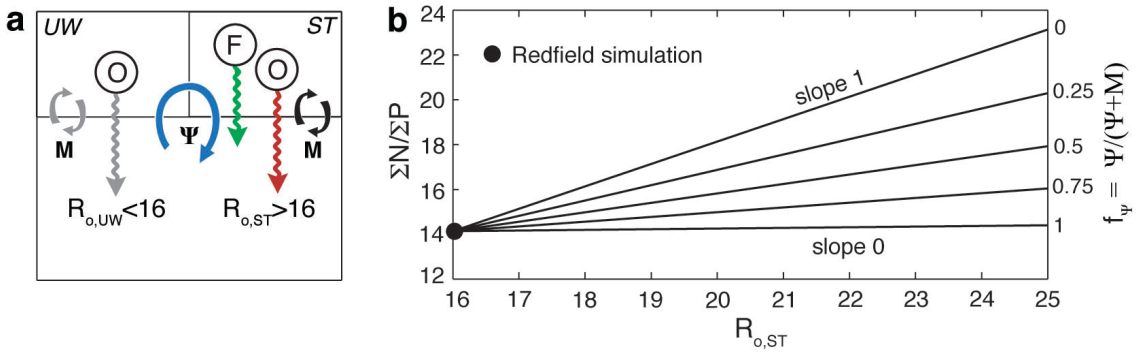

Figure 3.10. Role of ocean circulation illustrated in a 3-box model. **a,** Structure of the model, with two surface regions (upwelling – *UW*; subtropics – *ST*) and two circulation pathways (vertical exchange – **M**; overturning – **Ψ**). Diazotrophs are restricted to *ST*, and other plankton have diverse stoichiometry that is varied by raising $R_{o,ST}$, and reducing $R_{o,UW}$ to maintain a mean of 16. **b**, The response of ΣN/ΣP to stoichiometric diversity depends on f_ψ, the fraction of subtropical source-waters that first pass through *UW*. From Weber & Deutsch, 2012.

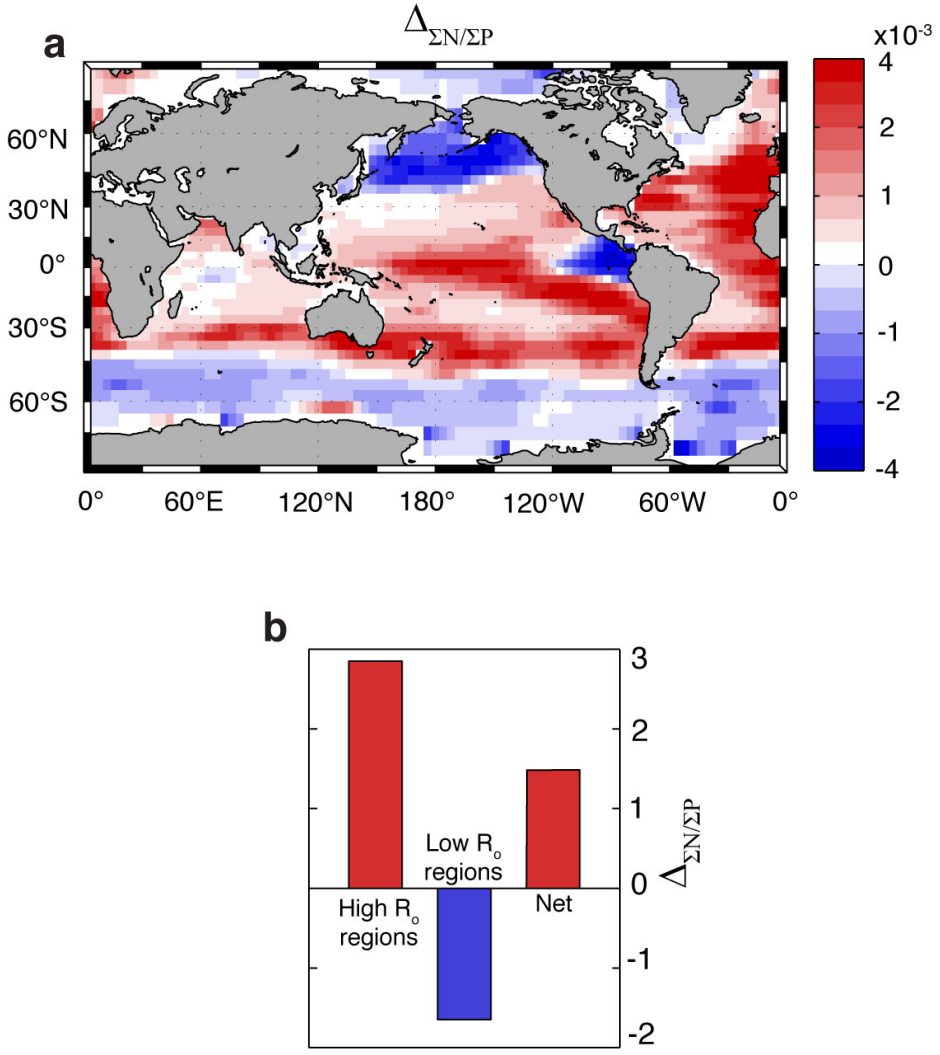

Figure 3.11. Influence of individual surface regions on ΣN/ΣP. **a,** Values of $\Delta_{\Sigma N/\Sigma P}$ represent the change in steady-state ΣN/ΣP (from Redfield case) prompted by introducing the grid cell's deviation of R_o from 16 (Fig. S4), while holding R_o=16 elsewhere (see Methods). **b,** Integral of $\Delta_{\Sigma N/\Sigma P}$ over regions of high R_o (>16) and low R_o (<16), and over the entire global domain (Net). High and low R_o regions exert opposite pressure on the ocean N reservoir, with the net effect of a slight increase in ΣN/ΣP over the Redfield case. From Weber & Deutsch, 2012.

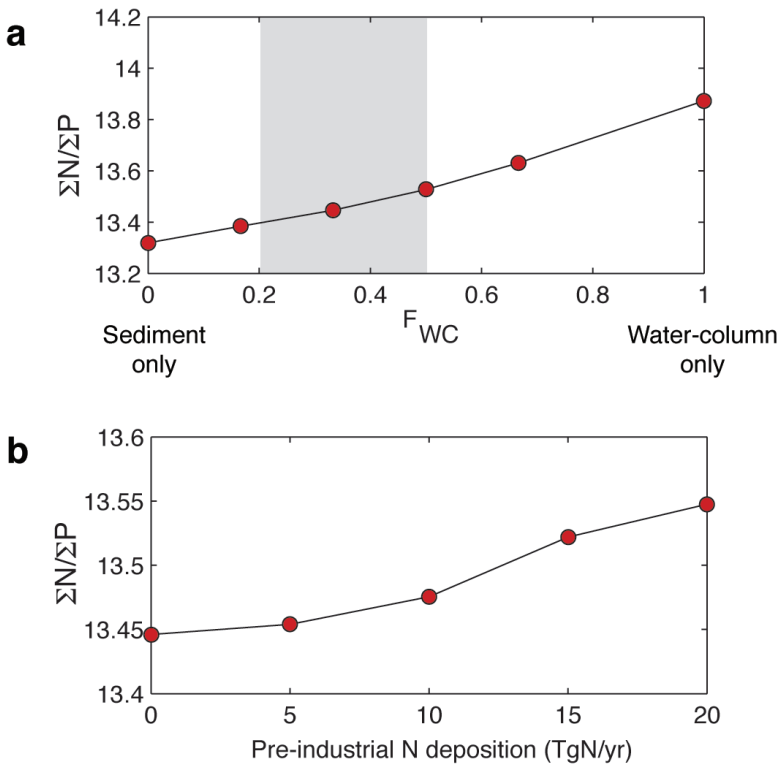

Figure 3.12. Sensitivity of N reservoir under Redfield conditions to other factors that might explain its low value. a Sensitivity to the partition of denitrification between water column and sediments. The shaded region represents isotopic constraints on F_{WC} – within this range, changes in the N reservoir are very small. b Sensitivity to additional N sources to the ocean, representing N deposition by lightning. These sources are considered to account for less than 20TgN/yr input in the pre-industrial era, and have little influence on ΣN/ΣP in our model.

CHAPTER 4

Local versus basin scale limitation of marine N_2-fixation

Abstract

Nitrogen (N) fixation by diazotrophic plankton is the primary source of this crucial nutrient to the ocean, but the factors limiting its rate and distribution are controversial. According to one view, the ecological niche of diazotrophs is controlled by the ocean, through internally generated N deficits that suppress the growth of their competitors. A second view posits control by the atmosphere, which restricts diazotrophs to regions where dust deposition satisfies their high iron requirement, thus segregating N sources from sinks. Here we use multiple geochemical signatures of N_2 fixation to show that the Fe-limitation of diazotrophs is strong enough to modulate the regional distribution of N_2-fixation within ocean basins – particularly the Fe-poor Pacific – but not strong enough to influence its partition between basins, which is instead governed by rates of N loss. This scale-dependent limitation of N_2 fixation reconciles local observations of Fe stress with inferred basin scale coupling of sources and sinks. Within the regime of intermediate Fe-control, the oceanic N reservoir would respond only weakly to the enhanced dust fluxes hypothesized for a glacial climate, but strongly to the reduced fluxes expected under anthropogenic climate warming.

4.1 Introduction

Over millennial timescales N_2-fixation replenishes the oceanic N reservoir, which is continually depleted by bacterial denitrification, maintaining the productivity of the ocean and its biological storage of carbon. The growth of diazotrophs and their ability to fix N_2 is sensitive to myriad environmental conditions (Karl et al 2002), but two are considered most important. First, a deficit of NO_3 in upwelling deep water is thought to favor diazotrophs by inhibiting their faster-growing competitors, who leave behind residual phosphate (PO_4) (Redfield et al 1963, Tyrrell 1999). Second, an abundant supply of trace metals – particularly Fe – that form cofactors to the nitrogenase enzyme is thought to be critical in sustaining rates of N_2-fixation (Falkowski 1997). These two hypotheses predict wildly different spatial patterns of N_2-fixation in the modern ocean, and imply opposing roles for the oceanic N cycle in the global climate system (Deutsch & Weber 2012, Gruber 2004).

Because windblown dust provides the primary conduit for Fe into the ocean, a strong Fe-dependence would produce N_2-fixation rates that mirror dust deposition, with highest values in the Atlantic and Indian basins (Mahowald et al 2006). This view is supported by the abundance of the important diazotroph *Trichodesmium* in the tropical Atlantic Ocean (Capone et al 2005, Moore et al 2009), and the global maximum of "excess" NO_3 observed in the underlying thermocline that has been attributed to remineralization of N-rich diazotrophs (Gruber & Sarmiento 1997, Hansell et al 2004). Furthermore, recent studies have uncovered molecular evidence for intensive Fe-

limitation of diazotroph growth in the Pacific Ocean, in which dust deposition is lowest. In contrast, a strong dependence on NO_3 scarcity should concentrate N_2-fixation in the Pacific Ocean, where recently denitrified waters upwell to the surface (Deutsch et al 2007).

Direct observations of N_2 fixation rates are still too sparse to discriminate between these possibilities (Luo et al 2012), especially in light of systematic underestimates of rates (Großkopf et al 2012) especially by unicellular cyanobacteria that dominate the diazotrophic community in the Pacific (Montoya et al 2004, Zehr et al 2001). While observations support a role for both Fe inputs and N losses in regulating marine N_2-fixation, the temporal and spatial scales at which they are expressed are poorly understood.

In this study, we used an ocean model combined with multiple geochemical quantities to constrain the relative influence of the supply of Fe and N deficits on rates and patterns of N_2-fixation.

4.2 Methods 1: ocean model

Our model simulates the growth of two phytoplankton groups on three nutrients (NO_3, PO_4 and Fe), source and sinks of fixed N, and the isotopic composition of NO_3, all in the context of a three-dimensional global circulation.

4.2.1 Circulation model

As in the previous study (Chapter 3), we used an Ocean General Circulation Model in which circulation is constrained to simultaneously satisfy both large-scale dynamical balances and hydrographic tracer observations (temperature, salinity, and ^{14}C) (DeVries & Primeau 2011). The majority of simulations employed a coarse configuration with horizontal resolution of 4°x4°, and 24 vertical layers including 2 in the top 75m. Simulations including a prognostic oxygen cycle (see below) were conducted in a finer configuration with horizontal resolution of 2°x2°. In all cases, annual-mean flow fields were extracted as a matrix (**A**), and biogeochemical simulations performed using the fast-spinup Transport Matrix Method (Khatiwala 2007).

4.2.2 Ecosystem model

We used the simple ecosystem model described by Weber & Destch (2012), and in Chapter 3 above. It simulates the cycles of PO_4 (P) and NO_3 (N), including dissolved organic matter dynamics, and contains "general" phytoplankton (O) and N_2-fixing diazotropic phytoplankton (F) that compete for resources. Modifications are described here, and new parameters listed in TABLE 1. The primary extension for this study is the addition of a prognostic Fe cycle (see below), in which Fe becomes a potentially limiting resource for plankton growth. The growth and mortality of the two plankton groups are thus governed by:

$$\frac{dO}{dt} = \mu_o \min\left(\frac{P}{P+K_P}, \frac{N}{N+K_N}, \frac{Fe}{Fe+K_{Fe}}\right) O - MO \quad (1)$$

$$\frac{dF}{dt} = \mu_F \min\left(\frac{P}{P+K_P}, \frac{Fe}{Fe+K_{Fe}}\right) F - MF \quad (2)$$

Here, μ_o and μ_F are the maximum growth rates of *O* and *F* respectively, as a function of ambient temperature and light conditions, and *M* represents phytoplankton mortality, including a quadratic term that scales with total biomass ($M = m_1 + m_2 B$, where $B = O + F$ and m_1 and m_2 are constants). Although this model lacks a representation of higher trophic levels, it was shown to accurately reproduce observed nutrient distributions and the broad biogeography of diazotrophic plankton, which are confined to warm oligotrophic subtropical gyre regions (Luo et al 2012). The elemental composition of non-diazotrophic phytoplankton is defined by the stoichiometric ratios R_O (N:P) and Q_O (Fe:P). Diazotrophs assimilate P and Fe in the ratio Q_F (Fe:P) and release NO_3 from newly fixed N, in a ratio R_F relative to PO_4 uptake. The majority of our simulations make the "Redfield assumption" (R_O=16 everywhere) for simplicity, but our results are tested for sensitivity to this parameter (Appendix 4A).

4.2.3 Denitrification

Because we intend to use tracer distributions to constrain the Fe limitation of N_2 fixation, we must ensure that other processes affecting these tracers are accurately represented. The most important of these processes is denitrification. As in Chapter 3, we impose the

pattern and rate of water-column denitrification derived from inverse model estimates of N losses (DeVries et al 2012a), with the Eastern Tropical North and South Pacific suboxic zones each contributing 25 TgN loss per year, and the Arabian Sea contributing 15TgN/yr (Fig. 3.1a). The distribution of benthic denitrification is governed by the flux of organic matter to the seafloor (Middelburg et al 1996), but rates are scaled to meet a specified global total (Fig. 3.1b). Because the global benthic flux is less well constrained, we conduct 4 simulations for each Fe-limitation scenario (i.e. each value of Q_F/Q_O), with total sediment N losses of 100, 140, 180 and 220 TgN/yr, bracketing the range estimated from observations (DeVries et al 2012b). Model results are presented as the average of this model ensemble, with inter-model standard deviation taken as an uncertainty estimate.

4.2.4 Fe cycle

We used the Fe cycle model described by Parekh et al (2004) and adapted for a three-dimensional global model by Parekh et al (2005), with minimal modifications. The conservation equation for the total dissolved Fe pool (Fe_T) is:

$$\frac{dFe_T}{dt} = AFe_T + J_{bio}(Fe_T) + S_{Fe_T} - J_{sc}(Fe) \qquad (3)$$

The second term represents the biological cycle of Fe_T, in which Fe is conserved but redistributed between the surface and the deep ocean by the biological pump. The uptake

and remineralization of Fe is controlled by the growth, mortality and Fe quotas of the two plankton groups:

$$J_{bio}(Fe_T) = -(Q_O J_{up,O} + Q_F J_{up,F}) + Q_{rem}(M(Q_O O + Q_F F)) \quad (4)$$

Here, $J_{up,O}$ and $J_{up,F}$ are the first terms on the RHS of Eqs. 1 and 2 respectively, and Q_{rem} is the remineralization operator as derived in Chapters 2 and 3.

In Eq. 3, S_{Fe} represents the sum of all sources of new dissolved Fe to the ocean. In this study, we consider windblown dust deposited on the surface ocean as the only major Fe source, although new evidence suggests that the release of soluble Fe from marine sediments may be an additional important source (Moore & Braucher 2008). The source of dissolved Fe is computed based on the distribution of dust deposition (J_{dust}) from an atmospheric modeling study (Mahowald et al 2006), assuming a constant fraction of Fe (f_{Fe}) in mineral dust, a constant proportion (α_{Fe}) of which is soluble in seawater:

$$S_{Fe} = f_{Fe}\alpha_{Fe}J_{dust} \quad (5)$$

The only modeled sink of Fe from the ocean as a whole is the scavenging of Fe onto sinking particles (the last term on the RHS of Eq. 3). However, this sink requires the simulation of a chemical system involving Fe-binding ligands that are dissolved in seawater. The total "dissolved" Fe pool is the sum of Fe that is bound to the ligand (L) in complexes (FeL), and "free" Fe (Fe'):

$$Fe_T = FeL + Fe' \quad (6)$$

Only free Fe is available for scavenging onto particles, which is represented as a first order removal:

$$J_{sc}(Fe) = k_{sc}Fe' \quad (7)$$

Since complexation occurs on very short timescales (relative to other processes represented in our model) the Fe-ligand system is assumed to go to equilibrium. The system can therefore be solved for Fe' by specifying the total ligand concentration (L_T = FeL+L'), and using the empirically-derived conditional stability constant for the reaction:

$$K_{FeL}^{cond} = \frac{[FeL]}{[Fe'][L']} \quad (8)$$

Because the distribution of Fe-binding ligands is poorly constrained, we take the approach of previous studies and assume a constant concentration, taking the value constrained using an inverse approach by Parekh et al (2004). Although this model of Fe cycling rests on a number of untested assumptions and poorly constrained parameters, it is able to capture the observed large-scale patterns in surface and intermediate-water dissolved Fe (Fig. 4.2).

The assumptions and deficiencies of the Fe-cycle model are explored further in Appendix 4A (sensitivity testing), and a study is proposed in section 4.7 (outlook) to address some of the uncertainties in this important elemental cycle.

4.2.5 O_2 cycle

A set of simulations was designed to test the effect of N_2-fixation on the distribution of water column denitrification between the Pacific and Indian Oceans, which can be compared to an observational constraint. In these model runs, the data-derived rates of water-column denitrification were replaced by a prognostic representation, necessitating

the simulation of dissolved oxygen (O_2). The O_2 cycle is simulated following standard OCMIP protocol:

$$\frac{dO_2}{dt} = AO_2 + K_W(O_{2,sat} - O_2) + r_{O:N}J_{bio,N} \quad (9)$$

Here, K_W is the piston velocity for O_2 gas exchange, $O_{2,sat}$ is the saturation O_2 concentration, $J_{bio,N}$ is the sum of biological production and remineralization N fluxes and $r_{O:N}$ is the ratio of oxygen production (or removal) to nitrate uptake (release) during organic matter production (remineralization). When the oxidant demands of remineralization would draw O_2 below zero, O_2 consumption is prevented and the residual oxidant demand is met through denitrification with the known stoichiometry of the net reaction, r_{den} = N-loss/N remineralization = 104/16 (Gruber & Sarmiento 1997).

To improve the representation of suboxic zones, simulations with the explicit O_2 cycle are conducted in a 2°x2° configuration of the observationally-constrained circulation model (DeVries et al 2012a). Uncertainty estimates were derived using two different transport operators, one of which employs an additional CFC-11 constraint, and by repeating our experiments with a longer DOM turnover timescale (TABLE 1).

4.2.6 ^{15}N cycle

In addition to nutrient concentrations, we simulated the isotopic distribution of NO_3 following the procedure described in (2012b). Each steady-state flux of N (J_N, including

biological uptake, reminearlization, N_2-fixation and benthic and water-column denitrification) is converted into a ^{15}N flux using a fractionation factor α:

$$J_{^{15}N} = \alpha \frac{^{15}N}{^{14}N} J_N \quad (10)$$

The governing equations for $^{15}NO_3$ and ^{15}DON are then cast in terms of the isotopic ratio $R = {}^{15}N/{}^{14}N$ producing a linear system that can be solved directly by matrix inversion for the steady state. These ratios are then converted into $\delta^{15}N$ values for comparison to observations, which are usually reported in this notation: $\delta^{15}N = (R_{sample} / R_{standard} - 1)*1000$, where the standard is atmospheric N_2. Because the degree of fractionation during certain process is still not accurately constrained, we perform a range of simulations with different values of the fractionation factor to quantify these uncertainties. See Table 4.1 for the enrichment factors (ε) we tested, which are related to fractionation factors by $\varepsilon=(1-\alpha)*1000$.

4.2.7 Fe-limitation scenarios

Simulations were designed to predict the steady-state patterns of N_2-fixation and geochemical tracers that are consistent with a wide range in the degree of Fe-limitation faced by diazotrophic communities. The Fe-dependence of diazotrophs was varied between simulations via the parameter Q_F, which determines the Fe quota required for their growth – as it increases they require more Fe and are more susceptible to Fe-limitation. Because the Fe quota of non-fixing plankton (Q_O) remains constant between

simulations, we distinguish our different model scenarios by Q_F/Q_O, which indicates the degree to which the diazotrophic Fe requirement exceeds that of the broader community. We vary this ratio over the interval $1 \leq Q_F/Q_O \leq 50$, which brackets the majority of laboratory observations.

Each simulation was brought to a steady state, defined as an N budget imbalance less than 1TgN/yr, taking around 10,000 model years. The model's Fe budget equilibrates on much shorter timescales of <1000yrs.

4.3 Methods 2: observational constraints

To determine the most likely degree of Fe control over diazotrophs in the modern ocean, we compared our different model predictions to a variety of geochemical quantities that are strongly influenced by N_2 fixation. Geochemical quantities provide the most appropriate metrics to test long-term regulation of N_2-fixation because they integrate its effect over time and space scales much longer than biological rate measurements. The diagnostics we employ are relatively insensitive to poorly constrained model parameters (see sensitivity testing, Appendix 4A), and are therefore robust indicators of the basin scale partition of N_2 fixation. Methods for calculating and comparing these metrics between observations and models are outlined below, and the results are discussed in section 4.4 (Fe-limitation regimes).

4.3.1 Pacific N* convergence

The Pacific Ocean receives the lowest Fe inputs of the three major basins, and is subject to the largest removal of fixed N through denitrification. The degree to which N_2-fixation is able to compensate N-losses within the Pacific is therefore a good indicator for the strength of Fe-limitation at the basin scale. The basinwide difference between N_2-fixation and denitrification must be balanced at steady state by an export of N deficits via ocean circulation, so can be inferred from the net transport convergence of N* into the basin (Deutsch et al 2001).

We placed an observational constraint on this quantity by computing the transport of observed N* in both directions across the gateways separating the Pacific from other ocean basins, which amounts to a series of matrix-vector multiplications using the Transport Matrix Method (Khatiwala 2007). For any gateway, the transport of N* into the Pacific (N^*_{conv}) can be computed as:

$$N^*_{conv} = \mathbf{A}_{IB}\mathbf{N}^*_B - \mathbf{A}_{BI}\mathbf{N}^*_B \quad (11)$$

Here, *I* is the indices of gridcells on the Pacific side (Inside) of the of the gateway, and *B* is the indices of gridcells on the on the other side (Boundary side).

Potential uncertainties in this calculation arise from three factors: (i) The nutrient data themselves; (ii) the model circulation fields; (iii) the precise geographic definition of the Pacific Ocean, which becomes important only if there is a strong N* gradient across the boundary regions. We used a Monte Carlo approach to account for these uncertainties, repeating the transport calculation while probing a pre-defined "parameter

space" for these three factors. Each iteration selects randomly from a set of three transport operators, randomly defines each Pacific Ocean gateway from a given latitude/longitude range, and produces a "realization" of the N* field by adding spatially-correlated noise to the observations.

Transport operators used in this calculation include (i) a higher-resolution (2°x2°) version of the observationally-constrained OGCM used in our ecosystem simulations (DeVries & Primeau 2011); (ii) a variation on this model that uses CFC concentrations as an additional constraint on circulation (DeVries et al 2012a); and (iii) annual-mean circulation fields from the 1°x1° observationally-constrained ECCO project model (Khatiwala 2007). Pacific Ocean gateways are defined as follows: The *Indonesian Throughflow* is a meridional transect between Australian and East Asian continents, varied between 113 and 117°E; The *Australian Antarctic Circumpolar Current* is a meridional transect between Australian and Antarctic continents, varied between 125 and 130°E; The *Drake Passage* is a meridional transect between South American and Antarctic continents, varied between 68 and 72°W. The *Bering Straight* is a zonal transect between Eurasian and North American continents, varied between 64-68°N.

Nutrient data realizations are constructed following the method described in DeVries & Primeau (2011). Briefly, each Monte Carlo simulation generates synthetic nutrient datasets by adding smoothed error fields to the objectively analyzed WOA09 climatology. Error fields are derived by taking a random draw from a Gaussian distribution with zero mean and variance estimated from the original dataset. This variance is taken as the sum of a contribution from the raw data (its standard error), and a

component associated with the objective mapping procedure (the difference between mapped data and raw data, averaged over each depth level). Error fields are then smoothed over a correlation length scale of 200km by solving a diffusion equation on the original data grid, and are finally interpolated onto the model grid. See DeVries & Primeau (2011) for full methods.

The Monte Carlo procedure was repeated 10,000 times to produce a probability density function for net Pacific N* convergence, although the PDF had converged after <5000 iterations. This PDF could then be compared to simulated values from our range of simulations, in which N* transport can be computed precisely without the iterative procedure (section 4.4).

4.3.2 Nutrient tracers

N_2-fixation leaves well-known regional signatures in the nutrient stoichiometry of the surface ocean, where diazotroph growth consumes "excess PO_4" (or $P^*=[PO_4] - [NO_3]/16$) (Deutsch et al 2007), and in the underlying thermocline, where the remineralization of their N-rich organic matter (Letelier & Karl 1998) releases an excess of NO_3 relative to PO_4, denoted N* ($N^* = [NO_3] - 16[PO_4]$) (Gruber & Sarmiento 1997). To use these tracers as constraints on the relative strength of environmental pressures on marine diazotrophs, we compared their concentration differences between a Fe-rich basin with little denitrification (North Atlantic Subtropical Gyre, NASG), and a Fe-poor basin with large denitrification zones (North Pacific Subtropical Gyre, NPSG).

We defined averaging masks to calculate representative tracer values NPSG and NASG to compare simulated tracer distributions to climatological observations from World Ocean Atlas 2009 (WOA09) (Garcia et al 2010). NPSG is defined as the oligotrophic North Pacific region where observed [NO_3] falls below 1μM, and bounded to the North by the 34psu isohaline, a proxy for the subtropical/subpolar front. NASG is defined as the oligotrophic North Atlantic region with observed [NO_3]<1μM, and bounded to the North by the 35.4psu isohaline (Fig. 4.3). Within these regions, simulated and observed P* is averaged over the top 75m (Fig. 4.4a), where primary production occurs in our model, and N* is averaged across the depth of the North Atlantic N* maximum (400-600m), which is interpreted as a signature of N_2-fixation in that basin (Fig. 4.4b). These basin-averages are denoted P^*_{NASG}, P^*_{NPSG}, N^*_{NASG} and N^*_{NPSG}. Their values are not strongly sensitive to small variations in the definitions of the averaging regions. We place error estimates on observed P^*_{NPSG}, P^*_{NASG}, N^*_{NPSG} and N^*_{NASG} by calculating these quantities for each month in the WOA09 monthly climatology and taking the standard deviation. These errors are then propagated into the calculation of interbasin differences, ΔP* and ΔN*, which are defined as:

$$\Delta P^* = P^*_{NPSG} - P^*_{NASG} \tag{12}$$

$$\Delta N^* = N^*_{NASG} - N^*_{NPSG} \tag{13}$$

These metrics of large-scale patterns in nutrient tracers provide a more robust constraint than the basin-mean values themselves. Although mean-ocean P* and N* do vary between Fe-limitation scenarios, they are also strongly sensitive to poorly-constrained

factors that regulate the ocean's N inventory whereas ΔP* and ΔN* are not (see Appendix 4A, sensitivity testing).

4.3.3 N isotopes

Newly fixed N released by diazotrophs has an isotopic composition very similar to atmospheric N_2, which has a $\delta^{15}N$ value of ~5‰ lighter than mean-ocean NO_3. The difference in $\delta^{15}NO_3$ between basins thus provides an additional geochemical constraint on the large-scale distribution of N_2-fixation. Because no climatological dataset exists for $\delta^{15}NO_3$ we used observations from individual studies at sites thought to be representative of the oligotrophic subtropical gyres. We used data from (Sigman et al 2009) from the Hawaii Ocean Timeseries (HOT) site in the central NPSG, and data from Knapp et al (2008) collected along transects in the Sargasso Sea close to the Bermuda Atlantic Timeseries (BATS) site (Fig. 4.3). These data are averaged over the shallow subsurface depth interval between 100-300m and reported with the standard error of the mean (Fig. 4.4c). Waters in this depth range should collect the isotopic signature of N_2-fixation while minimizing the influence of water column denitrification in the Pacific, which has a strong isotopic fractionation effect. Simulated $\delta^{15}NO_3$ is averaged from grid cells traversed by the Bermuda transect in NASG, and from the grid-cell containing the HOT site and its 8 lateral neighbors in NPSG. Simulated and observed $\delta^{15}NO_3$ are compared as interbasin differences, defined as $\Delta\delta^{15}N = \Delta\delta^{15}N_{HOT} - \Delta\delta^{15}N_{BATS}$.

4.3.4 Suboxic zones

As a final constraint, we look at the interbasin distribution of water column denitrification (WC), which is related to N_2-fixation through the sinking organic matter flux (see section 4.4, below). We quantify this as the fraction of total global WC that occurs in the Pacific Ocean suboxic zones (WC_{Pac}), rather than the Arabian Sea Suboxic Zone. It is calculated by integrating volumetric rates across the Pacific, and dividing by the global integral. This is then compared to the same diagnostic from an inverse model, in which denitrification rates were determined from several datasets, including excess-N_2 gas (DeVries et al 2012a).

4.4 Fe-limitation regimes

The changing patterns of N_2-fixation produced by raising Q_F/Q_O can be characterized as three distinct Fe-limitation regimes. When diazotrophs have similar Fe requirements to other phytoplankton ($Q_F/Q_O<5$, Regime 1) they grow successfully in any region with N-deficits strong enough to overcome their slower intrinsic growth rate. N_2-fixation is concentrated where denitrified waters are brought to the surface, and its partition between ocean basins closely resembles that of denitrification, with the Pacific contributing ~60%. Within the Pacific, N_2-fixation is focused towards the eastern and equatorial gyre margins, where strongly N-deficient waters upwell from suboxic zones (Fig. 4.5, 4.6a).

As the Fe requirement for diazotrophs rises ($5 \leq Q_F/Q_O \leq 25$; Regime 2), the distribution of N_2-fixation within the Pacific Ocean undergoes major reorganization. Diazotrophs are displaced from the Fe-poor eastern margin, and relocated westward within the subtropical gyres, where they are better fueled by dust from the East Asian and Australian continents. The proportion of total Pacific N_2-fixation found east of 160°W decreases from ~70% to ~40% over this regime, but the basin-scale rates remain relatively constant (Fig. 4.5, 4.6b). At even higher diazotroph Fe quotas ($Q_F/Q_O > 25$, Regime 3), their Fe demands cannot be met in the Western Pacific either, and N_2-fixation shifts out of the Pacific basin and into the Indian and tropical Atlantic oceans where Fe is more abundant. Its inter-basin partition diverges from that of N-losses and begins to resemble the distribution of atmospheric Fe inputs as Q_F/Q_O approaches 50 (Fig. 4.5, 4.6c).

The large-scale shifts in diazotrophic habitat induced by varying Fe limitation are associated with substantial changes in the geochemical quantities outlined in section 4.3. These predictions can be tested against established data to determine in which regime the modern ocean lies.

The most direct diagnostic of the basinwide rate of N_2-fixation is the degree to which it compensates basin-scale N losses. Under the weak to intermediate Fe-limitation of Regimes 1&2, N_2-fixation is able to closely balance denitrification to within ±5TgN/yr in the Fe-poor Pacific Ocean (Fig. 4.7a). In response to the strong Fe-limitation of Regime 3, N_2-fixation in the basin falls short of denitrification, with imbalances exceeding 20TgN/yr at $Q_F/Q_O > 30$ and approaching 50TgN/yr in the most Fe-limited

scenarios. The difference between biological sources and sinks of N must be balanced by a net export of N deficient water from the basin of similar magnitude, to close its N budget (Fig. 4.7a). The transport of a nitrate deficit into/out of the real Pacific Ocean can be directly estimated by summing the physical convergence of observed N* ($N^* = [NO_3] - 16[PO_4]$) across all of its boundaries (Deutsch et al 2001), accounting for uncertainty in ocean circulation and nutrient observations. The suite of 10,000 Monte Carlo calculations described in section 4.3.1 finds a transport convergence of just 1.3±14.7TgN*/yr into the Pacific, indicating a close balance between denitrification and N_2-fixation in the basin. When results are separated between the three ocean circulation models used, each one finds a net N* that is not significantly different from zero (Fig. 4.9). Our model is only compatible with this observation-based estimate in the low and intermediate Fe-limitation regimes (Fig. 4.7a).

The stoichiometric tracers N* and P* reveal striking differences between a Fe-rich basin with little denitrification (NASG), and a Fe-poor basin with large denitrification zones (NPSG). For a given denitrification rate, these tracer differences predominantly reflect the spatially and temporally integrated rates of N_2-fixation, making them a strong constraint on its distribution.

When N_2-fixation is weakly constrained by Fe (Regime 1), excess PO_4 is fully consumed by diazotrophs in all oligotrophic waters, so simulated surface P* is close to zero in both the North Atlantic and North Pacific Subtropical Gyres (NASG, NPSG respectively). Its basin scale difference ($\Delta P^* = P^*_{NPSG} - P^*_{NASG}$) is ~0μM, lower than the observed value of 0.09±0.04μM (Fig. 4.7b) computed from a monthly nutrient

climatology (Garcia et al 2010). As Q_F/Q_O increases through Regime 2, P* begins to accumulate in the eastern NPSG, fueling diazotroph growth downstream in the central and western gyre. Its basin difference reaches agreement with observations in the range $15<Q_F/Q_O<25$. Once Fe-scarcity precludes complete P* utilization even in the Western Pacific (Regime 3), it accumulates rapidly in the NPSG and simulated ΔP* diverges sharply from observations. As Q_F/Q_O is raised, the interbasin difference in thermocline N* ($\Delta N^* = N^*_{NASG} - N^*_{NPSG}$) exhibits similar behavior to ΔP*, increasing gradually through Regime 2 and sharply in Regime 3, departing significantly from observations at $Q_F/Q_O>30$ (Fig. 4.7c). The stoichiometric differences between Atlantic and Pacific Ocean, from surface and thermocline waters, both constrain the modern ocean to lay in the intermediate Fe-limitation regime.

The Fe-induced shifts in diazotroph habitat also alter large-scale patterns of organic matter export, and thus the relative rates of denitrification among different suboxic zones. As Q_F/Q_O is raised, diazotroph communities become increasingly separated from the low-O_2 waters of the Eastern Pacific, and eventually relocate towards corresponding waters in the Indian Ocean (Fig. 4.6). In simulations with prognostic rather than prescribed denitrification rates (see SOM), the accompanying shift in subsurface respiration from the Pacific to Indian Oceans decreases the fraction of global water column denitrification that occurs in the Pacific Ocean (WC_{Pac}) from ~90% at $Q_F/Q_O=1$ to ~40% at $Q_F/Q_O=50$ (Fig. 4.7d). Consistent with previous constraints, WC_{Pac} matches the observation-based estimate of 75±6% (DeVries et al 2012a) only in Regime 2.

Due to data paucity and uncertainty in model fractionation factors, $\delta^{15}NO_3$ provides a much weaker constraint on N_2-fixation than other tracer-based diagnostics. However, the observed gradient in shallow subsurface $\delta^{15}NO_3$ between HOT (Pacific) and BATS (Atlantic) of 2.3±0.7‰ is most compatible with our simulations when $Q_F/Q_O \leq 30$ (Fig. 4.8), supporting the conclusion drawn from the stronger constraints, above.

In summary, the intra-basin reorganization of N_2-fixation associated with an intermediate degree of diazotroph Fe-limitation (Regime 2), brings model predictions into closest agreement with the suite of observational constraints. In contrast, the interbasin shifts accompanying the transition to Regime 3, representing strong and widespread Fe-limitation, lead to a rapid violation of those constraints. These qualitative results are robust against other factors that influence diazotroph growth, stoichiometry and Fe-limitation (see Appendix 4A. sensitivity testing).

4.5 Local vs. basin-scale limitation

Within the second Fe-limitation regime, where observational constraints place the modern ocean, the proximal factors limiting diazotroph growth vary between ocean basins. N_2-fixation is locally limited by PO_4 throughout most of the Atlantic and Indian oceans, as indicated by low resource limitation factors (γ) for P relative to Fe ($\gamma_{Fe}/\gamma_P > 1$, Fig. 4.10a). In these regions, diazotrophs can obtain sufficient Fe to completely utilize the

excess PO_4 in upwelling water, either because atmospheric Fe inputs are large or because subsurface P* is scarce due to low NO_3 removal. In contrast, diazotroph communities in much of the low-latitude Pacific Ocean are subject to intensive Fe-limitation ($\gamma_{Fe}/\gamma_P<1$, Fig. 4.10a), and experience P-limitation only at the poleward and western margins of the subtropical gyres. Across vast areas of the tropics and eastern subtropics, N_2-fixation is inhibited or excluded in high-PO_4 surface waters of the Pacific due to Fe-scarcity, which results from low dust deposition rates and the upwelling of old waters with a long history of Fe-scavenging. In these regions, small-scale Fe additions, simulated by instantaneously increasing the atmospheric supply to a single surface gridcell by 1gFe/m^2/yr, can promote local diazotroph blooms and enhanced carbon drawdown (Fig. 4.10b).

The regulation of N_2-fixation rates by Fe inputs does not translate to larger spatial scales however. When the Fe supply is enhanced across the entire Pacific Ocean (agin by 1gFe/m^2/yr), N_2-fixation is stimulated in the strongly Fe-limited eastern and equatorial Pacific (Fig 4.10a), but diazotroph growth along these margins strips excess PO_4 from waters that flow westward across the basin and feed into the subtropics. Consequently, diazotroph communities that were fueled by shallow downstream PO_4 transport become starved of this nutrient, suppressing N_2-fixation throughout much of the subtropical gyres (Fig. 4.11a). Just a few decades after the onset of Fe fertilization, the reduced fixation rates in those downstream environments almost entirely offset the regional gains from fertilization (Fig. 4.11b). Thus, in the intermediate Fe limitation regime, Fe fertilization can redistribute N_2-fixation within the Pacific Ocean, but cannot raise its basin-wide rate,

which already balances N-losses within the Pacific (Fig. 4.7a) and is thus constrained by the production of N deficits through denitrification.

Taken together, our results can reconcile direct observations of Fe-limitation of diazotroph growth (Chappell et al 2012), with geochemical evidence for a spatial coupling of N sources and sinks (Deutsch et al 2007). The key distinction is that Fe-limitation operates at the scale of plankton communities, and even over larger biogeographical provinces, but does not control the partition of N_2-fixation between ocean basins. The Pacific Ocean contributes ~60% of global N_2-fixation despite receiving low Fe-inputs relative to the Indian and Atlantic oceans. At the basin scale, rates of N_2-fixation largely mirror the interbasin of denitrifrication, reflecting a mechanistic coupling of N sources and sinks over that scale.

4.6 Implications

A spatial proximity of diazotroph habitats to N removal has been assumed to imply stronger feedbacks regulating the N reservoir over time. We tested this assumption by simulating the response of N_2-fixation to the climatically forced variations of water-column denitrification inferred over both glacial and modern periods (Altabet et al 1995, Deutsch et al 2011). Within the intermediate regime of Fe-control implied by observational constraints, an instantaneous doubling of denitrification in suboxic zones is counteracted fast enough by N_2-fixation to limit oceanic N-loss to <10% of its current

reservoir, before a new steady state is reached (Fig. 4.12a). New N-deficits generated by enhanced denitrification in the Pacific are transported only through shallow circulation pathways before being counteracted by N_2-fixation within the basin. In order for such changes to significantly impact the N reservoir, new N deficits generated in the Pacific must penetrate the deeper ocean and traverse sluggish circulation pathways before they are compensated in the dustier Atlantic and Indian Oceans. This occurs only in the strong Fe-limitation regime (Fig. 4.12a), well outside the plausible range of tracer constraints (Fig. 4.7).

It has also been hypothesized that global N_2-fixation is itself subject to climate-forced variations in the Fe supply, in which enhanced dust fluxes associated with climate cooling are argued to stimulate N inputs to the ocean (Broecker & Henderson 1998, Falkowski 1997). However, because Fe additions are unable to raise N_2-fixation rates at the basin scale under contemporary Fe-limitation conditions (Fig. 4.11a), the potential of this mechanism to change the global N inventory is limited (Moore & Doney 2007). Raising global Fe inputs to the ocean by up to five times the modern rate allows for no more than a 5% increase in the N reservoir (Fig. 4.12b), even with the altered dust distribution inferred for the LGM (Mahowald et al 2006).

However, the N reservoir's stability under dustier climate regimes is in stark contrast to its behavior when dust deposition is reduced. As the Fe supply falls below its modern rate, the Pacific Ocean is soon unable to support enough N_2-fixation to balance its N losses, resulting in a sustained reduction in N_2-fixation rates and a substantial global N loss before reaching a new steady state. When atmospheric Fe sources are lowered to

25% of modern values, over 40% of oceanic fixed N is lost (Fig. 4.12b) and export production is reduced by a corresponding factor. These results raise the possibility that reduced dust fluxes expected under a warming climate (Mahowald et al 2006) could trigger a large-scale suppression of marine N_2-fixation, weakening the biological carbon pump.

4.7 Summary and outlook

This study investigated the relative importance Fe inputs from the atmosphere, and N-deficits produced through denitrification within the ocean, in limiting marine N_2-fixation. This is a critical question in determining whether the oceanic N inventory is modulate over millennial timescales by external forcings or buffered and regulated by stabilizing internal feedbacks. Simulations with varying degrees of Fe-limitation in diazotrophs showed that observed tracer constraints can only be reproduced when Fe limitation is strong enough to regulate the distribution of N_2-fixation within ocean basins, particularly in the Pacific where inputs are lowest. However, these constraints are rapidly violated when Fe-limitation becomes strong enough to redistribute N2-fixation between ocean basins, forcing it out of the Pacific and into the Atlantic and Indian Oceans where Fe is abundant. Therefore, although diazotroph growth may be limited by Fe at the community scale throughout most of the Pacific, its basin-scale rates are determined by the distribution of denitrification. N deficits produced through denitrification are thus

compensated over the short timescales of shallow circulation, and not exported to other basins through deep-ocean pathways. These findings have two important implications:

- The internal feedback of N_2-fixation on forced changes in denitrification operates quickly in the modern climate regime, because N anomalies can confined to the upper ocean. Variations in denitrification therefore have limited potential for changing the oceanic N reservoir.
- The response of N_2-fixation to external forcing of the Fe supply is complex and non-linear. Under the modern climate regime, enhanced Fe inputs can only redistribute N_2-fixation within ocean basins, with little influence on the N reservoir. However, reduced Fe inputs rapidly shift the ocean towards a strongly Fe-limited state, suppressing N_2-fixation throughout the Pacific and leading to significant N loss from the ocean.

The picture that emerges is of an oceanic N reservoir that must be strongly buffered to forcings associated with a cooling climate regime, such as during glaciations. Even if cooling resulted in reduced denitrification as hypothesized, N_2-fixation must have compensated that change over short timescales. Similarly, additional N_2-fixation stimulated in the Pacific by enhanced Fe inputs would have been compensated on short timescales by reduced fixation in other parts of the same basin. Climate warming is hypothesized to weaken Fe inputs to the ocean. Our simulations reveal that the resultant reduction in Pacific N_2-fixation would only be compensated over long timescales in other ocean basins.

However, a number of remaining uncertainties limit our ability to predict the response of N_2-fixation to anthropogenic climate warming. First, changes in rates and distribution of Fe-deposition are still debated. The warmer, moister climate should suppress Fe transport to the ocean (Mahowald et al 2006), whereas land use changes are predicted to have an opposite effect (Jickells et al 2005). Second, the ocean's internal Fe cycle is still not well understood. The parameters that control the Fe-ligand complexation system in current models are poorly constrained, and other processes are often neglected. Most important may be the release of Fe seafloor sediments, which has the potential to buffer Fe availability against variations in the atmospheric source. However, its modern rates and environmental sensitivities are unknown. A new study using an inverse method and a recent Fe data compilation (Moore & Braucher 2008) is being planned by the author to address these issues.

Finally, this chapter demonstrated that the strength of N_2-fixation feedback in response to external forcing can be understood by the distances and timescales over which N anamolies are compensated. Compensation within ocean over shallow circulation pathways results in strong feedbacks that minimize changes in the N reservoir, whereas the transport of N anomalies through the deep ocean over longer timescales weakens the feedback. This suggests that much can be learned about other feedbacks in the N cycle by examining the timescales on which they operate, and the factors that determine them. The next chapter of this dissertation will focus on understanding these timescales, and seeing what constraints they place on N reservoir changes.

Appendix 4A: Sensitivity testing

We tested the sensitivity of our primary results to those features of the model that might affect the distribution of N_2-fixation and the tracer constraints we employ. Specifically, we wish to ensure that the appearance of three distinct Fe-limitation regimes is robust, and that observations are always most consistent with the second regime, in which Fe controls the distribution of N_2-fixation within ocean basins, but not between them. We considered the following factors:

Variable R_O: For simplicity, we assumed a constant N:P requirement (R_O) of 16:1 in non N_2-fixing plankton in our primary simulations. However N:P uptake ratios vary between marine biomes according to the dominant plankton taxa (Martiny et al 2013, Weber & Deutsch 2010), and these variations are important in regulating the NO_3 content of the ocean as a whole (Weber & Deutsch 2012). We tested the sensitivity of our results to large-scale variations in R_O by repeating our simulations using the parameterization of ref. (Weber & Deutsch 2012), where community N:P is linked to the relative abundance of diatoms as gleaned from the silicic acid distribution. The competition between diazotrophs and high N:P plankton in this configuration raises the ocean's N reservoir, increasing global-mean NO_3 and N*, and reducing mean P*.

However, variable R_O has little effect on the changing patterns of N_2-fixation and accompanying tracer patterns produced by strengthening Fe-limitation. N_2-fixation transitions out of the Eastern Pacific and then the Pacific Ocean as a whole at similar

values of Q_F/Q_O to our default simulations, and ΔP* and ΔN* exhibit similar trends, increasing gradually in Regime 2 and sharply in Regime 3 (Fig. 4.13a-c). These inter-basin tracer differences thus provide robust constraints on the large-scale distribution of N_2-fixation, that are independent of factors controlling their mean concentrations. Simulations with variable R_O again reach best agreement with observed ΔP* and ΔN* constraints within the intermediate regime of Fe-limitation, in which Fe controls N_2-fixation locally, but not at the basin scale.

Growth rate handicap: In our default simulations, we assumed the intrinsic energetic expenditure associated with N_2-fixation (represented by a reduced maximum growth rate) to be relatively low, taking $\mu_F/\mu_O=0.9$. Therefore, the total competitive handicap faced by diazotrophs in our model is mostly associated with their heightened Fe requirements (at least when $Q_F/Q_O>1$). We tested whether a stronger 'intrinsic' handicap would affect our results by repeating our experiments but taking $\mu_F/\mu_O=0.7$ (Fig. 4.13d-f). Their reduced growth rate made it easier for Fe-limitation to exclude diazotrophs from regions with low dust deposition when their Fe requirements were raised, causing transitions between Fe-limitation regimes to occur at lower values of Q_F/Q_O. The interbasin shift of N_2-fixation from the Pacific towards the Indian and Atlantic Oceans now commences at Q_F/Q_O between 10 and 20, rather than at ~25 in our default simulations. However, the range of Q_F/Q_O in which model is consistent with observed ΔP* and ΔN* is also shifted correspondingly lower. In other words, even though the Fe-limitation regimes have been

shifted with respect to Q_F/Q_O, observations still support the regime of intermediate Fe-limitation in which denitrification and N_2-fixation remain coupled at the basin scale.

Diazotroph N/P: In our default simulations, diazotrophs are assumed to fix 50 moles of new N for each mole of P assimilated, corresponding to a high biomass N:P ratio (R_F), consistent with observations (LaRoche & Breitbarth 2005). It might be hypothesized that changing the ratio between PO_4 uptake and new NO_3 introduced through N_2-fixation would influence the simulated distribution of P* and N* tracers. To test the sensitivity of our results to this factor, we repeated our experiments but with R_F increased to 100, at the upper end of N:P ratios observed in diazotrophs (Karl et al 1992). However, this modification had little influence on the distribution of N_2-fixation or the Atlantic to Pacific difference in P* and N*, which again support the intermediate regime of Fe-limitation. Deutsch et al (2007) showed that because the majority of newly fixed N quickly becomes accessible to the broader community, increasing R_F allows for additional consumption of PO_4 by non-fixing phytoplankton, which in turn inhibits diazotroph growth. Therefore the net N_2-fixation achieved per unit of PO_4 drawdown is largely independent of R_F, explaining why surface ΔP^* is not sensitive to this parameter in our model. The lack of sensitivity in thermocline ΔN^* is probably explained by the relatively small fraction of newly fixed N that is exported from the surface ocean (10% in our model).

Fe-limitation scheme: Because this study aims to constrain the net influence of Fe on N_2-fixation, and not specific Fe-cycle processes or parameters, our main conclusions are independent of the exact treatment of the Fe cycle. To demonstrate this, we conducted a series of experiments that employed the much simpler parameterization of diazotroph Fe-limitation used by refs. (Somes et al 2010, Weber & Deutsch 2012). Instead of explicitly simulating dissolved Fe, the Fe-dependence of diazotroph growth is represented by scaling their maximum growth rate by the distribution of dust deposition onto the surface ocean. The scaled maximum growth rate (μ'_F) is given by:

$$\mu'_F = \mu_F \frac{J_{dust}}{J_{dust} + K_{dust}} \tag{14}$$

where J_{dust} is the dust flux from the atmosphere and K_{dust} is constant that determines the strength of this scaling, i.e. determines the degree to which μ'_F varies between regions of high and low dust deposition. Raising K_{dust} in this configuration is therefore the equivalent of raising Q_F/Q_O in the explicit Fe-cycle mode, and the three familiar regimes of Fe-limitation arise as before (Fig. 4.14). With K_{dust} between 0 and 0.02g/m^2/yr, the interbasin spread of N_2-fixation mirrors that of denitrification with ~60% occurring in the Pacific, and the majority found close to the Eastern upwelling zones (Regime 1). Between $0.02<K_{dust}<0.2$g/m^2/yr, N_2-fixation shifts towards the Western Pacific (Regime 2), and at higher values it shifts out of the Pacific and into the dustier basins (Regime 3). Within these regimes, simulated ΔP^* and ΔN^* exhibit similar behavior to their

counterparts in the explicit Fe-cycle model, and once again their comparison to observations supports the intermediate Fe-limitation regime, in which denitrification and N_2-fixation are coupled at the basin scale. These results suggest that any representation of Fe-limitation that captures the asymmetry in Fe supply between basins will lead to the same conclusions reached in this study.

Parameter	Definition	Units	Value or range
f_{Fe}	Fraction of Fe in mineral dust	unitless	0.035
α_{Fe}	Soluble fraction of Fe	unitless	0.01
β_{Fe}	Ligand binding strength	$(\mu MFe)^{-1}$	10^{5}
[L]	Fe-binding ligand concentration	μM	10^{-3}
k_{sc}	Scavenging rate of free Fe	day^{-1}	$1.1*10^{-3}$
Q_O	Fe:P ratio for non-diazotrophs	mmol/mol	0.47
Q_F	Fe:P ratio in diazotrophs	mmol/mol	0.47-23.5
ε_{WC}	Isotopic enrichment factor for water column denitrification	‰	25
ε_B	Isotopic enrichment factor for benthic denitrification	‰	0
ε_F	Isotopic enrichment factor for N_2-fixation	‰	0
ε_{prod}	Isotopic enrichment factor for nitrate assimilation	‰	5
ε_{prod}	Isotopic enrichment factor for remineralization	‰	0
$r_{O:N}$	O_2:N ratio in production/remineralization	unitless	9.3
r_{den}	NO_3 consumption: remineralization ratio in water column denitrification	unitless	7
ϕ_{DOM}	Fraction of plankton organic matter to DOM	unitless	0.1
τ_{DOM}	Turnover time of DOM	years	1 (1-2 in O_2 simulations)

Table 4.1 Parameters of the ecosystem/biogeochemical model. Other parameters are as in (Weber & Deutsch 2012).

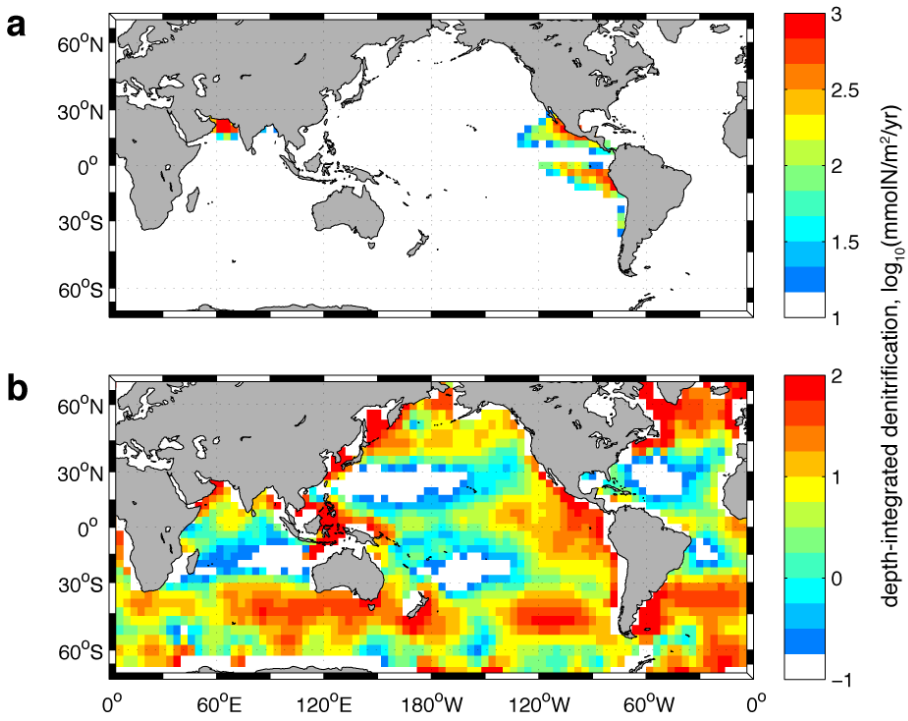

Figure 4.1 Model denitrification rates integrated over depth. **a,**Water column denitrification is distributed between the Eastern tropical North and South Pacific (25TgN/yr) and the Arabian Sea (15TgN/yr) **b,** Benthic denitrification is distributed based on the flux of organic matter to the seafloor, but is scaled to maintain a specified global rate, here 140TgN/yr.

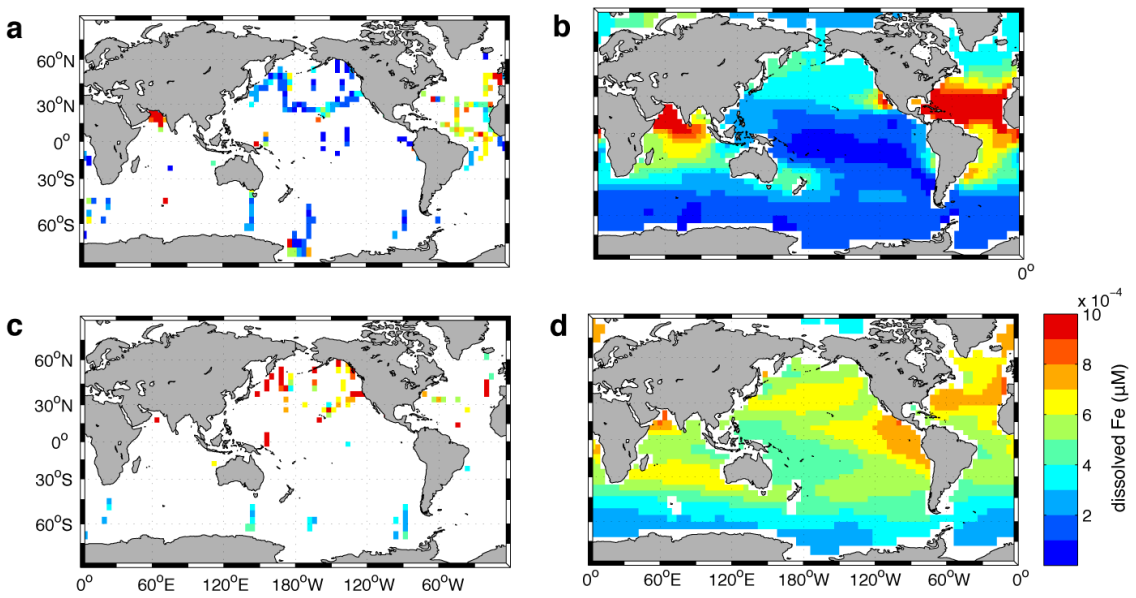

Figure 4.2 Dissolved Fe (free+complexed) distribution at the surface (**a,b**) and 1000 m (**c,d**) from observations (**a,c**) and simulations with $Q_F/Q_O = 20$ (**b,d**). **a,** Observed surface dissolved Fe largely mirrors the distribution of mineral dust deposition, with the highest concentrations in the tropical Atlantic and Indian Ocean. **b,** Simulated surface Fe reproduces these interbasin variations. **c,** The dominant pattern observed in intermediate waters (800-1100m) is a Northwards increase in all basins, with lowest values in the Southern ocean. **d,** Again this pattern is well reproduced in the model, although simulated concentrations in the North Pacific are somewhat low, possibly due to a missing source of Fe released from sediments.

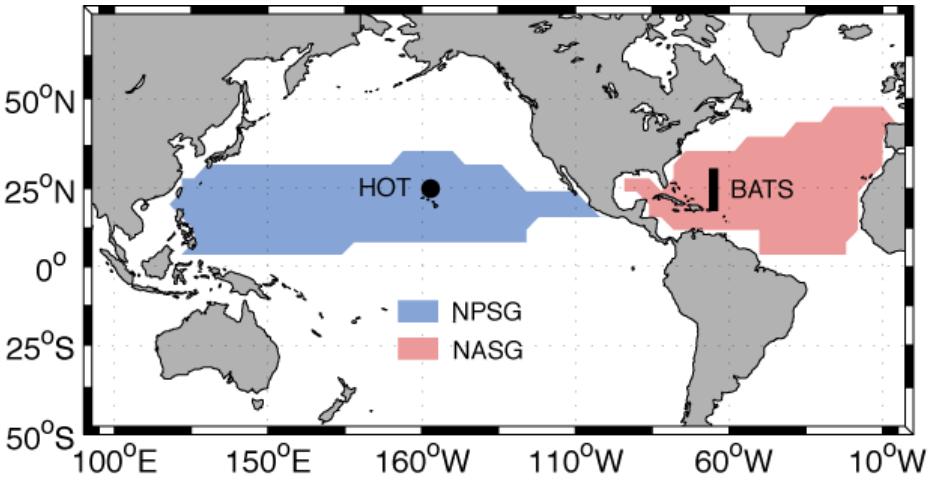

Figure 4.3 Locations for comparison to observational constraints. Simulated and observed climatological P* and N* are averaged across the shaded regions, representing the North Pacific (blue) and North Atlantic (red) Subtropical Gyres, to compute the interbasin tracer gradients we use as constraints. For $\delta^{15}NO_3$, these gradients are computed from individual localities – the HOT site in NPSG (black dot), and the Bermuda transect proximal to the BATS site in NASG (black line).

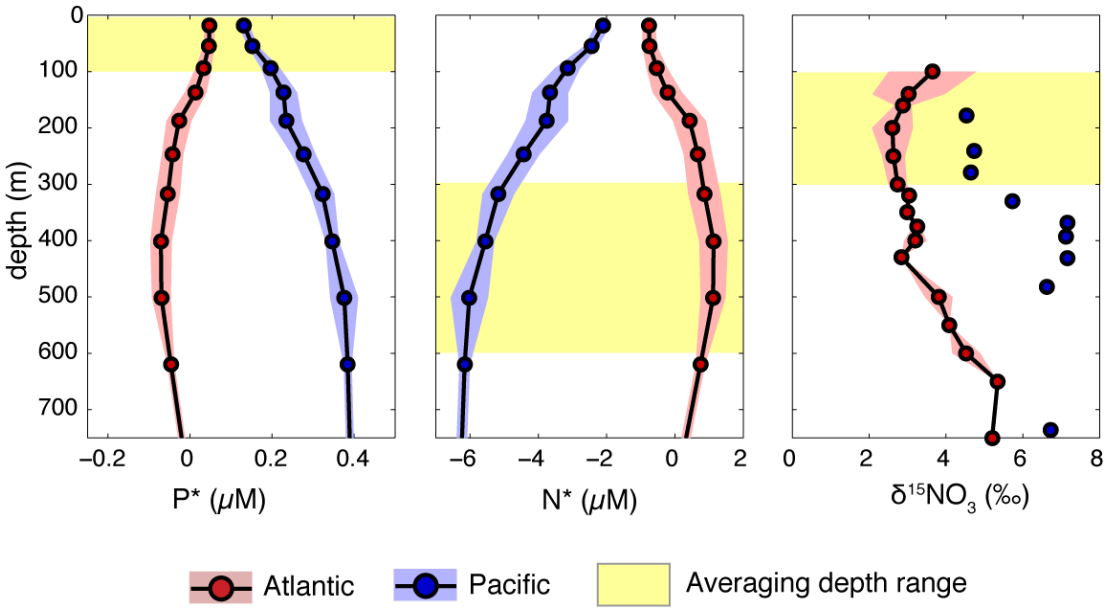

Figure 4.4 Observed tracer profiles (for regions shown in Fig. S5), showing depth ranges over which interbasin gradients are computed. **a,** P* profiles for NPSG and NASG. ΔP^* ($P^*_{NPSG} - P^*_{NASG}$) is calculated in surface waters (<75m), where nutrient uptake occurs in our model. **b,** N* profiles for NPSG and NASG. ΔN^* ($N^*_{NASG} - N^*_{NPSG}$) is calculated across the depth of the prominent N* maximum in the Atlantic Ocean (400-600m). **c,** $\delta^{15}NO_3$ profiles from HOT and BATS. $\Delta\delta^{15}NO_3$ is calculated in shallow subsurface waters (100-300m), which accumulate the isotopic signature of N_2-fixation.

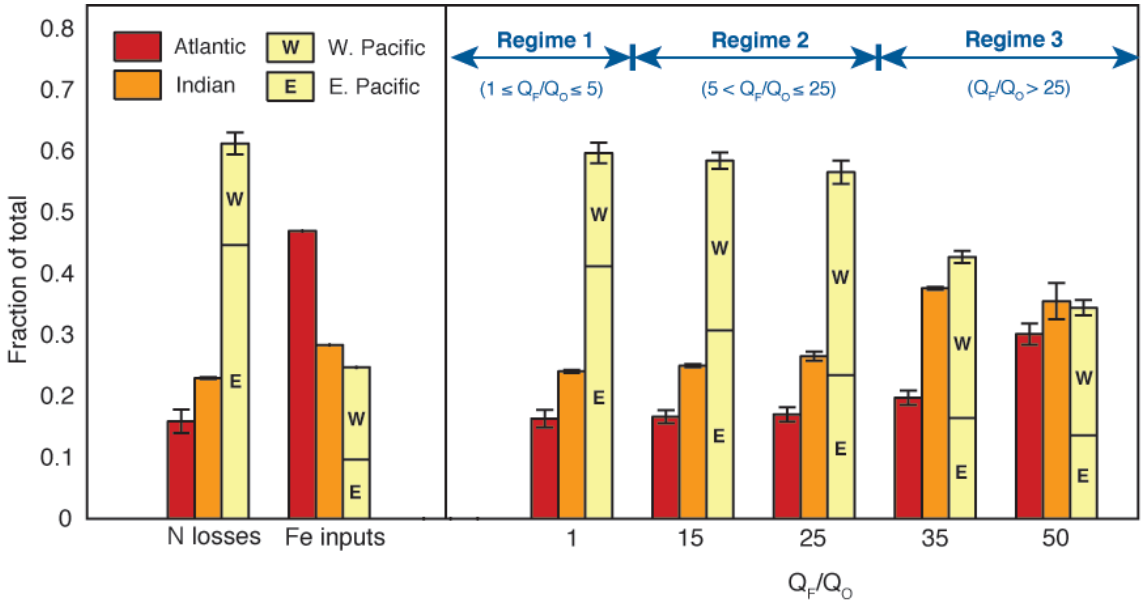

Figure 4.5. Distribution of simulated N_2-fixation (right hand side) and its environmental stimuli (left hand side). Basin-integrated rates are given as a fraction of the global total. N-losses comprise water column and benthic denitrification, which are prescribed using data-constrained estimates from inverse models. Fe inputs to the surface ocean are based on dust deposition rates predicted in an atmospheric model. The N_2-fixation distribution varies as diazotroph Fe requirements (Q_F) are raised relative to the fixed Fe requirement of other plankton (Q_O). Bar heights and errorbars for N-loss and N_2-fixation represent average and standard deviation across four model scenarios with different global rates of benthic denitrification (100, 140, 180, 220TgN/yr), which bracket the observationally-constrained range; The contribution of the Pacific to each process is divided between Western and Eastern portions, separated along 160°W.

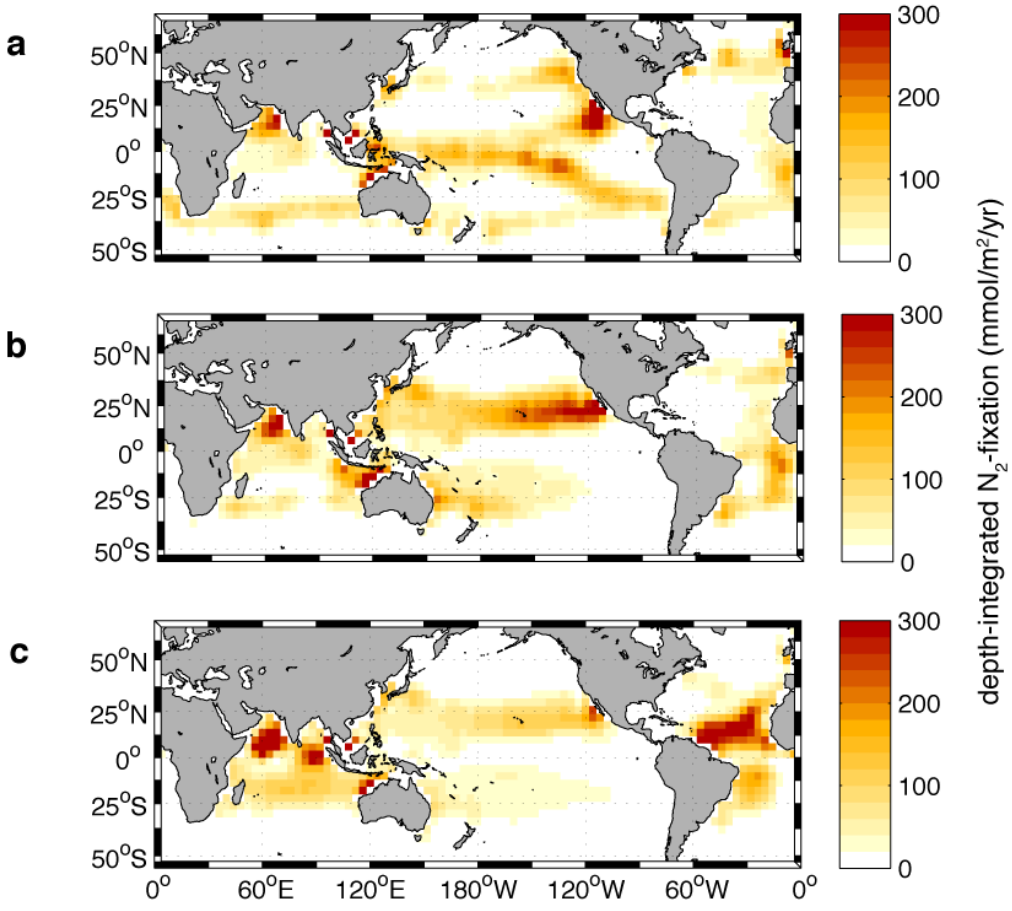

Figure 4.6 Distributions of N_2-fixation under the three Fe-limitation Regimes. **a,** Regime 1 (Q_F/Q_O=1), in which the large-scale distribution of N_2-fixation closely mirrors that of denitrification, and concentrates towards upwelling zones where N-deficient waters reach the surface. **b,** Regime 2 (Q_F/Q_O=20), in which N_2-fixation becomes more separated from the Eastern denitrification zones in the Pacific Ocean, but its interbasin spread remains unchanged from Regime 1. **c,** Regime 3 (Q_F/Q_O=50), in which Fe-limitation reduces N_2-fixation within the Pacific Ocean as a whole, and its interbasin distribution begins to mirror that of the atmospheric Fe source.

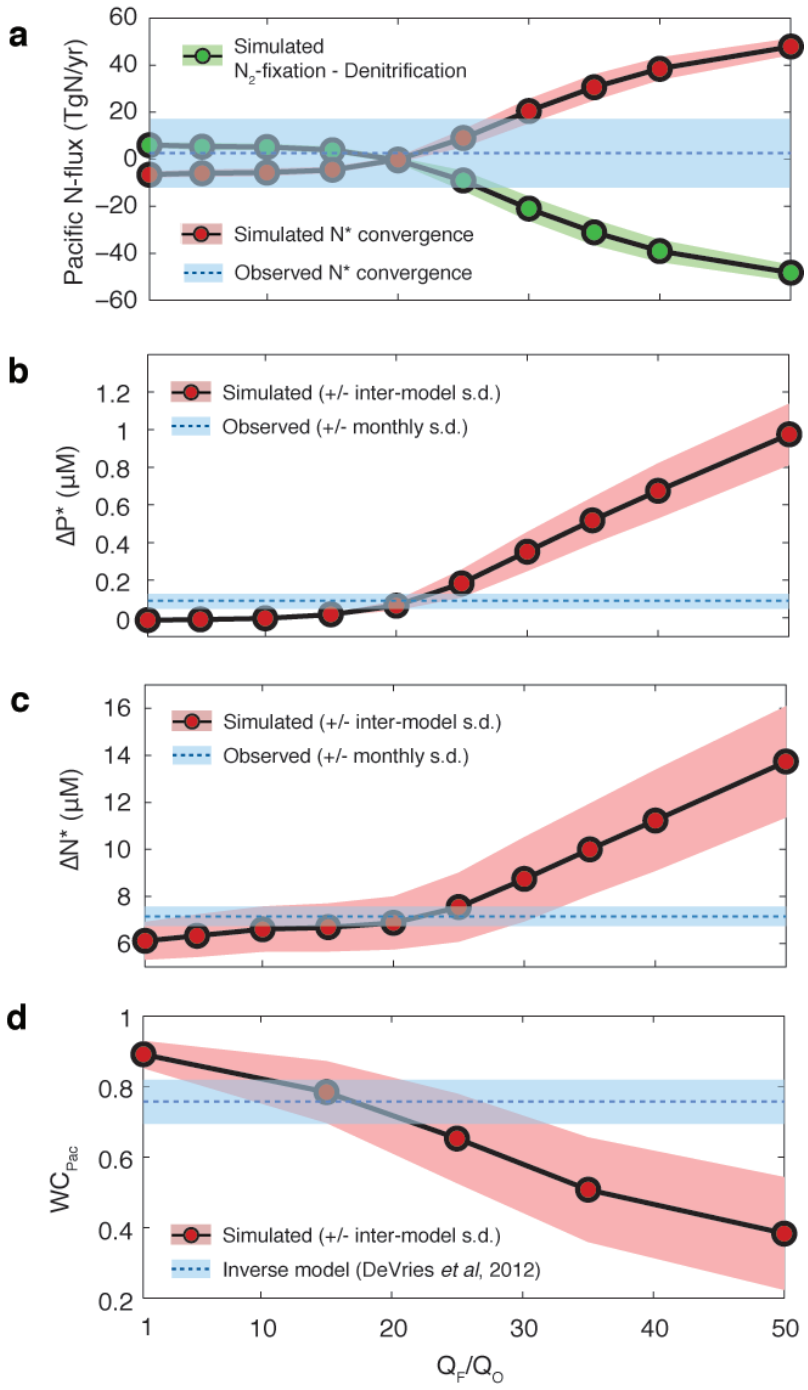

Figure 4.7. Geochemical constraints on the N_2-fixation regime of the modern ocean. Simulated quantities from model Fe-limitation scenarios are compared to observations (blue bars). **a,** N budget of the Pacific Ocean: the basin-scale difference between N_2-

fixation and denitrification (green dots) is balanced by a transport convergence of N* into the Pacific (red dots). Observational constraint applies to transport component, and gives mean and standard deviation of 10,000 Monte Carlo calculations of observed N* convergence in an ensemble of three circulation models (Fig. 4.9). **b,** Difference in surface P* ($[PO_4]$-$[NO_3]/16$) and **c**, difference in thermocline N* ($[PO_4]$-$[NO_3]/16$) between North Pacific and North Atlantic Subtropical Gyres ($\Delta P^*=P^*_{NPSG}–P^*_{NASG}$; $\Delta N^*=N^*_{NASG}–N^*_{NPSG}$). Observed values are computed from WOA09 annual-mean climatology with error envelopes representing standard deviation between months in the monthly climatology. In **a**-**c**, simulated values and error envelopes represent mean and standard deviation of four benthic denitrification scenarios for each Q_F/Q_O. **d,** Fraction of global water-column denitrification confined to the Pacific Ocean (WC_{Pac}) in simulations with explicit O_2-cycle. Simulated values represent mean and standard deviation of four simulations with different transport models and DOM parameterizations; observational constraint is from an inverse model calculation.

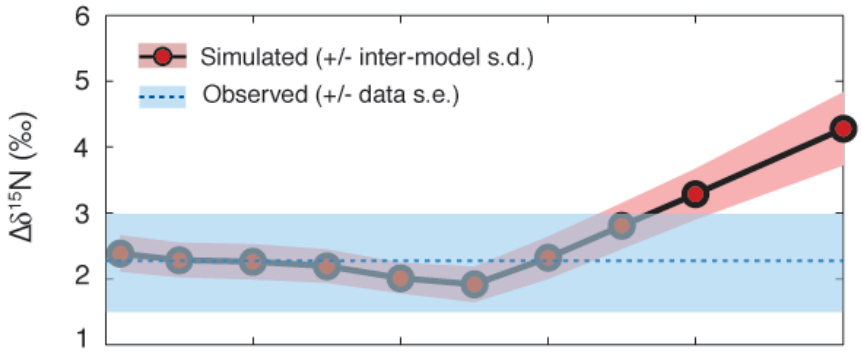

Figure 4.8. Isotopic constraint on Fe-limitation of N_2-fixation. $\Delta\delta^{15}N$ quantifies the isotopic difference between shallow subsurface waters in the North Pacific and North Atlantic subtropical Gyres, based on the representative HOT and BATS locations ($\Delta\delta^{15}N_{HOT}$ - $\Delta\delta^{15}N_{BATS}$). Simulated values and error envelopes represent mean and standard deviation from four benthic denitrification scenarios. The data constraint is derived from the mean and standard error of observations from individual studies at the two sites, rather than climatological data. Due to the paucity of data, the observed value is subject to large uncertainty and is thus a weak constraint on Q_F/Q_O, excluding only the most strongly limited cases ($Q_F/Q_O>40$) in which N_2-fixation is strongly focused in the tropical Atlantic Ocean.

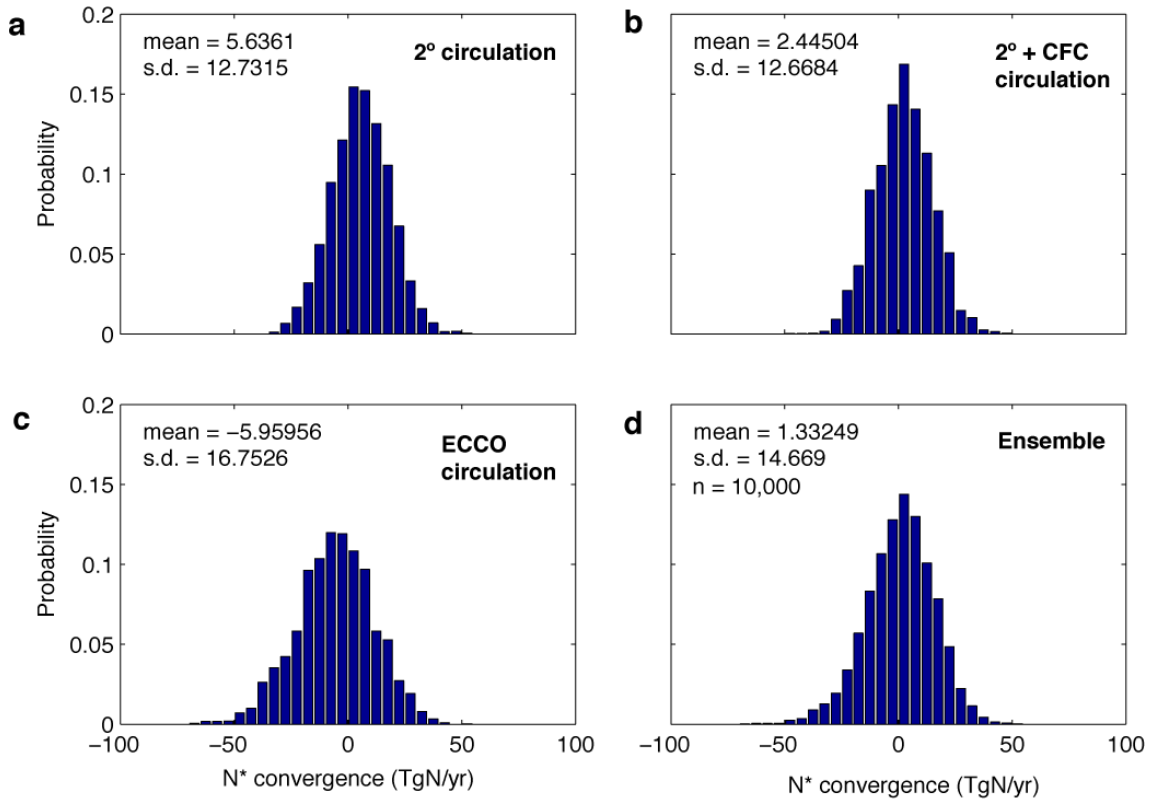

Figure 4.9 Probability density functions for transport convergence of observed N* into the Pacific Ocean, calculated in three circulation models with errors propagated from the nutrient data. PDFs are shown for individual circulation models: **a,** 2° observationally-constrained circulation model; **b,** A second configuration of the 2° model with added CFC constraint; **c,** Annual-mean circulation from the ECCO project model. **d,** PDF from the ensemble of 3 models, from which the range reported in Fig. 4.7a is derived.

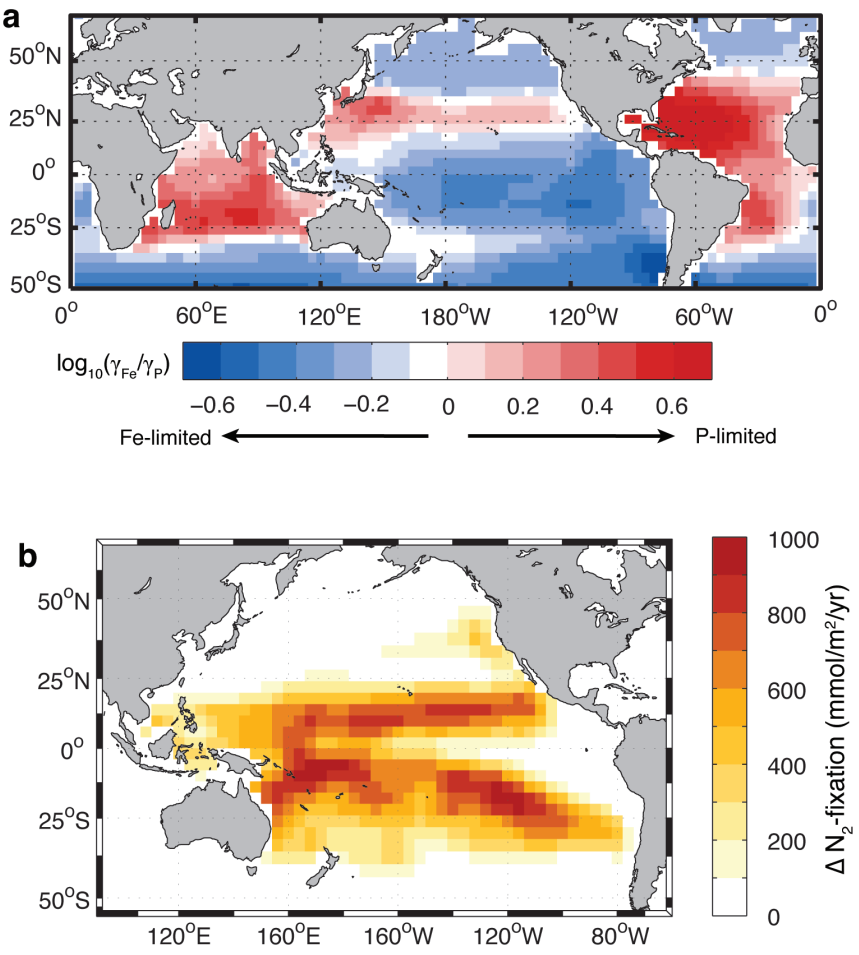

Figure 4.10 Local-scale limitation of N_2-fixation rates under modern-ocean conditions (Q_F/Q_O=20). **a**, Comparison of nutrient limitation factors for model diazotrophs: γ_{Fe}=Fe/(Fe+K_{Fe}), γ_P=PO_4/(PO_4+K_P), where K_{Fe} and K_P are half-saturation constants for diazotroph growth on Fe and PO_4 respectively. Values of $\log_{10}(\gamma_{Fe}/\gamma_P)$ separate regions where diazotrophs are Fe-limited (negative) and PO_4-limited (positive).**b,** N_2-fixation stimulated by local Fe fertilization in the Pacific Ocean. The value in each grid cell represents the increase in column-integrated N_2-fixation at that locality (relative to default simulation, with Q_F/Q_O=20) 1yr after the Fe supply to that grid-cell (and no others) is enhanced by 1gFe/m^2/yr. Regions in which diazotroph growth is initially Fe-limited (**a**) exhibit large increases in N_2-fixation, as diazotrophs rapidly consume the excess PO_4 that has accumulated in those surface waters.

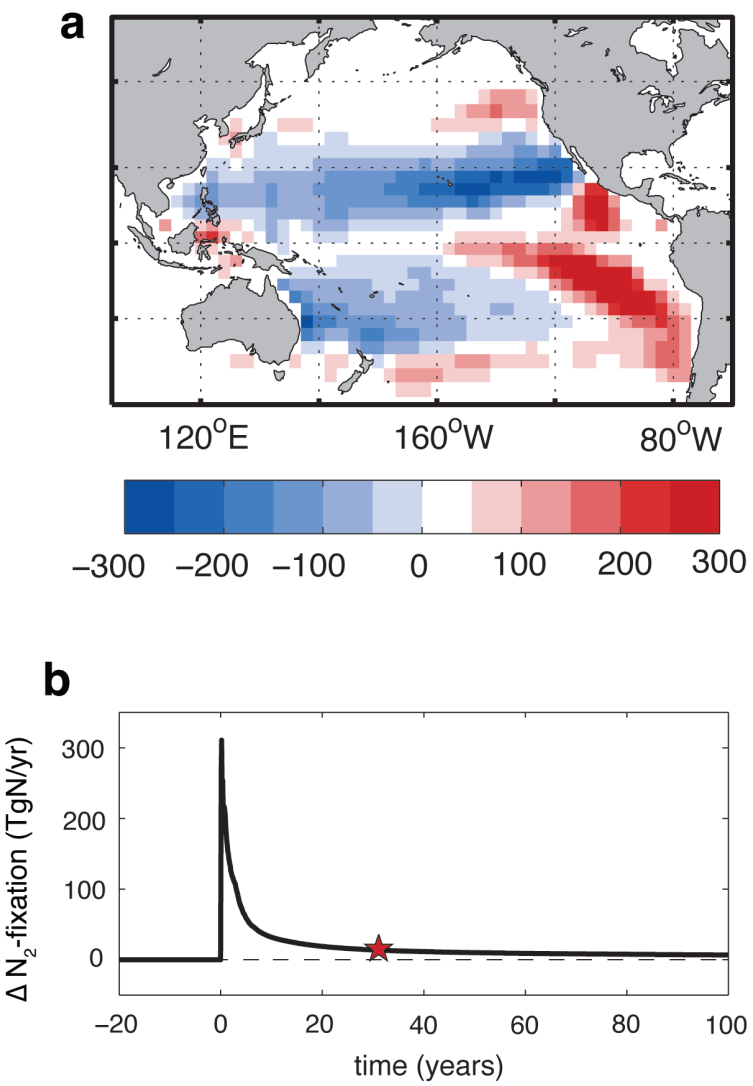

Figure 4.11 Basin-scale limitation of N_2-fixation. **a** Change in column-integrated N_2-fixation 30yrs after the atmospheric Fe supply is raised by 1g/m^2/yr across the Pacific. Regions in which N_2-fixation is raised (positive) are almost exactly offset by those where it is lowered (negative), yielding a net increase less than 10TgN/yr after 30yrs of fertilization (**b**). **b** Shows the basin-scale N_2-fixation anomaly (above previous steady-state value), star shows time point at which **a** is drawn.

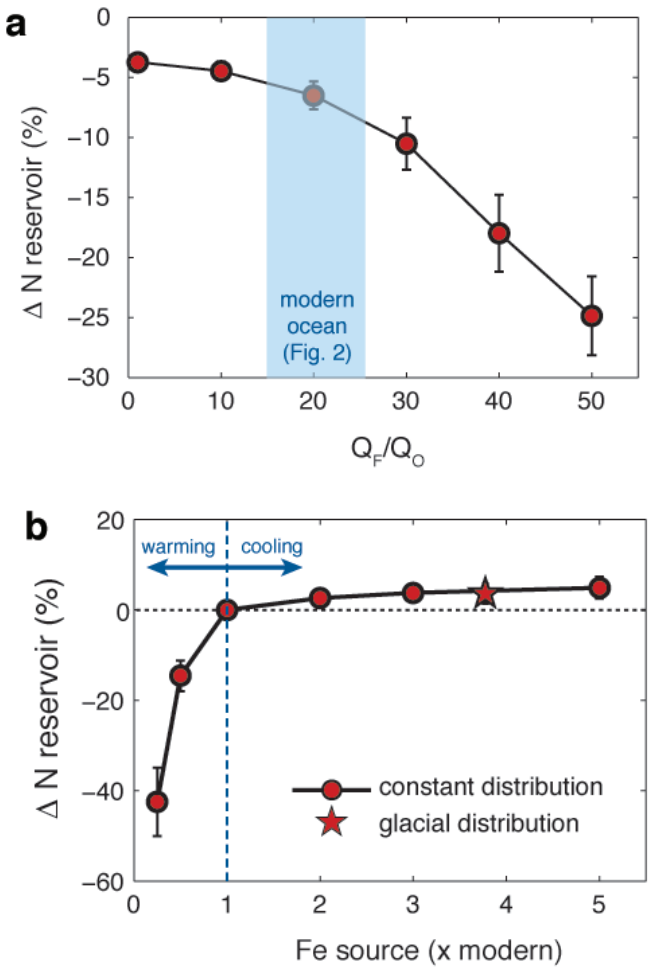

Figure 4.12 Sensitivity of the ocean N reservoir to climate forcing. a, Change in steady-state N reservoir following a doubling of global water-column denitrification, as a function of diazotroph Fe-limitation regimes. Blue band indicates the range of Q_F/Q_O allowed by modern-ocean constraints. b, Change in N reservoir induced by altering Fe inputs to the ocean, for Q_F/Q_O=20. Glacial simulations use dust deposition fluxes predicted for the Last Glacial Maximum, others scale the modern distribution by a constant factor. In a&b, simulated values and error bars give mean and standard deviation of four benthic denitrification scenarios.

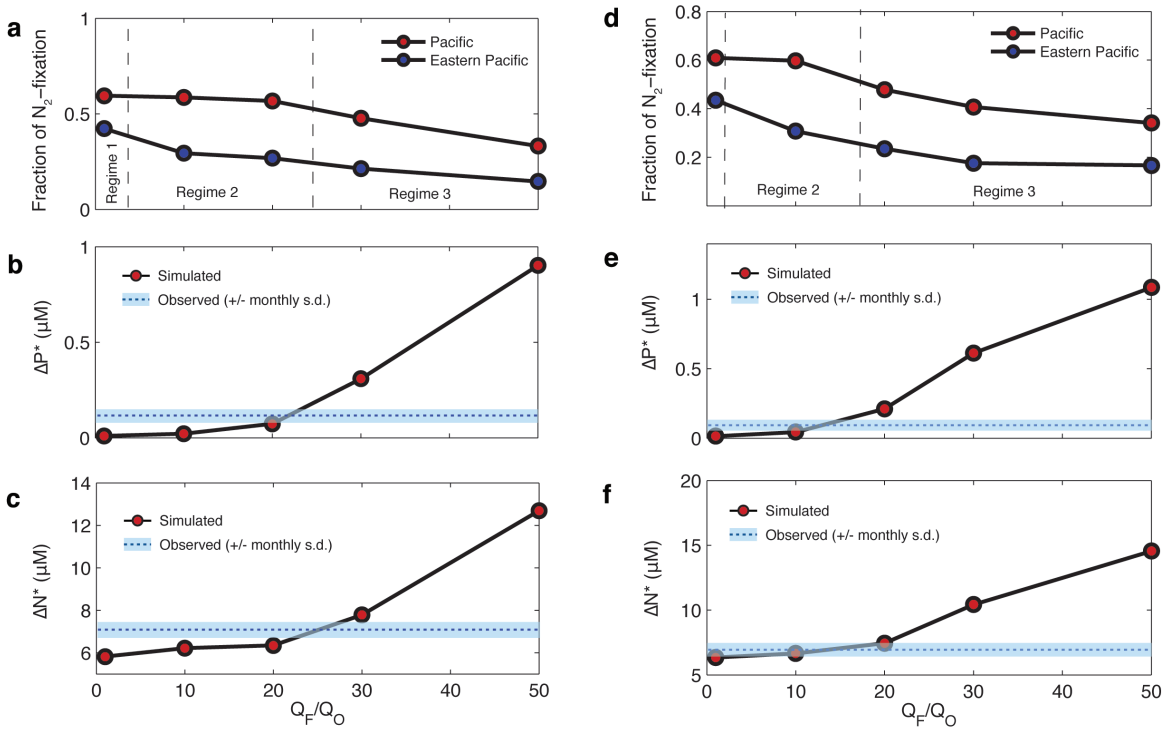

Figure 4.13. Sensitivity testing to factors that control competition between diazotrophs and non-fixing plankton: **a-c** N:P ratio of non-fixing plankton and **d-f** growth rate handicap of diazotrophs. **a,d** Contribution of Pacific and Eastern Pacific to global N_2-fixation, **b,e** surface P* constraint and **c,f** thermocline N* constraint.

a With variable R_o the model reproduces the same large-scale changes observed in our default simulations, at similar values of Q_F/Q_O **b&c**, Predicted tracer distributions are again most consistent with observed ΔP* and ΔN* constraints when Q_F/Q_O falls between 20 and 25, corresponding to Regime 2. Note the lack of error bars on simulated values, as only one benthic denitrification rate was tested here.

d, When μ_F is reduced, similar shifts in the large-scale N_2-fixation distribution are observed, but the transitions occur at lower values of Q_F/Q_O, reflecting the increased susceptibility of diazotrophs to Fe-limitation due to their lower growth rate. **e&f** Again, the model is only in agreement with observed ΔP* and ΔN* when Fe-limitation produces a westward shift of N_2-fixation within the Pacific, but is not strong enough to force it from the basin as a whole.

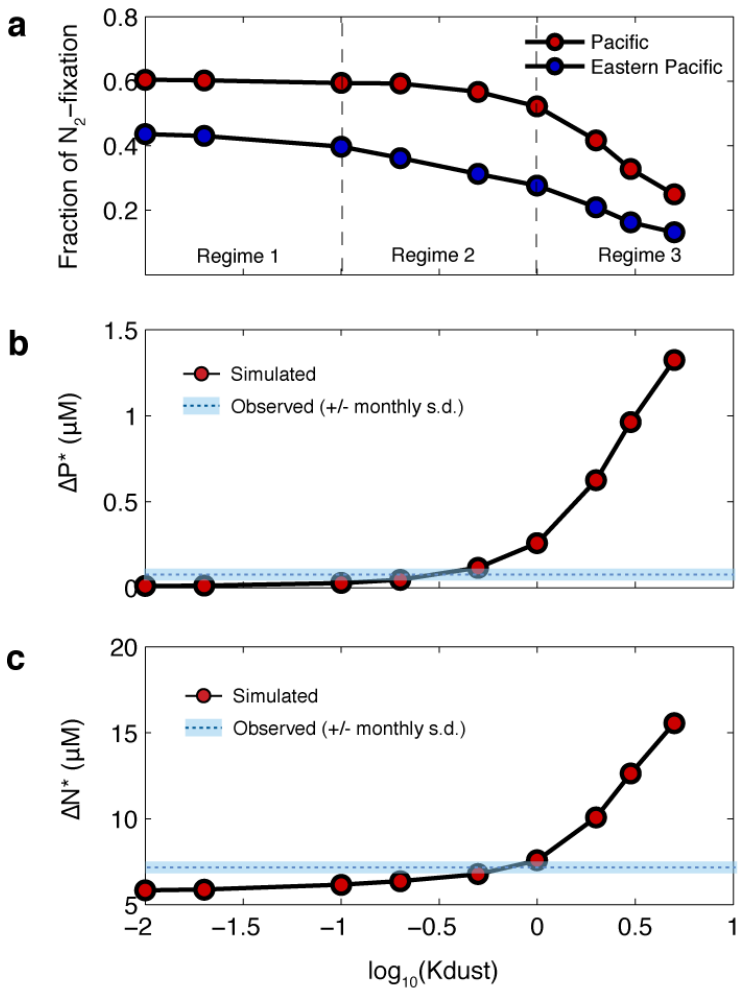

Figure 4.14 Sensitivity testing to representation of Fe-limitation, in which the explicit Fe-cycle of default simulations is switched for a simpler parameterization that scales atmospheric dust fluxes. **a,** Strengthening this scaling (i.e. raising K_{dust}) produces the same patterns of N_2-fixation as the explicit model. The ΔP* (**b**) and ΔN* (**c**) constraints again support the intermediate Fe-limitation regime, where Fe limitation dictates the distribution of N_2-fixation within the Pacific, but not its interbasin spread.

CHAPTER 5

Understanding feedback timescales in the ocean N cycle

Abstract

The ocean's dominant sources and sinks of fixed nitrogen (N) – N_2-fixation and denitrification – are subject to external forcings that push the N budget out of balance. At the same time, negative feedbacks couple those fluxes to the fixed N reservoir itself, and strive to restore a balance. The stability of the N reservoir is governed by the magnitude of forcings on the N budget, and the timescales over which the restorative feedbacks operate. We show that feedback responses comprise two components that operate over very different timescales: (i) a rapid response, occurring on timescales of decades to a few hundred years, in which the feedback damps N anomalies transported through the upper ocean and (ii) a gradual damping, on millennial timescales, of anomalies that pass through the deep ocean. The millennial damping timescale is set by the removal efficiency of upwelling anomalies by the feedback, whereas the partition between short and long modes reflects the probability of forced anomalies leaking into the deep ocean, controlled by the coupling of forcing and feedback regions. By diagnosing these properties in a linearized ocean biogeochemical model, we show that the feedback through N_2-fixation is strongest, as it minimizes leakage into the deep ocean and damps

deep anomalies on the shortest timescales. This feedback is sufficient to prevent significant perturbation of the N reservoir, unless N_2 fixation is strongly limited by Fe.

5.1 Introduction

Fixed nitrogen limits primary production and organic carbon export throughout the majority of the global ocean. The oceanic N reservoir is thus the primary factor controlling the strength of the biological carbon pump – one of the processes that maintains a strong gradient of dissolved inorganic carbon between the surface and the deep ocean, sequestering carbon out of contact with the atmosphere. Owing to its leverage over the ocean-atmosphere partition of CO_2, the N reservoir has been identified as a potential driver of long-term climate change (Galloway et al 2004).

Because the major N sources and sinks – N_2-fixation and denitrification – are linked through negative feedbacks, the oceanic N budget is continually restored towards a balanced state (Gruber 2004). Any variation in the N reservoir thus requires an external forcing on the budget to upset this balance. Forcing mechanisms have been identified for each N budget process, which may operate on millennial and shorter timescales. N_2-fixing plankton (diazotrophs) have a high requirement for iron (Fe), which is supplied to the ocean from land via windblown dust (Falkowski 1997). This supply is sensitive to climatic factors including the extent of desert regions, wind patterns and the hydrological cycle, which favor greater Fe inputs under cold dry climate regimes (Lambert et al 2008,

Mahowald et al 1999). On the other hand, water column and sediment denitrification rates are strongly dependent on thermocline oxygenation and sea level respectively, both linked to global temperature and climate (Christensen et al 1987, Ganeshram et al 1995).

The ability of these forcings to raise and lower the ocean's N reservoir and carbon storage is governed by the timescale over which they can maintain an imbalance in the ocean's N budget, before internal feedbacks restore a steady state. For a forcing on one N-budget flux, this feedback may be achieved both through a self-damping of the forced flux, and a compensating adjustment of the other fluxes. In both cases, the feedback manifests through the sensitivity of N budget fluxes to the N reservoir itself. A higher N reservoir stimulates productivity and the rain of organic matter into suboxic zones and onto the seafloor, increasing water-column (WC) and benthic (B) denitrification; an N replete ocean also selects against diazotrophic plankton and reduces N_2-fixation (F). Each response would act to curtail an initial increase in the N reservoir.

Attempts have been made to quantify feedback responses to specific climate forcings using data constraints, most notably for the last deglaciation when isotopic records suggest a strong climate forcing on WC (Deutsch et al 2004, Eugster et al 2013). However, no general framework exists to explain the timescales over which feedbacks operate, and the role of ocean circulation in setting those timescales is particularly poorly understood. This study aims to build a mechanistic understanding of the factors governing feedback timescales, and the relative strengths of the three feedback processes in response to various forcings.

5.2 Conceptual model

The dynamics of the ocean N reservoir in response to external forcing can be summarize by the simple conceptual model:

$$\frac{d\bar{N}'}{dt} = f(t) - \lambda\bar{N}' \quad (1)$$

Here, $\bar{N}$ represents the mean-ocean concentration of fixed N (mainly NO_3), and $\bar{N}'$ represents a perturbation to that mean. Perturbations are produced through a time-varying external forcing $f(t)$ on the N budget, which may act on any N budget process. The forced imbalance is then compensated through negative feedbacks, driven by the sensitivity of N budget processes to the N reservoir, represented by the damping of N perturbations: $-\lambda\bar{N}'$. Assuming a simple step forcing of amplitude A ($f(t) = A$), that is applied instantaneously at t=0, N perturbations accumulate over time following:

$$\bar{N}' = \frac{A}{\lambda}(1 - e^{-\lambda t}) \quad (2)$$

until a steady state is reached in which the accumulation of anomalous N has given rise to feedback processes large enough offset the forcing:

$$\bar{N}' = \frac{A}{\lambda} = A\tau, \ \ \tau = 1/\lambda \quad (3)$$

The susceptibility of the total N pool to temporal change is thus dependent upon the amplitude of forcings on its budget, and the characteristic timescale τ over which restorative feedbacks operate (Fig. 5.1). For forcing amplitudes >100TgN/yr, only feedbacks that operate on timescales shorter than ~1000 years will prevent significant

(>10%) variations in the N reservoir. Should these feedbacks operate over timescales much longer than 1000yrs, smaller forcings will be sufficient to generate large N perturbations. Because a perturbation to the N reservoir must simultaneously invoke a response from each N budget process, its damping rate may be the thought of as the sum of contributions from WC, B and F: $\lambda = \lambda_{WC} + \lambda_B + \lambda_F$. It follows that whichever process operates on the shortest timescale (largest λ) will act as the strongest feedback on a given perturbation.

In order to characterize these timescales, it will be useful to separate the three feedbacks and examine the response of each, in isolation, to various forcings. The separation is first performed in a three-dimensional ocean ecosystem-biogeochemical model, which is used to conduct simulations with single active feedbacks under idealized forcings. This model is then simplified through linearization to draw analogy to a hierarchy of box models and derive a mechanistic understanding of feedback timescales.

5.3 Feedback timescales in an ecosystem-biogeochemical model

In this part of the study, we use the ecosystem-biogeochemical model described in Chapters 3 and 4 (Weber & Deutsch 2012), coupled to a coarse-resolution, observationally constrained ocean circulation model (DeVries & Primeau 2011). The model simulates the cycles of PO_4, NO_3, Fe, dissolved organic matter, and contains a "general" non-fixing class of phytoplankton, and a diazotrophic class, which compete in

the upper 75, of the water column. Initial simulations are conducted under the "most likely" Fe-limitation scenario of Chapter 4, in which diazotrophs require ~20 times more Fe than non-fixing plankton.

5.3.1 Model spinup

The model was spun up with all feedback processes operative. Water column denitrification is simulated based on the remineralization of organic matter in observed suboxic zones, using the standard stoichiometry for NO_3 removal to remineralization (Gruber & Sarmiento 1997); benthic denitrification is governed by the flux of organic matter onto the seafloor, using the data-constrained relation of (DeVries et al 2012b); N_2-fixation is determined by competitive dynamics between diazotrophic and non-fixing plankton, and confined it to oligotophic subtropical gyres where diazotrophs thrive. The model is integrated to a steady state is reached, in which N_2-fixation balances the two denitrification sinks to within 1TgN/yr, which takes ~5,000yrs. At steady state, the model has WC, B and F rates of 70, 120 and 190TgN/yr respectively.

5.3.2 Separation of feedbacks

We separate the three feedbacks in our model, such that each further simulation contains a single *operative* feedback associated with one N budget process, while the two

remaining N budget processes are held constant. For WC and B this is achieved by decoupling their rates from organic matter remineralization, holding them constant to rates in the spinup. For F this is achieved by 'killing' the model diazotroph (μ_F=0), and simulating N_2-fixation as a constant source of N, with rate and distribution taken from the spinup.

5.3.3 Forcings

We perform simulations with three idealized forcings, representing the forcing of each N budget process. They are not intended to represent a forced response to any particular environmental stimuli, only to generate N anomalies that are consistent with an overall weakening or strengthening of that process. The forcing is handled by adding an anomalous sink of NO_3 to the ocean, with distribution equivalent to that of WC, B or F in the spinup simulation, scaled to produce a global rate of 50TgN/yr.

5.3.4 Simulation results

We tested the response of each feedback, operating in isolation, to each forcing yielding a total of 9 simulations (3 forcings, 3 feedbacks). The N budget for each forcing-feedback combination (grouped by feedback) is shown in Fig. 5.2. Each simulation begins with an N-budget of imbalance of 50TgN/yr, reflecting the amplitude of the forcing, which then

decays over time as the feedback process compensates. The simple conceptual model of Section 5.2, predicts the an N budget imbalance (source-minus-sink, *SMS*) will decay according to a first order relation:

$$SMS(N) = Ae^{-t/\tau} \quad (4)$$

where τ is the characteristic timescale of the feedback. However, the N budget of the ecosystem model exhibits more complex behavior, undergoing a period of rapid initial adjustment, before the remaining imbalance decays over the following millennia. This implies that a feedback operates on different portions of the anomalous N pool (i.e. compensates different portions of the forcing) over different timescales, i.e.:

$$SMS(N) = f_1 Ae^{-t/\tau_1} + f_2 Ae^{-t/\tau_2} + \ldots + f_n Ae^{-t/\tau_n} \quad (5)$$

where $\tau_{1\rightarrow n}$ represent the temporal spectrum of the feedback, and $f_{1\rightarrow n}$ represent the fraction of the feedback that occurs in each band.

The long millennial timescale over which each feedback operates, after the initial adjustment, is largely independent of the forcing on which it operates: ~6500yrs for WC, ~5000yrs for B, and ~1500yrs for F. However, the partition of feedback's response between the initial adjustment and the long millennial-scale damping varies significantly between forcings.

To gain a deeper understanding of the partition between short and long responses, we employ a linearized version of our model to allow for a number of simple timescale diagnostics.

5.4 Linearized N cycle model

Before simplifying the ecosystem-biogeochemical model, it is worth considering the sequence of events through which a feedback operates on N anomalies, and their associated timescales. Because each N-cycle feedback depends on the uptake of N anomalies by phytoplankton in the surface ocean, this sequence can summarized as follows:

a) Transport of the N anomaly to the surface ocean.
b) Uptake of the N anomaly by phytoplankton, resulting in anomalous primary production.
c) Conversion of anomalous primary production to an anomalous source or sink of fixed N.

Of this sequence, step a) seems simplest, with a timescale controlled by the location at which N anomlies are produced (i.e. location of forcing), and the circulation pathways that transmit them to the surface. Step c) is more complex, and varies between the each feedback process. It will be useful to define a *removal efficiency* (r) of the feedback, which is quantified as the number of moles of anomalous NO_3 that get removed from the ocean for every 1 mole of anomalous N uptake up by phytoplankton in the surface.
For WC, *r* is determined by the fraction of organic matter produced by anomalous N uptake that remineralizes in suboxic water and the stoichiometry of denitrification. It is high in regions with subxoic water columns, but zero throughout most of the ocean (Fig. 5.3a). Removal efficiency for B is governed by the portion of organic matter exported

from the surface that reaches the seafloor, which varies regionally depending on bathymetry (Fig. 5.3b). In diazotrophic habitats, anomalous N uptake by non-fixing plankton is accompanied by anomalous PO_4 uptake, which should drive a net change in N_2-fixation that entirely compensates uptake anomaly. The N_2-fixation feedback thus has a removal efficiency of 1 whenever other environmental factors (such as Fe) do not inhibit diazotroph growth (Fig. 5.3c).

In the sequence above, steps a) and c) are conducive to linearization assuming the removal efficiency of feedbacks is represented as constant in time (see Section 5.5 for limitations of this assumption). The uptake of nutrient anomalies in the surface ocean (step b) is governed by complex ecosystem dynamics, which cannot be linearized. For simplicity, we assume that primary production results in a linear damping of NO_3 anomalies in the surface, equivalent to assuming production is N-limited. The main limitation of this approach is thus that it will overestimate feedback strength when anomalies are supplied to the high nutrient low chlorophyll (HNLC) where this assumption does not hold. However, it allows us to investigate how ocean circulation and removal efficiency limit feedback timescales, which may then be further modified by ecosystem processes.

5.4.1 Linearization

We start with the general form of the conservation equations for NO_3 (N) and PO_4 (P), in which transport is simulated using the Transport Matrix (**A**):

$$\frac{dN}{dt} = \mathbf{A}N + J_{up}(N) + J_{rem}(N) + J_F(N) - J_{WC}(N) - J_B(N)$$
$$\frac{dP}{dt} = \mathbf{A}P + J_{up}(P) + J_{rem}(P) + J_F(P) \quad (6)$$

The J terms on the right hand side of the first equation represent biogeochemical fluxes of N, comprising (in turn) the net uptake of N from the surface ocean during the production of "regular" organic matter by phytoplankton; release of N during the remineralization of sinking organic matter; release of newly-fixed N during the remineralization of diazotrophic organic matter; net removal of N by water column denitrification; and finally the net removal of N by benthic denitrification. The first three terms on the RHS represent the ocean's internal cycling of N, which conserves the N reservoir, whereas the final three terms represent sources and sinks to and from the ocean as a whole, i.e. the N budget. The ocean's P budget is closed, and PO_4 is simply cycled internally within the ocean – note J_F in the P equation represents the uptake of PO_4 by diazotrophs, which is then redistributed via remineralization, rather than a source or sink of PO_4 to/from the ocean.

The major simplification (discussed above) is to the biological uptake term, in which a suite of ecosystem process are replaced by a linear first-order damping of surface NO_3, giving $J_{up}(N) = -\lambda_{bio}N$, or $\mathbf{Q_{up}}N$, where $\mathbf{Q_{up}}$ is a sparse matrix with $-\lambda_{bio}$ on the diagonal for surface grid cells. The sinking and remineralization of organic particles is assumed to occur instantaneously, so can be represented as the redistribution of the uptake flux by a linear operator $\mathbf{Q_{rem}}$. This operator is further divided into two components, one representing remineralization in the water column ($\mathbf{Q_{rem,WC}}$), and

another representing remineralization of organic matter that reaches seafloor sediments ($\mathbf{Q_{rem,B}}$), which returns respired nutrients to the overlying bottom-waters, representing a 'reflective' bottom boundary condition. The method for building these two remineralization operators is described fully in DeVries et al (2012b).

Assuming that water-column and benthic denitrification have a time-invariant removal efficiency, those processes can also be represented through linear operators ($\mathbf{Q_{WC}}$ and $\mathbf{Q_B}$, see derivation below). Diazotroph growth results in the uptake of "excess" PO_4 ($P^* = [PO_4] - [NO_3]/R_O$) and that *net* N_2-fixation rates in high-recycling regimes are not dependent on the N:P ratio of diazotrophs themselves, but rather on the N:P of competing non-diazotrophic plankton (R_O). Assuming that diazotroph growth can again be represented as a linear damping of P* at rate $-\lambda_{fix}$ (which is equal to λ_{bio} in the subtropics, and zero elsewhere), N_2-fixation can also be represented by a linear operator, $\mathbf{Q_F}$. Assuming N-limited primary production, we then obtain:

$$\begin{aligned} \frac{dN}{dt} &= (\mathbf{A} + \mathbf{Q_{up}} + \mathbf{Q_{rem}} - \mathbf{Q_{wc}} - \mathbf{Q_D})N + R_O \mathbf{Q_F} P^* \\ \frac{dP}{dt} &= \mathbf{A}P + (\mathbf{Q_{up}} + \mathbf{Q_{rem}} - \mathbf{Q_{wc}} - \mathbf{Q_D})N / R_O - \mathbf{Q_F} P^* \end{aligned} \tag{7}$$

Because this is a linear system in N and P, we can break the nutrient terms into mean values and perturbations, and assume that "background" cycles are in steady state. System 7 can then be rewritten in terms of nutrient anomalies, to which we add an additional term to represent the production of N anomalies through external forcing:

$$\begin{aligned} \frac{dN'}{dt} &= (\mathbf{A} + \mathbf{Q_{up}} + \mathbf{Q_{rem}} - \mathbf{Q_{wc}} - \mathbf{Q_D})N' + R_O \mathbf{Q_F} P^{*\prime} + f(t) \\ \frac{dP'}{dt} &= \mathbf{A}P' + (\mathbf{Q_{up}} + \mathbf{Q_{rem}} - \mathbf{Q_{wc}} - \mathbf{Q_D})N' / R_O - \mathbf{Q_F} P^{*\prime} \end{aligned} \tag{8}$$

The resulting model describes the biological cycling of P and N anomalies, and the damping of N anomalies via N budget feedbacks.

One advantage of the linearized system is that each feedback can be easily separated and simulated in isolation, by setting the other feedback operators to zero. When simulating either denitrification feedback, we set λ_{fix}=0, and thus the anomalous N cycle is independent of P:

$$\frac{dN'}{dt} = \mathbf{B}N' + f(t), \quad where$$
$$\mathbf{B} = \mathbf{B_{WC}} = \mathbf{A} + \mathbf{Q_{up}} + \mathbf{Q_{rem}} + \mathbf{Q_{wc}} \quad or \qquad (9)$$
$$\mathbf{B} = \mathbf{B_B} = \mathbf{A} + \mathbf{Q_{up}} + \mathbf{Q_{rem}} + \mathbf{Q_B}$$

This equation is similar to Eq. 1 but simulates the spatial structure of N anomalies as well as the mean, and by analogy all the information regarding feedback timescales is contained in the operator **B**. In the case of the N_2-fixation feedback, it is most convenient to combine Eqs. 9 and 10 into a single equation for P* that can be simplified to:

$$\frac{dP^{*'}}{dt} = \mathbf{B}P^{*'} + f(t)/R_O, \quad where \qquad (10)$$
$$\mathbf{B} = \mathbf{B_F} = \mathbf{A} + \mathbf{Q_F}$$

By comparing the operators $\mathbf{B_{WC}}$, $\mathbf{B_B}$ and $\mathbf{B_F}$, a key distinction between feedbacks becomes apparent. Anomalous N uptake, which drives the WC and B feedbacks, occurs in any region where N anomalies surface, even regions in which no feedback process can be stimulated (e.g. above oxygenated waters for WC). On the other hand, anomalous P* uptake is associated only with N_2-fixation, and thus P* anomalies that surface outside of the subtropics continue to circulate until they reach diazotrophic habitats, rather than being exported to deeper waters.

5.4.2 Feedback operators

Water column denitrification rates are governed by the remineralization of organic matter in suboxic water:

$$J_{WC} = r_{N,denit:org} J_{rem,WC} \Leftrightarrow O_{2,obs} < O_{2,crit} \quad (11)$$

where $r_{N,denit:org}$ is the stoichiometry of denitrification (see section 5.3). The "if and only if" statement $\Leftrightarrow$ is handled by creating a mask from the observed monthly climatology of O_2, which quantifies that fraction (ϕ_{sub}) of each grid cell, both spatially and over the seasonal cycle, that is suboxic (i.e. O_2 lower than a critical threshold $O_{2,crit}$). The linear operator relating water column denitrification to surface NO_3 concentrations is then:

$$\mathbf{Q_{WC}} = \Phi \mathbf{Q_{rem},}_{WC} \quad (12)$$

where $\mathbf{\Phi}$ is matrix with $r_{N,denit:org}\phi_{sub}$ on the diagonal. Values of $O_{2,crit}$ and $r_{N,denit:org}$ were optimized to produce rates of WC consistent with tracer constraints in the modern ocean (DeVries et al 2012a).

Benthic denitrification is often parameterized as a non-liner function of the organic-matter rain rate onto the seafloor sediments (Bohlen et al 2012, Middelburg et al 1996). However, DeVries (2012b) showed that a similar spatial distribution and depth structure, which is consistent with tracer constraints, can be obtained using a linear relation to organic matter deposition, with an additional scaling dependent on bottom-water oxygenation. The linear operator relating benthic denitrification to NO_3 is then:

$$\mathbf{Q}_B = \mathbf{F}\mathbf{Q_{rem},}_B \quad (13)$$

where **F** is a matrix with the scaling factor on the diagonal.

The N_2 fixation operator $\mathbf{Q}_{fix}$ is simply a sparse matrix with λ_{fix} on the diagonal. To maintain a realistic distribution of N_2-fixation, occurring only in oligotrophic subtropical gyres, we set $\lambda_{fix}=0$ when $T_{obs}<15°C$ and $N_{obs}>2\mu M$, and $\lambda_{fix}= \lambda_{bio}$ elsewhere.

5.4.3 Simulations

The linearized model is forced by the same three forcings described in section 5.3.3, and each forcing-feedback combination is again simulated in isolation. Each experiment requires the integration of just one equation: N' for both denitrification feedbacks, and P*' for N_2-fixation. Forcings are again assumed to represent an instantaneous increase in one N budget represented by "switching on" on a source of N' (or P*') at t=0. Simulations are conducted using a fast matrix exponential method, and integrated until the N budget reaches a steady state.

We note at this point that the N_2-fixation forcing adds P* anomalies directly to the subtropical surface ocean, where they can be immediately operated on by the N_2-fixation feedback, meaning the entire feedback occurs almost instantaneously in that case. We consider this case u realistic, because any environmental stimuli that forces a change in N_2-fixation (e.g. a reduction in the Fe supply) should also prevent an immediate feedback in the same location. We thus do not discuss this case, until returning to think about Fe limitation at the end of the chapter.

5.5 Linear model results

5.5.1 Timescale deconstruction

The N budget from linearized simulations again exhibits a period of rapid adjustment over fast (sub-millennial) timescales, followed by gradual decay over thousands of years. To identify the dominant feedback timescales, Eq. 5 was fit to the N budget of each simulation, allowing four modes to be selected with the following constraints:

i) $0\text{yr}<\tau_1<10\text{yr}$ (decadal mode)

ii) $10\text{yr}<\tau_2<100\text{yr}$ (interdecadal mode)

iii) $100\text{yr}<\tau_3<1000\text{yr}$ (centennial mode)

iv) $\tau_4=\tau_M>1000\text{yr}$ (millennial mode)

Using just these four modes, a >99% fit to each model N budget was achieved.

The deconstruction reveals a unique spectrum for each forcing-feedback combination (Fig. 5.4). As with the ecosystem-biogeochemical model simulations, the most striking feature of these spectra is that for a given feedback, the partition of the total response between temporal modes varies, but the timescale associated with the longest, millennial mode is constant: ~7500yrs for WC, ~3500yrs for B, ~1500yrs for F. For WC and B, these values represent a departure on the order of ~1000yrs from the results of the ecosystem-biogeochemical model, which result from the simplifications made during the linearization, and can probably be understood due to the difference in nutrient utilization

between the two configurations. In the linearized configuration, the universal millennial timescale for each feedback can be understood mathematically by noting that the characteristic timescales governing the linear systems represented in Eqs 9 and 10 are given the eigenvalues of the **B** matrices matrix. Because each eigenmode must decay over time, on long timescales the system must be governed by the gravest mode, and thus the millennial timescale for each forcing is just the inverse of the gravest eigenvalue of the matrices $\mathbf{B_{WC}}$, $\mathbf{B_B}$, $\mathbf{B_F}$.

The partition of the initial adjustment between decadal, interdecadal and centennial modes yields important information regarding the coupling of forcing and feedback processes over observable timescales, and timescales relevant to anthropogemic climate change, and will be investigate in a further study. However, changes in the oceanic N reservoir and global-scale productivity are very small over this adjustment period. Instead, >95% of the total reservoir change occurs during the millennial feedback mode. For the purposes of understanding N reservoir perturbations, we can thus group all but the millennial mode into a "fast response" that operates on localized N perturbations and has little influence on the N reservoir as a whole. A perturbation to the oceanic N reservoir in response to any forcing thus depends on two factors:

a) the timescale over which the longest, millennial mode of the feedback operates (τ_M)
b) the fraction of the forcing that must be compensated over that millennial timescale, rather than on shorter timescales

In the remainder, we seek a mechanistic understanding of these two factors (f_M).

5.5.2 Nutrient lifetimes

The characteristic timescales over which a feedback compensates a forcing are equivalent to the timescales on which the feedback process removes a nutrient anomalies produced by a forcing, which will be referred to as the *lifetime* of the anomaly. From the preceding, it is obvious that anomalies have a whole spectrum of lifetimes, yet the perturbation to the N reservoir (before a new steady-state is reached), depends on the *mean lifetime* of the nutrient anomaly (Γ), because

$$\bar{N}' = A / \Gamma \tag{14}$$

where A is again the amplitude of the forcing. The distribution of Γ for nutrient anomalies starting their life in each grid cell of the ocean model can be computed as:

$$\mathbf{B}^{*}\Gamma = 1 \tag{15}$$

where $\mathbf{B}^{*}$ is the adjoint of $\mathbf{B_{WC}}$, $\mathbf{B_B}$, $\mathbf{B_F}$ depending on the operative feedback. This is analogous to computing the remaining lifetime of a water parcel before reaching the surface – its first passage time, (Primeau 2005) – except the transport operator is replaced with the full transport-cycling-feedback operator **B**. For each feedback, the mean lifetime of nutrient anomalies in the upper ocean vary significantly spatially (Fig. 5.5), reflecting their proximity to regions of high removal efficiency: close to suboxic zones for WC, regions with shallow sediments for B, the subtropical surface for F. However, these spatial variations curtail with depth, and below ~1000m nutrient anomalies have a relatively homogeneous lifetime, close to the millennial damping timescale (τ_M) diagnosed for each feedback: ~7500yrs, ~3500yrs and ~1500yrs respectively (Fig. 5.5).

The mean lifetime of a nutrient anomaly averages across components that are removed over the entire spectrum of feedback timescales (Fig. 5.4). The similarity between deep-ocean nutrient lifetimes and the longest feedback timescale (inverse of the gravest eigenvalue) suggests that this millennial mode is associated with the gradual damping of anomalies that penetrate the deep ocean (>1000m). The mean lifetime of nutrient anomalies generated in the upper ocean may then be thought to reflect the average of two components: a fraction of the anomaly that is removed over short (centennial or faster) timescales without ever passing through the deep ocean, and the remainder that penetrates the deep ocean and then must be removed over millennial timescales. These components correspond to the initial adjustment and millennial damping periods of the feedback response, respectively.

Two factors then determine the ability of forcing, operated on by a given feedback, to change the oceanic N reservoir: (i) the fraction of anomalies produced by the forcing that must pass through the deep ocean before their removal, and (ii) the lifetime of deep-ocean nutrients with respect to the feedback process. The latter is completely independent of the forcing, and can be understood exclusively as a product of ocean circulation timescales and the *removal efficiency* of the feedback (Section 5.6.1), whereas the former is determined by both of these factors *and* the spatial structure of the forcing (Section 5.6.2).

5.6 Discussion

5.6.1 Understanding deep-ocean nutrient lifetimes

The factors controlling the lifetime of deep-ocean nutrient anomalies vary between the N_2-fixation and the two denitrification feedbacks. We first seek an understanding of lifetimes with respect to the two denitrification fluxes, using a hierarchy of box models that place the conceptual model of section 5.2 in a more realistic physcial context (Fig. 5.6). In these models, an N cycle feedback is just represented by the removal of a fixed fraction of N export from the surface ocean, where that fraction is equivalent to the removal efficiency, *r*.

In the simplest case, the ocean is broken into a surface (0-100m) and deep-ocean (100-4000m) compartment (Fig. 5.6a). Given that an N anomaly residing in the deep ocean stands a probability *r* of being removed each time it passes through the surface, it must on average cycle $1/r$ times between the surface and abyss before being removed. The time required for each cycle is limited by the mixing rate (Ψ) between these two compartments, because the biological uptake rate of N in surface ocean is very short in comparison. The lifetime of the anomaly is thus

$$\Gamma = T_{deep} / r \qquad (16)$$

where T_{deep} is the residence time of deep ocean waters (V_{deep}/Ψ).

In the real ocean, the removal efficiency (*r*) of a feedback varies between regions (e.g. between regions with suboxic and oxic water columns for WC). This is mimicked by splitting the surface of the box model into a region with yield r_1 and another with yield r_2 (Fig. 5.6b). The lifetime of a deep-ocean N anomaly is then

$$\Gamma = \frac{T_{deep}}{f_A r_1 + (1 - f_A) r_2} \tag{17}$$

where f_A is the fraction of deep-ocean waters are ventilated in surface region 1. The denominator here is then *mean removal efficiency* ($\bar{r}$), which is weighted according to the ventilation region of deep waters.

A final consideration must be made for analogy to the GCM. In the preceding model, nutrient anomalies must cycle 1/r through the homogeneous deep pool, in which waters reside for ~1000yrs. In reality, following an anomaly's first passage to the surface over timescale T_{deep}, the fraction 1-r (that is removed by the feedback) is not returned evenly throughout the deep ocean, but predominantly in thermocline waters from which its next passage to the surface occurs on timescales much shorter than T_{deep}. This behavior can be captured by adding a thermocline compartment (box 3) between the surface (boxes 1 & 2) and deep ocean (box 4) in the box model (Fig. 5.6c). Following biological export, the fraction $\phi_3(1-\bar{r})$ of a nutrient anomaly is remineralized in box 3 and $\phi_4(1-\bar{r})$ in box 4, where $\phi_3 + \phi_4 = 1$ and $\phi_3 > \phi_4$, reflecting preferential remineralization in shallower waters. The anomaly's remaining passages to the surface are completed over the timescale $T_{rem}=\Phi_3 T_3 + \Phi_4 T_4$ (where T_3 and T_4 are the mean passage times from the two subsurface boxes to the surface), which is much shorter than T_{deep}. The lifetime of a deep-ocean anomaly is then:

$$\Gamma = T_{deep} + (1/\bar{r} - 1) T_{rem} \tag{18}$$

This can be recognized as the sum of an infinite series, in which every term represents an additional 'cycle' traversed by the remaining fraction of the initial anomaly:

$$\Gamma = T_{deep} + (1-r)T_{rem} + (1-r)^2 T_{rem} + ...(1-r)^n T_{rem} \quad (19)$$

An analogy to this simple series exists for the linearized 3-dimensional ocean model. Instead of integrating the model forward in time explicitly, the removal of a deep ocean nutrient anomaly can be thought to occur over of a series of discrete "cycles", each involving:

(i) The transport of the entire subsurface nutrient pool to the surface, producing the surface nutrient distribution $H(\mathbf{x_S})$. $H(\mathbf{x_S})$ simply represents the portion of subsurface pool that is next exposed in each surface grid cell, and its method of computation is discussed in Holzer & Primeau (2013).

(ii) The export and remineralization of the surface distribution, to produce a new subsurface distribution, given by $(\mathbf{Q_{up}} + \mathbf{Q_{rem}})H(\mathbf{x_S})$.

(iii) The removal of a portion of that remineralized pool via the feedback process, given by $\mathbf{Q_{WC}}H(\mathbf{x_S})$ or $\mathbf{Q_B}H(\mathbf{x_S})$.

Just as in the box model series (Eq. 19), each of these "cycles" is associated with a characteristic timescale and mean removal efficiency. The timescale is just the mean surfacing time of subsurface waters (the "first passage time" of Primeau, 2005), weighted by their nutrient content. The first passage time is computed using the adjoint to the transport operator by solving:

$$\mathbf{A}^* \tau_{fp} = 1 \quad (20)$$

subject to τ_{fp}=0 in the surface. The mean removal efficiency of the cycle $\bar{r}$, i.e. the difference between nutrient reservoirs at the beginning and end of the cycle, is equal to

the spatially-varying pattern of r associated with each feedback weighted by $H(\mathbf{x_S})$, analogous to the same term in the box model.

The first two cycles are illustrated in Fig. 5.7a. In Cycle 1, a homeogeneous deep ocean N anomaly is transported to the surface, over a mean timescale, T_1, of ~700yrs, which is independent of the operative feedback. The resulting surface distribution $H_1(\mathbf{x_S})$ is shown in Fig. 5.7b. The timescale associated with Cycle 2 depends on how N anomalies are redistributed through the water column following their passage to the surface, which varies slightly between WC and B feedbacks (depending on where anomalies are removed). However, it is largely controlled by the depth structure of nutrient remineralization, which partitions most of the exported N into upper ocean waters, where the resupply timescale is short (<100yrs). For both WC and B, the mean resupply timescale for Cycle 2 (T_2), and for all remaining cycles is ~80yrs. The only significant difference between the feedbacks is the mean removal efficiency $\bar{r}$ associated with each cycle, which is ~1.5% for WC and ~3% for WC. Although WC has a very high removal efficiency for N anomalies that surface above suboxic zones, this comprises only a small fraction of the total anomaly pool. B has a low removal efficiency, but spread more evenly through the ocean, even in high latitudes where the majority of N anomalies actually surface (Fig. 5.7b,c). Integrating across the series in Eq. 19 for GCM "cycles", the difference in $\bar{r}$ between WC and B explains their millennial damping timescales of ~7500yrs and ~3500yrs respectively.

The millennial damping timescale associated with the N_2-fixation feedback has a simpler interpretation. P* anomalies are not continually exported and cycled through the

water column, rather they follow circulation pathways until they reach diazotrophic habitats where they removed at high efficiency. The lifetime of deep-ocean P* anomalies with respect to N_2-fixation of 1500yrs is therefore just their transport passage time to the subtropics, which can be derived by solving Eq. 2 subject to τ_{fp}=0 in the subtropical surface only.

5.6.2 Understanding deep-ocean leakage

We now turn our attention to the fraction of a nutrient anomaly (produced by a forcing) that passes through the deep ocean before its removal by a feedback process, and must then be damped on the long timescales described above. This comprises both anomalies that are produced by via forcing in the deep ocean itself, and a portion of anomalies produced in the upper ocean that *leak* into the abyss before their removal from the ocean. Because the forcings we prescribe are largely confined to the upper ocean, the leakage of upper ocean anomalies must be the primary component. The deconstruction performed in Fig. 5.4 demonstrates that the degree of leakage varies both as a function of the forcing and feedback process.

To illustrate why different feedbacks allow different portions of the same upper-ocean N anomaly to leak into the deep ocean, we return to the four-box model developed in the last section (Fig. 5.6c). For an anomaly produced in thermocline compartment (box 3), its probability of leaking into the deep ocean (before being removed by the operative feedback) is again given by the sum of an infinite series. During its transport out of the

thermocline, an anomaly has probability $\Psi_2/(\Psi_1+\Psi_2)$ of leaking into the deep through circulation. Of the fraction that reaches the surface, another portion $(1-\bar{r})\phi_4$ leaks into the deep ocean through remineralization, whereas $(1-\bar{r})\phi_3$ is returned to the thermocline for the next cycle. Following the series through the probability tree shown in Fig. 5.8a, the total fraction of a thermocline N anomaly that leaks into the deep ocean is given by:

$$f_{deep} = 1 - r\sum_{i=1}^{\infty}\left(\frac{\Psi_1}{\Psi_1+\Psi_2}\right)^i\left((1-\bar{r})\phi_3\right)^{i-1} \tag{21}$$

which for a given circulation is just a function of the mean removal efficiency of the feedback.

As Eq. 19, an analogy to Eq. 21 can be computed in the GCM (Fig. 5.8b). An upper ocean anomaly is again transported to the surface to produce the surface distribution $G(\mathbf{x_S})$, but components that cros the 1000m horizon on route to the surface is assumed to have leaked into the deep ocean ("circulation leakage", Fig. 5.8b), and do not reach the surface to be included in $G(\mathbf{x_S})$. The surface anomaly is then redistributed over depth, allowing further leakage ("remineralization leakage", Fig. 5.8b) before the next cycle commences. For an anomaly generated evenly throughout the upper ocean, we find that ~80% leaks into the deep ocean when operated on by either the WC or B feedback, but only ~40% is when operated on by the N_2-fixation feedback.

For each feedback, we repeated the above diagnosis for the more realistic WC, B and F forcings described in Section 5..3.3, each time computing the probability of nutrient anomalies leaking into the deep ocean. Values of f_M estimated by this method compare remarkably well to those derived by deconstructing our simulations in Section

5.5.1 (Fig. 5.9), supporting the interpretation that the longest feedback mode represents the portion of a forced anomalies that pass through the deep ocean before removal.

The difference between the leakage fraction for any forcing/feedback pair, and the baseline in which that feedback operates on a uniform upper ocean anomaly, reflects the degree of coupling between the forcing/feedback pair. The WC feedback is generally quite "leaky", allowing 80% of a uniform upper ocean anomaly to pass into the deep ocean due to the low mean removal efficiency of this process. However, this leakage is drastically reduced when the feedback is operating on a forcing of WC itself, because anomalies produced by WC are much more likely to hit the surface above suboxic zones before passing into the deep ocean. Similarly, the N_2-fixation feedback allows less leakage for an anomaly produced by WC than it does for the uniform forcing, because waters from the suboxic zones have a relatively direct pathway to the subtropical surface through equatorial upwelling and divergence. The benthic denitrification feedback, on the other hand, lacks a strong spatial to any forcing, and the majority of forced anomalies must always leak into the deep ocean, and then be damped over long timescales.

5.6.3 Feedback strengths

For each forcing feedback pair, the overall feedback strength can be quantified as a percentage change in the N reservoir that can be induced per TgN/yr of forcing. Lower values indicate a stronger feedback response, capable of holding N reservoir perturbations to smaller magnitudes. To first order, this feedback strength is just the

product of the two factors explored above – the damping timescale of deep ocean anomalies, and the fraction of forced anomalies that must pass through the deep ocean (Fig. 5.10a).

WC is generally the weakest feedback, due to its long damping timescale of deep-ocean N amomalies (>7000yrs), particularly when operating on N_2-fixation and benthic denitrification forcings, which are spatial decoupled from the feedback. In these cases, a relatively modest forcing of magnitude 50TgN/yr on F or B can change the oceanic N reservoir by ~50%. When operating on a forcing on WC itself, the WC feedback is somewhat stronger due to spatial coupling, which reduces the leakage of N anomalies into the deep ocean. The benthic denitrification feedback is stronger in general than WC, due to the shorter damping timescale of deep-ocean anomalies (~3500yrs), and holds N reservoir perturbations to ~25% for a forcing of 50TgN/yr. Its strength is largely independent of the nature of the forcing, because in each case ~80% of the anomalies produce are allowed to leak into the deep ocean. Finally, the N_2-fixation feedback is strongest of all, having both the shortest damping timescale of deep ocean anomalies (~1500yrs), and most efficiently preventing leakage into the deep ocean for each forcing. The N_2-fixation feedback is thus the most important factor stabilizing the N reservoir and preventing its perturbation in response to climate forcing. If the N_2-fixation feedback operates at full strength, changes in the N reservoir must be confined to <25% even for N budget perturbations up to 200TgN/yr (Fig. 5.10a).

5.6.4 Fe limitation of N_2-fixation feedback

Because the N_2-fixation feedback is most important in minimizing N reservoir perturbations, we must consider the factors that might limit the strength of this feedback. The most important factor that can limit P* utilization by diazotrophic plankton is a shortage of Fe. Fe limitation can be represented in our linear model by confining the surface ocean region in which P* anomalies are utilized to areas with increasingly large Fe inputs. We excluded N_2-fixation first from the Pacific Ocean, and then the Indian (reflecting their relative Fe inputs). Each successive reduction lengthens the lifetime of deep ocean P* anomalies with respect to N_2-fixation, because the mean removal efficiency of the surface ocean is reduced (Fig. 5.10b). Also, for each forcing, the fraction of its anomalies that leak into the deep ocean also increases with Fe limitation, further enhancing the potential for changes in the N reservoir (Fig. 5.10b). When N_2-fixation is excluded from the Pacific Ocean F remains the strongest feedback, but when confined to just the Atlantic Ocean the damping timescale of deep anomalies by F becomes longer than for B. In this case, climate forcing of B and WC of magnitude 50TgN/yr is able to perturb the N reserve by ~25%. Understanding the Fe limitation of the N_2-fixation feedback is thus critical in understanding the stability of ocean productivity (Chapter 4).

5.7 Limitations

Our linearized model has revealed how circulation timescales and removal efficiencies combine to govern feedback strengths. However, there are limitations to this approach. First, to linearize the model we had to assume that feedback removal efficiencies (although variable in space) are constant in time, which may be invalid in particular for the WC feedback. Variations in N export do not only influence the remineralization of organic matter in pre-existing suboxic zones, but change the oxidant demand in subsurface waters and the size of the suboxic zones themselves (Ganeshram et al 2000) – in other words, the removal efficiency of the WC feedback should also change in response to forcing, which may increase the strength of this feedback, and should be investigated further. Furthermore, the linearization of nutrient consumption may have overestimated feedback strengths in high latitude regions, where nutrients are not fully consumed. This is probably the cause of disparity in the timescale of millennial feedback modes for benthic denitrification between the ecosystem and linearized models, and should again be studied further.

5.8 Summary and Outlook

This study investigated the timescales over which N cycle feedbacks operate, and the mechanistic underpinnings of those timescales. We used a linearized model to characterize the feedback response of three N budget processes – water column denitrification, benthic denitrification and N_2-fixation – in isolation to forcing on each of

those processes. The study revealed that the response comprises two components – a rapid initial adjustment through the upper ocean, in which the accumulation of N anomalies is insignificant relative to the total reservoir of N, and a long millennial response involving the damping of deep-ocean anomalies, over which significant perturbations to the N reservoir can occur. The potential for a forcing to change the N reservoir thus depends on the fraction of anomalies it produces that "leak" into the deep ocean, and the lifetime of those deep ocean anomalies with respect to the operative N cycle feedbacks.

Separating feedbacks into these two components provides a simple but powerful tool to understand the relative strength of the three feedbacks: F>B>WC. N_2-fixation is the strongest feedback and precludes major perturbations to the reservoir, both because it damps deep-ocean anomalies over the shortest timescale, and most efficiently prevents the leakage of upper-ocean anomalies into the abyss. Both factors result from the high "removal efficiency" of upwelling anomalies by F due to the broad extent of diazotrophic habitats. If, however, diazotrophs are confined to small regions of the ocean with high Fe inputs, the feedback is drastically weakened.

In the future, we hope to use a similar modeling approach with to investigate the strength of feedbacks in response to specific forcings, where data constraints can be used to minimize the uncertainties outlined in Section 5.7. The timescales diagnosed here appear to be consistent with a slow compensation of the deglacial forcing on WC by the WC feedback (Deutsch et al 2004), and a faster (but delayed) response through N_2-fixation (Ren et al 2009), which have been argued for based on isotopic constraints.

We have also largely overlooked the "initial adjustment" phase of the feedback response, because the millennial mode is the more important constraint on N reservoir perturbations. However, the timescales over which this initial adjustment occurs may be important in understanding localized ecosystem processes and temporal trends. Deutsch and Weber (2012) hypothesized that multiple signatures of increasing N_2-fixation recoded in the Hawaii Ocean Timeseries (Karl et al 1997, Karl et al 2001a) may be coupled to an interdecal variations in denitrification in the Eastern Tropical North Pacific subxoic zone (Deutsch et al 2011). The simple model presented in this chapter will provide a useful tool to assess the mechanistic underpinnings of this coupling.

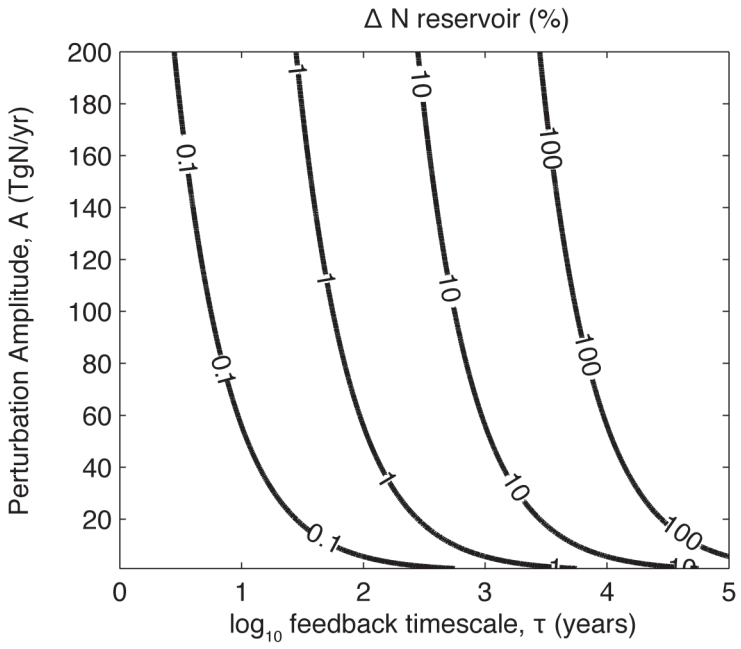

Figure 5.1 Conceptual model for N reservoir perturbations. The total perturbation produced before a new steady state is reached is determined by the amplitude of external forcing and the timescale over which restorative feedbacks operate. For feedback timescales longer than 1000yrs, forcing amplitudes of order 100TgN/yr can produce significant (>10%) changes in the N reservoir.

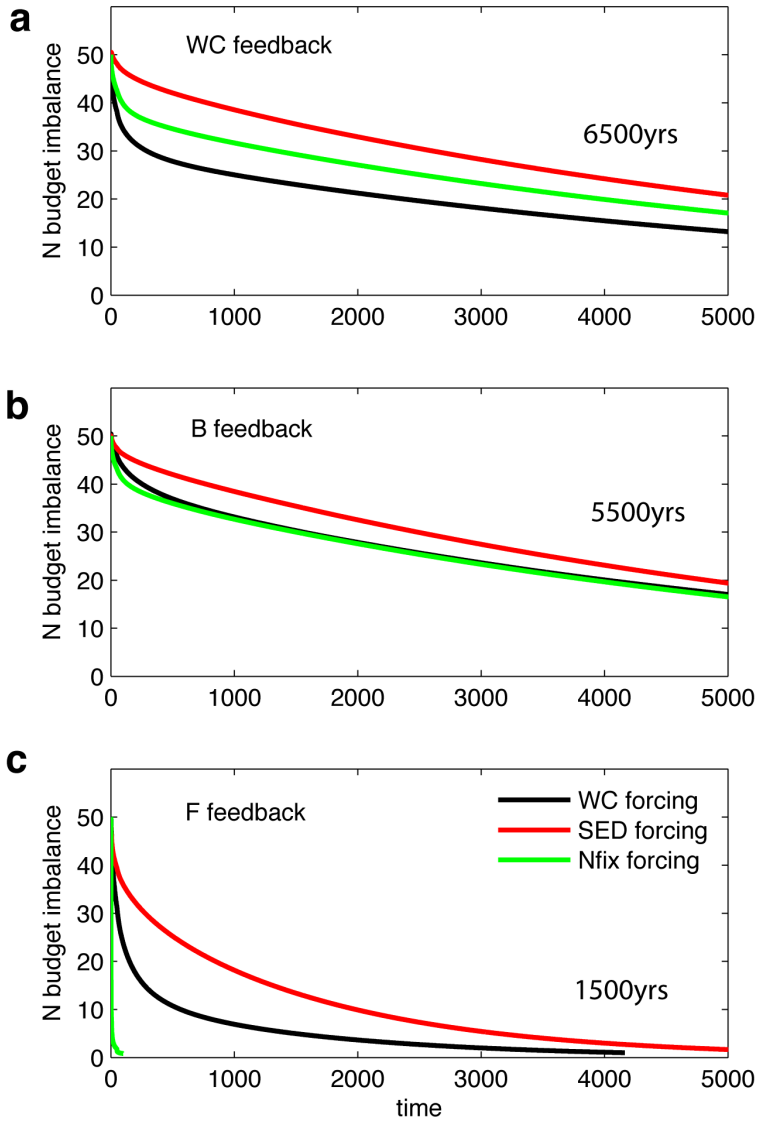

Figure 5.2 N budget from 9 similautions in an ecosystem-biogeochemical model. Each simulation has one external forcing (represented by line color) of magnitude 50TgN/yr, and one operative feedback: **a** water column denitrification feedback only; **b** Benthic denitrification feedback only; **c** N_2-fixation feedback only. For a given feedback, different fractions of each forcing are compensated on short timescales during the initial adjustment, but the timescale of the feedback following the initial adjustment is independent of forcing: 6500yrs for WC, 5500yrs for B and 1500yrs for F.

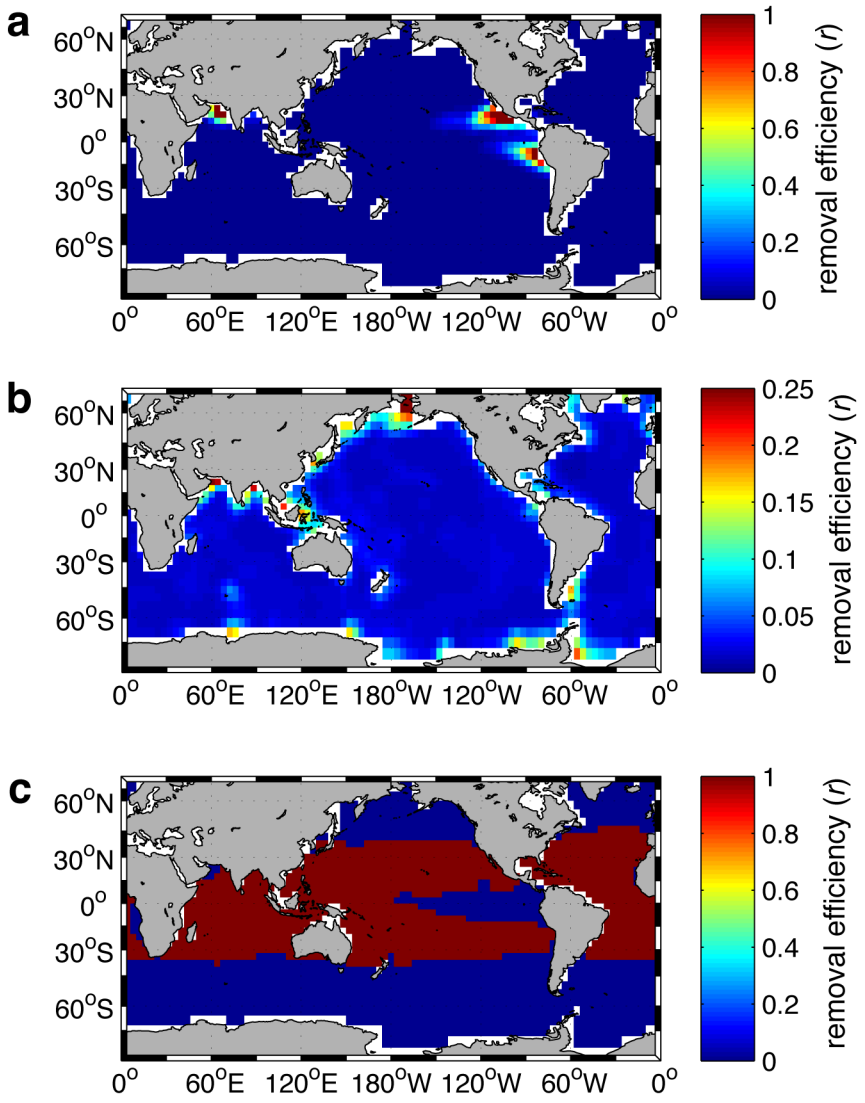

Figure 5.3 Removal efficiency for each feedback: **a** WC feedback; **b** B feedback; **c** F feedback. Values represent the number of moles of N that are removed from the ocean (integrated across depth) per mole of anomalous N uptake in the surface ocean.

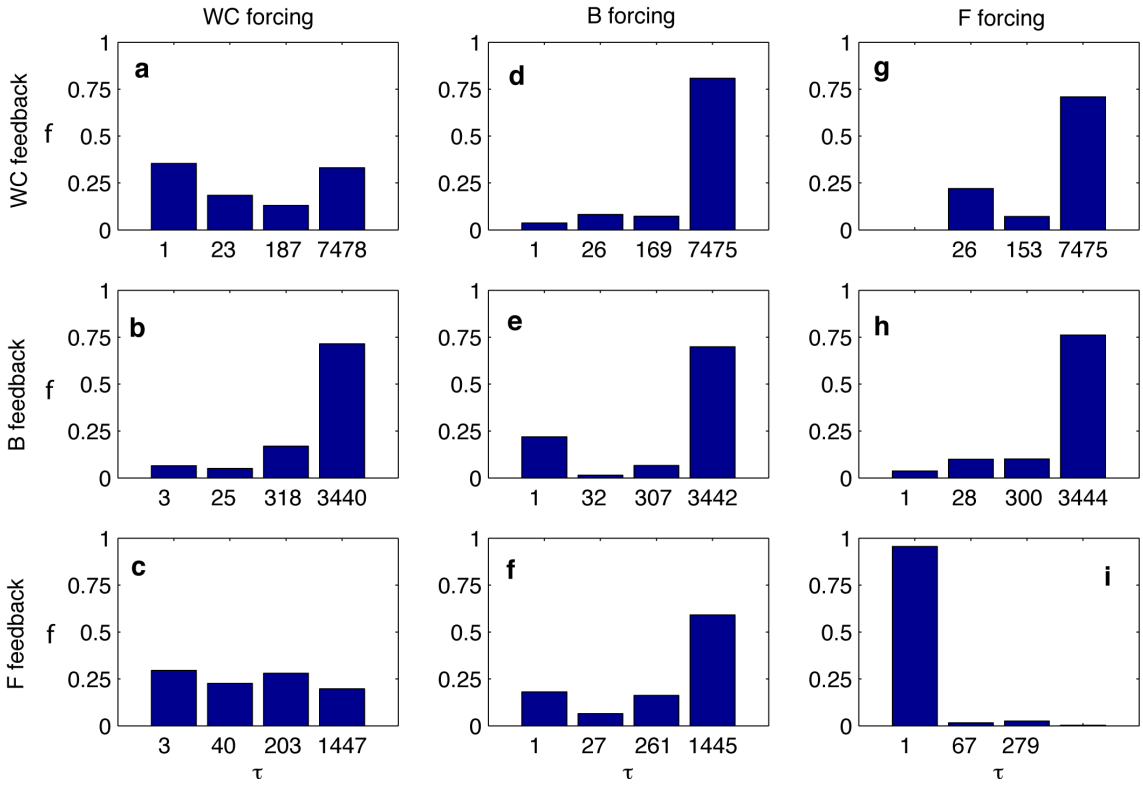

Figure 5.4 Deconstruction of feedbacks in linearized simulations. The set of simulations from Fig. 5.2 was repeated in a linearized version of the model, and Eq. 5 was fit to the N budget allowing four temporal modes with timescales (τ) of 1-10yrs, 10-100yrs, 100-1000yrs and >1000yrs, each of which comprise a fraction (*f*) of the complete feedback response.

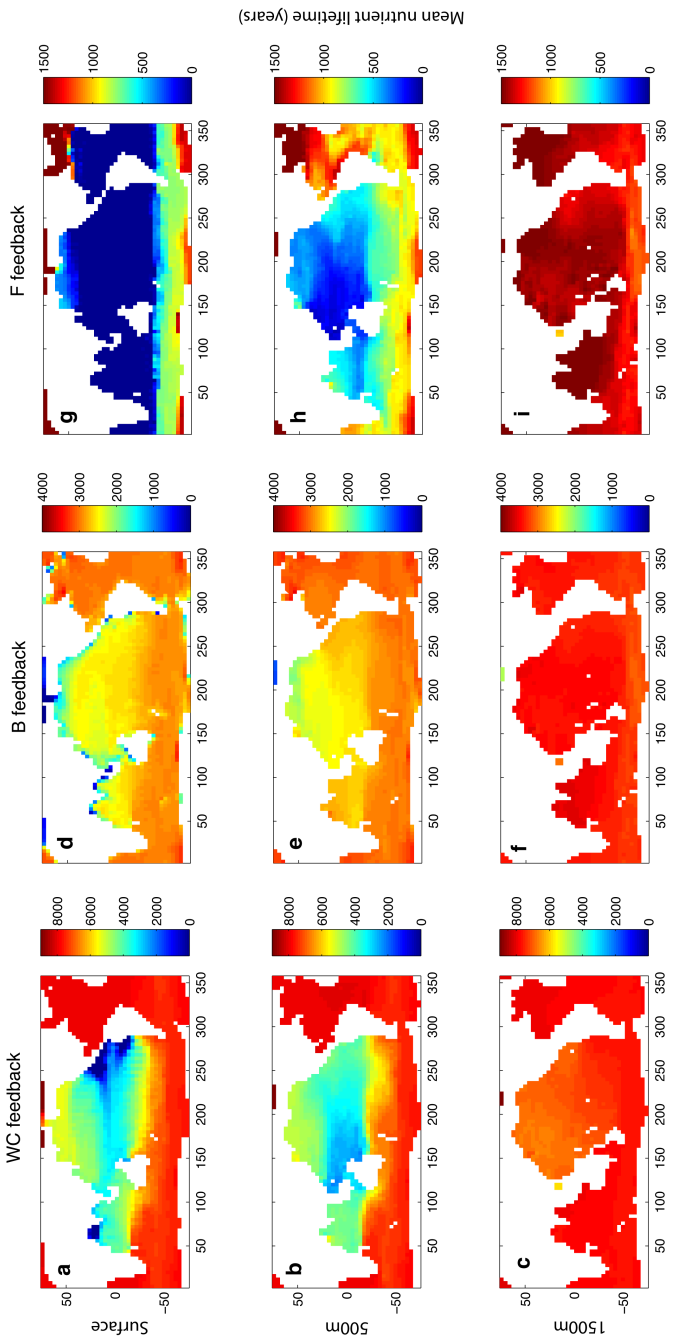

Figure 5.5 Mean lifetime of nutrient anomaly generated in each grid cell with respect to the WC (**a-c**), B (**d-f)** and F (**g-i)** feedbacks, at three depth intervals. Below ~1000m, lifetimes become relatively homogeneous and close to the timescale of the millennial feedback mode (Fig. 5.4), suggesting that the millennial mode represents the damping of deep ocean N anomalies.

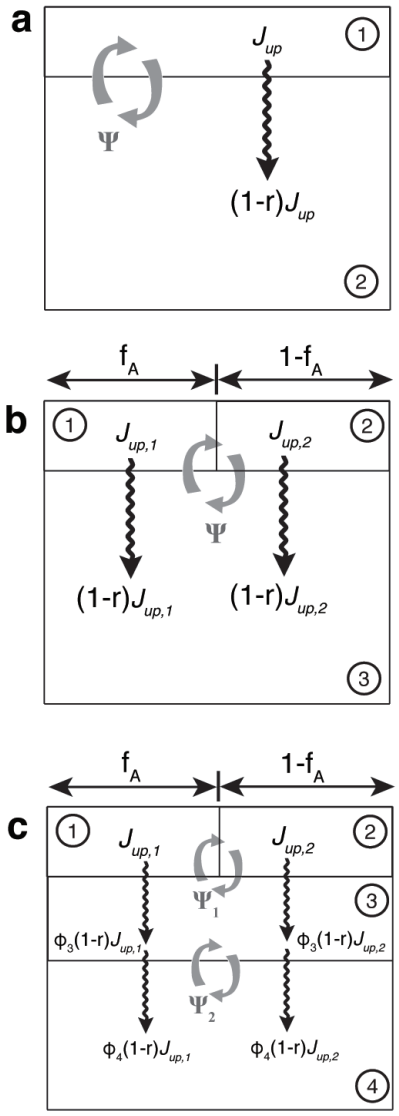

Figure 5.6 Hierarchy of box models used to interpret millennial damping timescale of N anomalies. **a** 2-box model, in which the feedback is represented by the removal of a fraction *r* (the removal efficiency) of anomalous N uptake (J_{up}). **b** 3-box model in which the surface is split into regions with different removal efficiencies. **c** 4-box model in which a thermocline compartment is added between the surface and deep ocean, creating a faster resupply pathway for remineralized nutrients to the surface.

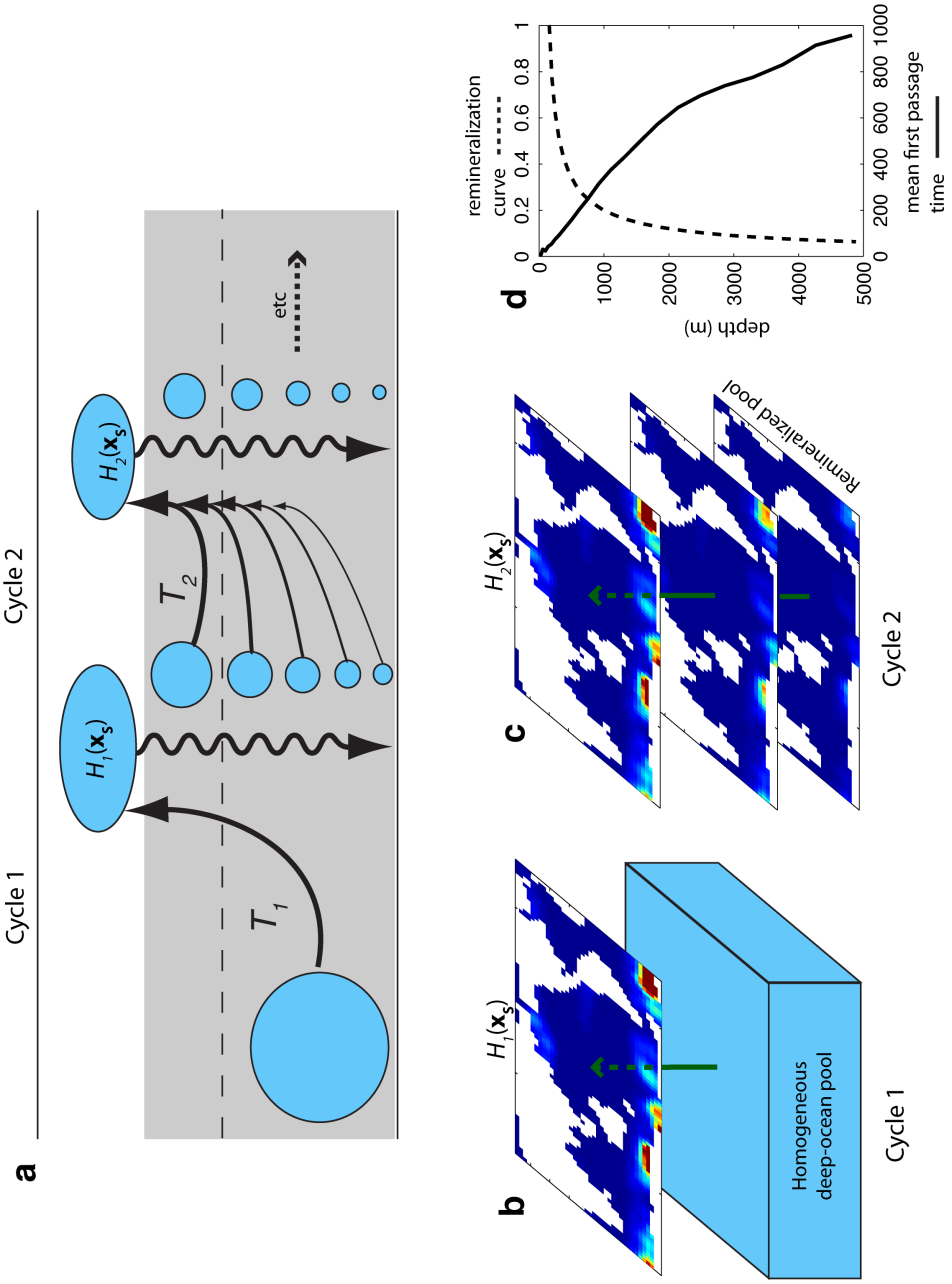

Fig. 5.7 Method for computing analogues of box model "cycle" timescales in the GCM. **a** Demonstration of first two cycles. A homogeneous deep ocean nutrient is transported to the surface, producing the surface distribution $H_1(\mathbf{x}_S)$ (**b**), over timescale T_1. The surface distribution is then exported and remineralized, before being transported to the surface again (**c**). The timescale associated with this second cycle (T_2) is significantly shorter because nutrients are mainly remineralized in shallow waters with shorter passage times to the surface (**d**).

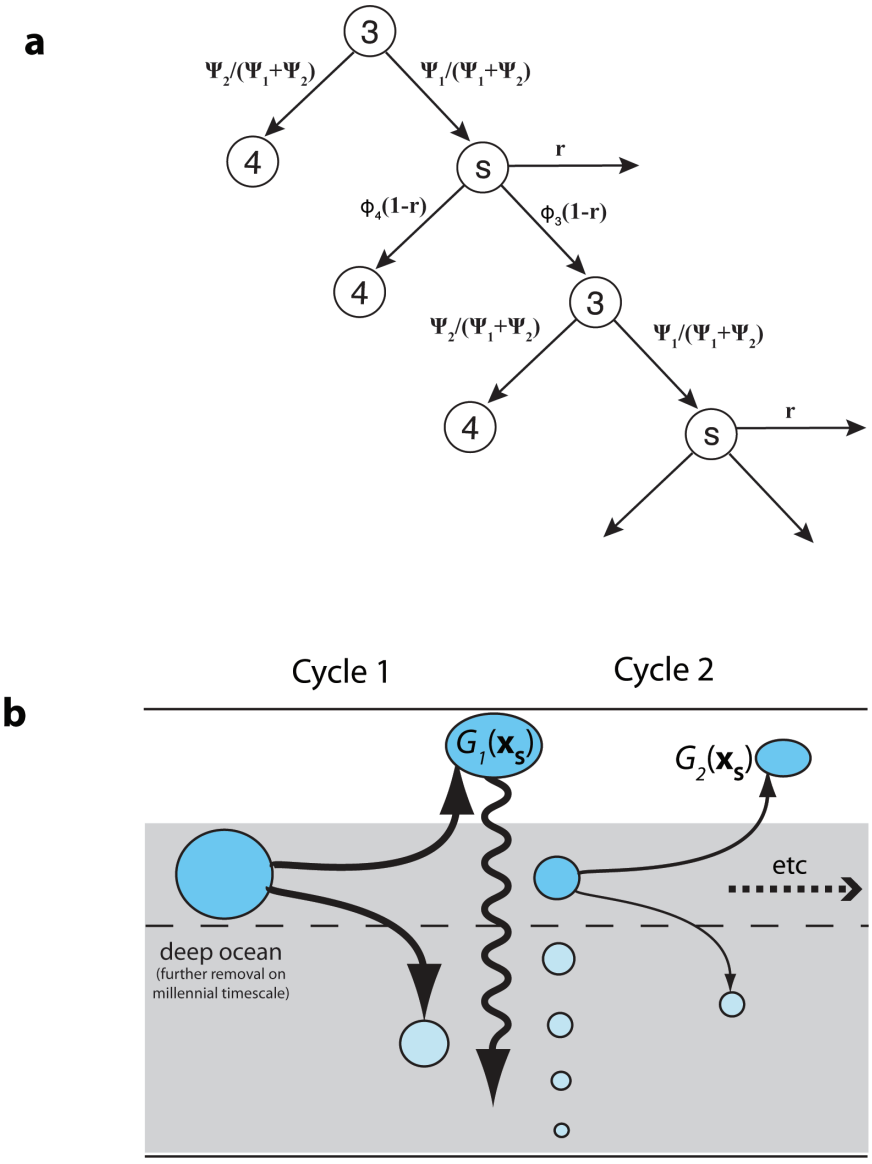

Figure 5.8 Method for computing leakage of upper ocean N anomalies into the deep ocean. **a** In the 4-box model (Figure 5.6), this corresponds to the probability of anomaly passing into box 4 (the deep ocean), before being removed from the ocean as a whole by the feedback process. S represents the surface (box 1 and 2 combined). **b** This series can be computed in the GCM, by simulating a series of "cycles" as in Figure 5.7. Nutrient anomalies that that passes below 1000m, either by circulation or remineralization, are not returned to the surface during the next cycle, and cycles are repeated until anomalies have either passed into the deep ocean or been removed by the feedback.

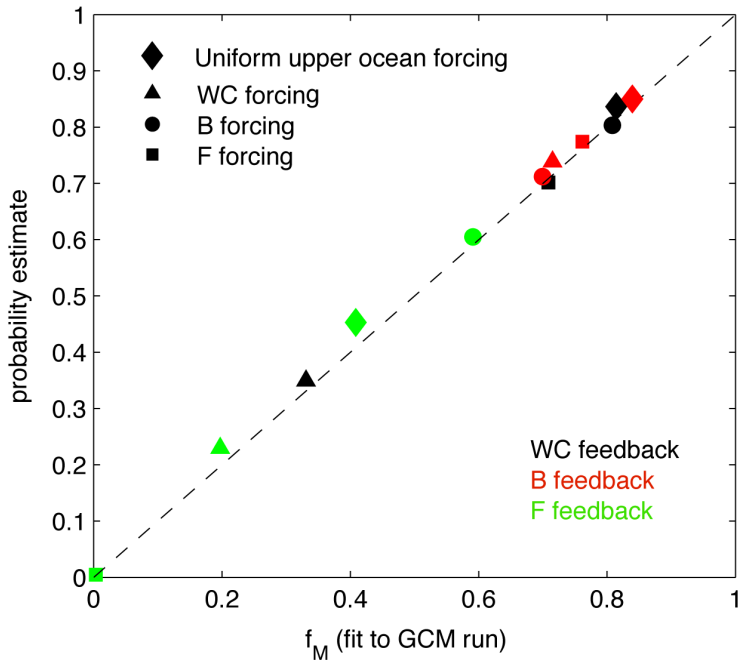

Figure 5.9 Comparison between fraction of forced anomalies that leak into deep ocean (y-axis), computed following method of 5.8, and fraction of feedback associated with millennial mode (from deconstruction in Fig. 5.4). The close agreement supports the interpretation that this millennial feedback mode represents the damping of anomalies that penetrate the deep ocean.

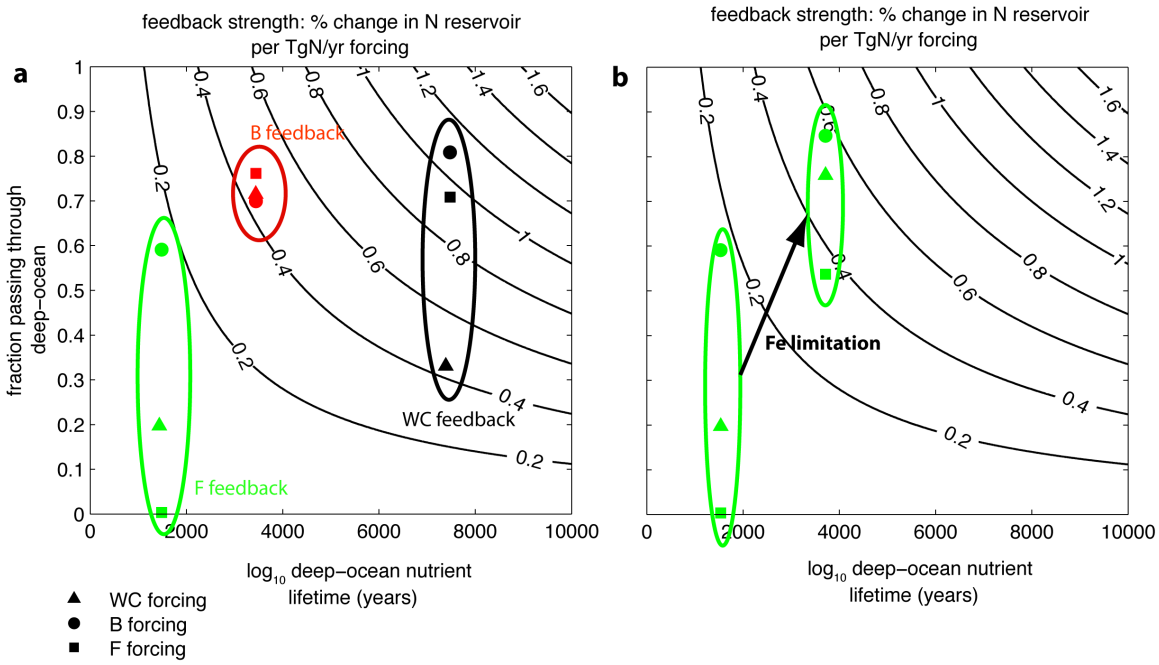

Figure 5.10 a Feedback strengths for each forcing-feedback pair, quantified as % change in the N reservoir per TgN/yr of forcing (smaller values represent stronger feedback). Feedback strength depends on the damping timescale of deep ocean anomalies, and the fraction of forced anomalies that pass through the deep ocean. The F feedback is by far the strongest, unless N_2 fixation is confined to small regions with high Fe inputs. In **b**, it is confined to the Atlantic Ocean only in the second set of points, significantly weakening the feedback.

CHAPTER 6

Summary and Conclusions

6.1 Summary of key results

This dissertation has examined the flexibility of the N reservoir with respect to direct forcing of the N budget, and with respect to the "setpoint" of the nutrient thermostat, as determined by N:P requirements of non-diazotrophic plankton. The four studies presented here revealed a number of important biological and physical processes that control the magnitude of the N reservoir at steady state, and its response to external forcings. The key findings of these studies can be summarized as follows:

- The N:P requirements of marine phytoplankton vary over large scales in the ocean, between biomes with distinct taxonomic composition. The tight correlation between oceanic PO_4 and NO_3, which has previously been taken to indicate a "universal stoichiometry" in plankton communities, is maintained despite large-scale stoichiometric variability by ocean circulation, which mixes remineralized nutrients between biomes. The Redfield N:P ratio of mean plankton biomass merely reflects the current configuration of high and low N:P biomes in the ocean, and does not represent a fundamental biological constraint.

- Because the "setpoint" of the nutrient thermostat is controlled by competitive dynamics between diazotrophs and non-diazotrophic, it is biased upwards towards the high N:P requirements of subtropical phytoplankton. This upwards bias is required in order to simulate a realistic oceanic N reservoir, because inefficient transport pathways between regions of benthic denitrification and N_2-fixation allow N deficits to penetrate the deep ocean, producing a low N reservoir in a "Redfieldian" Ocean. Ocean circulation also transports the stoichiometric signature of remote low N:P plankton into the subtropics, curtailing the upwards bias of the ocean's nutrient ratio and ensuring that the mean N:P ratio of planktons remains an important factor in the thermostat mechanism.
- The ability of external N-budget forcings to change the oceanic N reservoir depends on whether the N anomalies it produces "leak" into the deep ocean before stimulating a restorative feedback. Once in the deep ocean, nutrient anomalies have a long lifetime governed by mixing timescales and the removal efficiency of the operative feedbacks. The N_2-fixation feedback has the greatest removal efficiency and is thus the most important process stabilizing the N oceanic reservoir. The reservoir is strongly buffered against perturbations unless Fe limitation prevents a feedback through N_2-fixation.
- Multiple geochemical indicators suggest that N_2-fixation in the modern ocean is limited at local scales by Fe, but at the basin scale it is strongly coupled to N loss through denitrification. Therefore, Fe does not prevent a strong feedback of N_2-fixation on forced changes in denitrification, and enhanced Fe inputs are not able

to significantly expand the oceanic N reservoir, as has been hypothesized for the Last Glacial Maximum. On the other hand, reduced Fe inputs can force the ocean towards an Fe-limited state, weakening the N_2-fixation feedback and allowing significant oceanic N loss.

6.2 Conclusions – synthesis view of N reservoir dynamics

From these findings, a picture emerges of an oceanic N reservoir that is regulated by stoichiometrically diverse plankton, and is strongly buffered against external forcing by an efficient N_2-fixation feedback. However, two scenarios can be identified under which the N reservoir may undergo major perturbation, with consequences for ocean productivity and global climate:

1. A significant reduction in Fe inputs to the ocean, excluding diazotrophs from the Pacific Ocean. N deficits must then accumulate throughout the deep ocean, before a new steady state is reached in which N_2-fixation is concentrated in the Fe-rich Atlantic Ocean. A reduced Fe supply has been predicted under anthropogenic climate warming, largely due to perturbation of the hydrological cycle and atmospheric circulation. However, the magnitude of this change is subject to large uncertainty, particularly with respect to the role of land use change. Predicting the response of the N reservoir to these forcings will require an improved

understanding of the oceanic Fe cycle, particularly with respect to a proposed buffering mechanism by sedimentary Fe release ((Moore & Braucher 2008).

2. A strong forcing on the "setpoint" of the ocean nutrient thermostat, which must be mediated by large-scale changes in oceanic conditions that favor either high or low N:P plankton. A number of past and future changes in plankton bioegeography have been hypothesized, but their influence on stoichiometric patterns and the N reservoir have not been considered. During the last glacial maxiumum, Fe inputs may have allowed diatoms to expand their range in the low latitude ocean (Brzezinski et al 2002), yet a proliferation of low N:P plankton should be expected to lower the oceanic N reservoir and carbon storage, working against the observed trend in pCO_2. Over the next century, warming and stratification of the upper ocean may expand the range of oligotophic biomes (Polovina et al 2008) and the high N:P cyanobacteria that inhabit them, broadening the niche of diazotrophic plankton and gradually adding new N to the ocean. Our ability to make quantitative predictions regarding these scenarios is limited an incomplete understanding of relationships between elemental stoichiometry and the ecological traits that govern competition between phytoplankton taxa. A strategy combining new observational studies and ecosystem modeling will be required to make progress in this important area.

References

Altabet MA, Francois R, Murray DW, Prell WL. 1995. Climate-related variations in denitrification in the Arabian Sea from sediment $^{15}N/^{14}N$ ratios. *Nature* 373: 506-09

Alvain S, Moulin C, Dandonneau Y, Loisel H. 2008. Seasonal distribution and succession of dominant phytoplankton groups in the global ocean: A satellite view. *Global Biogeochemical Cycles* 22: -

Anderson LA, Sarmiento JL. 1994. Redfield ratios of remineralization determined by nutrient data analysis. *Global Biogeochemical Cycles* 8: 65-80

Anderson RF, Ali S, Bradtmiller LI, Nielsen SHH, Fleisher MQ, et al. 2009. Wind-Driven Upwelling in the Southern Ocean and the Deglacial Rise in Atmospheric CO2. *Science* 323: 1443-48

Arrigo KR, Robinson DH, Worthen DL, Dunbar RB, DiTullio GR, et al. 1999. Phytoplankton community structure and the drawdown of nutrients and CO_2 in the Southern Ocean. *Science* 283: 365-67

Benitez-Nelson CR. 2000. The biogeochemical cycling of phosphorus in marine systems. *Earth-Science Reviews* 51: 109-35

Bertilsson S, Berglund O, Karl DM, Chisholm SW. 2003. Elemental composition of marine Prochlorococcus and Synechococcus: Implications for the ecological stoichiometry of the sea. *Limnol. Oceanogr.* 48: 1721-31

Bohlen L, Dale AW, Wallmann K. 2012. Simple transfer functions for calculating benthic fixed nitrogen losses and C: N: P regeneration ratios in global biogeochemical models. *Global Biogeochemical Cycles* 26

Brandes JA, Devol AH, Deutsch C. 2007. New developments in the marine nitrogen cycle. *Chemical Reviews* 107: 577-89

Broecker WS. 1982. Glacial to Interglacial Changes In Ocean Chemistry. *Progress In Oceanography* 2: 151-97

Broecker WS, Henderson GM. 1998. The sequence of events surrounding Termination II and their implications for the cause of glacial-interglacial CO_2 changes. *Paleoceanography* 13: 352-64

Brzezinski MA, Pride CJ, Franck VM, Sigman DM, Sarmiento JL, et al. 2002. A switch from $Si(OH)_4$ to NO_3^- depletion in the glacial Southern Ocean. *Geophysical Research Letters* 29: art. no.-1564

Capone DG, Burns J, Montoya JP, Subramaniam A, Mahaffey C, et al. 2005. Nitrogen fixation by Trichodesmium spp.: An important source of new nitrogen to the tropical and subtropical North Atlantic Ocean. *Global Biogeochemical Cycles* 19: doi:10.1029/2004GB002331

Capone DG, Zehr JP, Paerl HW, Bergman B, Carpenter EJ. 1997. Trichodesmium, a globally significant marine cyanobacterium. *Science* 276: 1221-29

Chappell PD, Moffett JW, Hynes AM, Webb EA. 2012. Molecular evidence of iron limitation and availability in the global diazotroph Trichodesmium. *The ISME Journal* 6: 1728-39

Christensen JP, Murray JW, Devol AH, Codispoti LA. 1987. Denitrification in continental shelf sediments has major impact on the oceanic nitrogen budget. *Glob. Biogeochem. Cycles* 1: 97-116

Codispoti L. 2007. An oceanic fixed nitrogen sink exceeding 400 Tg N a< sup>? 1</sup> vs the concept of homeostasis in the fixed-nitrogen inventory. *Biogeosciences* 4: 233-53

Codispoti LA. 1989. Phosphorus vs. Nitrogen Limitation of New and Export Production In *Productivity of the Ocean: Past and Present*, ed. WH Berger, VS Smetacek, G Wefer, pp. 377-94: John Wiley and Sons, Ltd

Codispoti LA. 1995. Biogeochemical cycles - Is the ocean losing nitrate? *Nature* 376: 724

Codispoti LA, Brandes JA, Christensen JP, Devol AH, Naqvi SWA, et al. 2001. The oceanic fixed nitrogen and nitrous oxide budgets: Moving targets as we enter the anthropocene? *Scientia Marina* 65: 85-101

Codispoti LA, Christensen JP. 1985. Nitrification, denitrification, and nitrous oxide cycling in the eastern tropical Pacific Ocean. *Marine Chemistry* 16: 277-300

De Baar HJW, Van Leeuwe MA, Scharek R, Goeyens L, Bakker KMJ, Fritsche P. 1997. Nutrient anomalies in Fragilariopsis kerguelensis blooms, iron deficiency and the nitrate/phosphate ratio (A.C. Redfield) of the Antarctic Ocean. *Deep-Sea Research, Part II* 44: 229-60

Dentener F, Drevet J, Lamarque JF, Bey I, Eickhout B, et al. 2006. Nitrogen and sulfur deposition on regional and global scales: A multimodel evaluation. *Global Biogeochemical Cycles* 20: -

Deutsch C, Brix H, Ito T, Frenzel H, Thompson L. 2011. Climate-forced variability of ocean hypoxia. *science* 333: 336-39

Deutsch C, Gruber N, Key RM, Sarmiento JL, Ganaschaud A. 2001. Denitrification and N_2 fixation in the Pacific Ocean. *Global Biogeochemical Cycles* 15: 483-506

Deutsch C, Sarmiento JL, Sigman DM, Gruber N, Dunne JP. 2007. Spatial coupling of nitrogen inputs and losses in the ocean. *Nature* 445: 163-67

Deutsch C, Sigman DM, Thunell R, Meckler AN, Haug GH. 2004. Isotopic Constraints on the Glacial/Interglacial Oceanic Nitrogen Budget. *Global Biogeochemical Cycles* 18: doi:10.1029/2003GB002189

Deutsch C, Weber T. 2012. Nutrient Ratios as a Tracer and Driver of Ocean Biogeochemistry. *Annual Review of Marine Science* 4: null

DeVries T, Deutsch C, Primeau F, Chang B, Devol A. 2012a. Global rates of water-column denitrification derived from nitrogen gas measurements. *Nature Geoscience* 5: 547-50

DeVries T, Deutsch C, Rafter PA, Primeau F. 2012b. Marine denitrification rates determined from a global 3-dimensional inverse model. *Biogeosciences Discuss.* 9: 14013-52

DeVries T, Primeau F. 2011. Dynamically and Observationally Constrained Estimates of Water-Mass Distributions and Ages in the Global Ocean. *J. Phys. Oceanogr.* 41: 2381-401

Egge JK, Aksnes DL. 1992. Silicate as Regulating Nutrient in Phytoplankton Competition. *Marine Ecology-Progress Series* 83: 281-89

Elderfield H, Rickaby REM. 2000. Oceanic Cd/P ratio and nutrient utilization in the glacial Southern Ocean. *Nature* 405: 305-10

Elser JJ, Sterner RW, Gorokhova E, Fagan WF, Markow TA, et al. 2000. Biological stoichiometry from genes to ecosystems. *Ecology Letters* 3: 540-50

Eugster O, Gruber N, Deutsch C, Jaccard SL, Payne MR. 2013. The dynamics of the marine nitrogen cycle across the last deglaciation. *Paleoceanography*

Falkowski PG. 1997. Evolution of the nitrogen cycle and its influence on the biological sequestration of CO_2 in the ocean. *Nature* 387: 272-75

Falkowski PG. 2000. Rationalizing elemental ratios in unicellular algae. *Journal of Phycology* 36: 3-6

Finkel ZV, Quigg A, Raven JA, Reinfelder JR, Schofield OE, Falkowski PG. 2006. Irradiance and the elemental stoichiometry of marine phytoplankton. *Limnol. Oceanogr.* 51: 2690-701

Fu FX, Warner ME, Zhang YH, Feng YY, Hutchins DA. 2007. Effects of increased temperature and CO2 on photosynthesis, growth, and elemental ratios in marine Synechococcus and Prochlorococcus (Cyanobacteria). *Journal of Phycology* 43: 485-96

Fu FX, Zhang YH, Leblanc K, Sanudo-Wilhelmy SA, Hutchins DA. 2005. The biological and biogeochemical consequences of phosphate scavenging onto phytoplankton cell surfaces. *Limnol Oceanogr* 50: 1459-72

Galloway JN, Dentener FJ, Capone DG, Boyer EW, Howarth RW, et al. 2004. Nitrogen cycles: past, present, and future. *Biogeochemistry* 70: 153-226

Ganeshram RS, Pedersen TF, Calvert SE, McNeill GW, Fontugne MR. 2000. Glacial-interglacial variability in denitrification in the world's oceans: Causes and consequences. *Paleoceanography* 15: 361-76

Ganeshram RS, Pedersen TF, Calvert SE, Murray JW. 1995. Large changes in oceanic nutrient inventories from glacial to interglacial periods. *Nature* 376: 755-58

Garcia H, Locarnini R, Boyer T, Antonov J. 2010. World Ocean Atlas 2009, vol. 4, Nutrients (Phosphate, Nitrate, Silicate), NOAA Atlas NESDIS, vol. 71. *US Gov. Print. Off., Washington, DC*

Geider RJ, La Roche J. 2002. Redfield revisited: variability of C : N : P in marine microalgae and its biochemical basis. *European Journal of Phycology* 37: 1-17

Green SE, Sambrotto RN. 2006a. Net community production in terms of C, N, P and Si in the Antarctic Circumpolar Current and its influence on regional water mass characteristics. *Deep-Sea Research Part I-Oceanographic Research Papers* 53: 111-35

Green SE, Sambrotto RN. 2006b. Plankton community structure and export of C, N, P and Si in the Antarctic Circumpolar Current. *Deep-Sea Research Part Ii-Topical Studies in Oceanography* 53: 620-43

Großkopf T, Mohr W, Baustian T, Schunck H, Gill D, et al. 2012. Doubling of marine dinitrogen-fixation rates based on direct measurements. *Nature* 488: 361-64

Gruber N. 2003. The dynamics of the marine nitrogen cycle and its influence on atmospheric CO_2 variations In *Carbon-Climate Interactions*, ed. M Follows, T Oguz, pp. 97-148. New York: John Wiley & Sons

Gruber N. 2004. The dynamics of the marine nitrogen cycle and its influence on atmospheric CO2 variations In *The ocean carbon cycle and climate*, pp. 97-148: Springer

Gruber N, Sarmiento JL. 1997. Global patterns of marine nitrogen fixation and denitrification. *Global Biogeochemical Cycles* 11: 235-66

Hansell DA, Bates NR, Olson DB. 2004. Excess nitrate and nitrogen fixation in the North Atlantic Ocean. *Marine Chemistry* 84: 243-65

Heldal M, Scanlan DJ, Norland S, Thingstad F, Mann NH. 2003. Elemental composition of single cells of various strains of marine Prochlorococcus and Synechococcus using X-ray microanalysis. *Limnol. Oceanogr.* 48: 1732-43

Holzer M, Primeau FW. 2013. Global teleconnections in the oceanic 1 phosphorus cycle: patterns, paths, and 2 timescales. *Journal of Geophysical Research: Oceans*

Jickells T, An Z, Andersen KK, Baker A, Bergametti G, et al. 2005. Global iron connections between desert dust, ocean biogeochemistry, and climate. *Science* 308: 67-71

Jin X, Gruber N, Dunne JP, Sarmiento JL, Armstrong RA. 2006. Diagnosing the contribution of phytoplankton functional groups to the production and export of

particulate organic carbon, CaCO3, and opal from global nutrient and alkalinity distributions. *Global Biogeochemical Cycles* 20: -

Karl D, Letelier R, Tupas L, Dore J, Christian J, Hebel D. 1997. The role of nitrogen fixation in biogeochemical cycling in the subtropical North Pacific Ocean. *Nature* 388: 533-38

Karl D, Michaels A, Bergman B, Capone D, Carpenter E, et al. 2002. Dinitrogen fixation in the world's oceans. *Biogeochemistry* 57/58: 47-98

Karl DM, Bidigare RR, Letelier RM. 2001a. Long-term changes in plankton community structure and productivity in the North Pacific subtropical gyre: The domain shift hypothesis. *Deep-Sea Research Part Ii-Topical Studies in Oceanography* 48: 1449-70

Karl DM, Bjorkman KM, Dore JE, Fujieki L, Hebel DV, et al. 2001b. Ecological nitrogen-to-phosphorus stoichiometry at station ALOHA. *Deep-Sea Research Part Ii-Topical Studies in Oceanography* 48: 1529-66

Karl DM, Letelier R, Hebel DV, Bird DF, Winn CD. 1992. Trichodesmium blooms and new production in the North Pacific gyre In *Marine Pelagic Cyanobacteria: Trichodesmium and other Diazotrophs*, ed. EJ Carpenter, pp. 219-37: Kluwer Academic Publishers

Karl DM, Michaels AF. 2001. Nitrogen cycle In *Encyclopedia of Ocean Sciences*, ed. JH Steele, KK Turekian, SA Thorpe, pp. 1876-84. London: Academic Press

Keeling RF, Körtzinger A, Gruber N. 2010. Ocean deoxygenation in a warming world. *Annual Review of Marine Science* 2: 199-229

Khatiwala S. 2007. A computational framework for simulation of biogeochemical tracers in the ocean. *Global Biogeochemical Cycles* 21: -

Khatiwala S, Visbeck M, Cane MA. 2005. Accelerated simulation of passive tracers in ocean circulation models. *Ocean Modelling* 9: 51-69

Klausmeier CA, Litchman E, Daufresne T, Levin SA. 2004. Optimal nitrogen-to-phosphorus stoichiometry of phytoplankton. *Nature* 429: 171-74

Knapp AN, DiFiore PJ, Deutsch C, Sigman DM, Lipschultz F. 2008. Nitrate isotopic composition between Bermuda and Puerto Rico: Implications for N_2 fixation in the Atlantic Ocean. *Global Biogeochemical Cycles* doi:10.1029/2007GB003107

Kopczynska EE, Weber LH, El-Sayed SZ. 1986. Phytoplankton species composition and abundance in the Indian sector of the Antarctic Ocean. *Polar Biology* 6: 161-69

Kuypers MM, Sliekers AO, Lavik G, Schmid M, Jørgensen BB, et al. 2003. Anaerobic ammonium oxidation by anammox bacteria in the Black Sea. *Nature* 422: 608-11

Kwon EY, Primeau F. 2006. Optimization and sensitivity study of a biogeochemistry ocean model using an implicit solver and in situ phosphate data. *Global Biogeochemical Cycles* 20

Lam P, Kuypers MMM. 2011. Microbial Nitrogen Cycling Processes in Oxygen Minimum Zones. *Annual Review of Marine Science* 3: 317-45

Lambert F, Delmonte B, Petit JR, Bigler M, Kaufmann PR, et al. 2008. Dust-climate couplings over the past 800,000 years from the EPICA Dome C ice core. *Nature* 452: 616-19

Landolfi A, Dietze H, Koeve W, Oschlies A. 2013. Overlooked runaway feedback in the marine nitrogen cycle: the vicious cycle. *Biogeosciences (BG)* 10: 1351-63

LaRoche J, Breitbarth E. 2005. Importance of the diazotrophs as a source of new nitrogen in the ocean. *Journal of Sea Research* 53: 67-91

Lenton TM, Klausmeier CA. 2007. Biotic stoichiometric controls on the deep ocean N : P ratio. *Biogeosciences* 4: 353-67

Lenton TM, Watson AJ. 2000. Redfield revisited 1. Regulation of nitrate, phosphate, and oxygen in the ocean. *Global Biogeochemical Cycles* 14: 225-48

Letelier RM, Karl DM. 1998. Trichodesmium spp. physiology and nutrient fluxes in the North Pacific subtropical gyre. *Aquatic Microbial Ecology* 15: 265-76

Longhurst A. 1995. Seasonal cycles of pelagic production and consumption. *Progress in Oceanography* 36: 77-167

Luo Y-W, Doney S, Anderson L, Benavides M, Berman-Frank I, et al. 2012. Database of diazotrophs in global ocean: abundances, biomass and nitrogen fixation rates. *Earth System Science Data* 4: 47-73

Mahowald N, Kohfeld K, Hansson M, Balkanski Y, Harrison SP, et al. 1999. Dust sources and deposition during the last glacial maximum and current climate: A comparison of model results with paleodata from ice cores and marine sediments. *Journal of Geophysical Research - Atmospheres* 104: 15895-916

Mahowald NM, Muhs DR, Levis S, Rasch PJ, Yoshioka M, et al. 2006. Change in atmospheric mineral aerosols in response to climate: Last glacial period,

preindustrial, modern, and doubled carbon dioxide climates. *Journal of Geophysical Research-Atmospheres* 111: -

Martin JH, Gordon RM, Fitzwater S, Broenkow WW. 1989. VERTEX: phytoplankton/iron studies in the Gulf of Alaska. *Deep-Sea Research* 36: 649-80

Martin JH, Knauer GA, Karl DM, Broenkow WW. 1987. VERTEX: carbon cycling in the northeast Pacific. *Deep-Sea Research* 34: 267-85

Martiny AC, Pham CT, Primeau FW, Vrugt JA, Moore JK, et al. 2013. Strong latitudinal patterns in the elemental ratios of marine plankton and organic matter. *Nature Geoscience* 6: 279-83

Middelburg JJ. 1989. A simple rate model for organic matter decomposition in marine sediments. *Geochim. Cosmochim. Acta* 53: 1577-81

Middelburg JJ, Soetaert K, Herman PMJ, Heip CHR. 1996. Denitrification in marine sediments: A model study. *Global Biogeochemical Cycles* 10: 661-73

Mills MM, Arrigo KR. 2010. Magnitude of oceanic nitrogen fixation influenced by the nutrient uptake ratio of phytoplankton. *Nature Geosci* 3: 412-16

Montoya JP, Holl CM, Zehr JP, Hansen A, Villareal TA, Capone DG. 2004. High rates of N-2 fixation by unicellular diazotrophs in the oligotrophic Pacific Ocean. *Nature* 430: 1027-31

Moore CM, Mills MM, Achterberg EP, Geider RJ, LaRoche J, et al. 2009. Large-scale distribution of Atlantic nitrogen fixation controlled by iron availability. *Nature Geoscience* 2: 867-71

Moore J, Braucher O. 2008. Sedimentary and mineral dust sources of dissolved iron to the world ocean. *Biogeosciences* 5: 631-56

Moore JK, Doney SC. 2007. Iron availability limits the ocean nitrogen inventory stabilizing feedbacks between marine denitrification and nitrogen fixation. *Global Biogeochemical Cycles* 21: -

Moore JK, Doney SC, Lindsay K. 2004. Upper ocean ecosystem dynamics and iron cycling in a global three-dimensional model. *Global Biogeochemical Cycles* 18: -

Orsi AH, Whitworth TW, Nowlin WD. 1995. On the meridional extent and fronts of the Antarctic Circumpolar Current. *Deep-Sea Research*

Parekh P, Follows MJ, Boyle E. 2004. Modeling the global ocean iron cycle. *Global Biogeochemical Cycles* 18

Parekh P, Follows MJ, Boyle EA. 2005. Decoupling of iron and phosphate in the global ocean. *Global Biogeochemical Cycles* 19

Polovina JJ, Howell EA, Abecassis M. 2008. Ocean's least productive waters are expanding. *Geophys. Res. Lett.* 35: L03618

Price NM. 2005. The elemental stoichiometry and composition of an iron-limited diatom. *Limnol. Oceanogr.* 50: 1159-71

Primeau F. 2005. Characterizing transport between the surface mixed layer and the ocean interior with a forward and adjoint global ocean transport model. *J. Phys. Oceanogr.* 35: 545-64

Quigg A, Finkel ZV, Irwin AJ, Rosenthal Y, Ho TY, et al. 2003. The evolutionary inheritance of elemental stoichiometry in marine phytoplankton. *Nature* 425: 291-94

Redfield AC. 1958. The biological control of chemical factors in the environment. *American Scientist* 46: 205-21

Redfield AC, Ketchum BH, Richards FA. 1963. The Influence of Organisms on the Composition of Seawater In *The Sea, Vol. 2*, ed. MN Hill, pp. 26-77. New York: Interscience

Ren H, Sigman DM, Meckler AN, Plessen B, Robinson RS, et al. 2009. Foraminiferal Isotope Evidence of Reduced Nitrogen Fixation in the Ice Age Atlantic Ocean. *Science* 323: 244-48

Rubin SI, Takahashi T, Chipman DW, Goddard JG. 1998. Primary productivity and nutrient utilization ratios in the Pacific sector of the Southern Ocean based on seasonal changes in seawater chemistry. *Deep-Sea Res Pt I* 45: 1211-34

Sarmiento JL, Gruber N. 2006. *Ocean Biogeochemical Dynamics*. Princeton: Princeton University Press. 503 pp.

Sarmiento JL, Toggweiler JR. 1984. A new model for the role of the oceans in determining atmospheric pCO_2. *Nature* 308: 621-24

Schlitzer R. 2002. Carbon export fluxes in the Southern Ocean: results from inverse modeling and comparison with satellite-based estimates. *Deep-Sea Research Part Ii-Topical Studies in Oceanography* 49: 1623-44

Sigman DM, DiFiore PJ, Hain MP, Deutsch C, Karl DM. 2009. Sinking organic matter spreads the nitrogen isotope signal of pelagic denitrification in the North Pacific. *Geophysical research letters* 36

Somes CJ, Schmittner A, Altabet MA. 2010. Nitrogen isotope simulations show the importance of atmospheric iron deposition for nitrogen fixation across the Pacific Ocean. *Geophysical Research Letters* 37

Sterner RW, Elser JJ. 2002. *Ecological stoichiometry : the biology of elements from molecules to the biosphere*. Princeton, N.J. ; Oxford: Princeton University Press. xxi, 439 p. pp.

Takahashi T, Broecker WS, Langer S. 1985. Redfield ratio based on chemical data from isopycnal surfaces. *Journal of Geophysical Research* 90: 6907-24

Tyrrell T. 1999. The relative influences of nitrogen and phosphorus on oceanic primary production. *Nature* 400: 525-31

Ward BB, Devol AH, Rich JJ, Chang BX, Bulow SE, et al. 2009. Denitrification as the dominant nitrogen loss process in the Arabian Sea. *Nature* 461: 78-81

Weber T, Deutsch C. 2012. Oceanic nitrogen reservoir regulated by plankton diversity and ocean circulation. *Nature* 489: 419-U105

Weber TS, Deutsch C. 2010. Ocean nutrient ratios governed by plankton biogeography. *Nature* 467: 550-54

Wu JF, Sunda W, Boyle EA, Karl DM. 2000. Phosphate depletion in the western North Atlantic Ocean. *Science* 289: 759-62

Zehr JP, Kudela RM. 2011. Nitrogen Cycle of the Open Ocean: From Genes to Ecosystems. *Annual Review of Marine Science* 3: 197-225

Zehr JP, Ward BB. 2002. Nitrogen cycling in the ocean: New perspectives on processes and paradigms. *Applied and Environmental Microbiology* 68: 1015-24

Zehr JP, Waterbury JB, Turner PJ, Montoya JP, Omoregie E, et al. 2001. Unicellular cyanobacteria fix N-2 in the subtropical North Pacific Ocean. *Nature* 412: 635-38

Zhang YC, Rossow WB, Lacis AA, Oinas V, Mishchenko MI. 2004. Calculation of radiative fluxes from the surface to top of atmosphere based on ISCCP and other global data sets: Refinements of the radiative transfer model and the input data. *Journal of Geophysical Research-Atmospheres* 109: -